Benjamin Allcock March 2017

The downstream response to pharmacologically induced endoplasmic reticulum stress in two human cell lines.

A thesis submitted for the degree of Master of Science,

School of Biosciences,

Durham University

Supervisor: Dr Adam Benham

Abstract

Endoplasmic reticulum stress and the unfolded protein response are implicated in a number of diseases, from cancer to ankylosing spondylitis. Understanding the mechanisms underlying this response and how these may differ between cell types is important in beginning to address potential pharmacological therapies. This thesis investigated the effect of the pharmacological endoplasmic reticulum stress inducer tunicamycin, and the isoflavine tyrosine kinase inhibitor genistein on the downstream pathways of the subsequent unfolded protein response. This was investigated in the two human cell lines HeLa and HT1080.

The investigations in this thesis found that tunicamycin induced differential activation of downstream unfolded protein response pathways in the two cell lines. The first main finding was that the HT1080 cells exhibited chronic activation of stress related phosphorylation pathways in comparison to the more transient response of the HeLa cells. Both cell lines showed a peak expression of the pro-survival proteins after 10 minutes of tunicamycin treatment, as well as showing longer-term responses to stress with later induction of the phosphorylated-Stat3 protein. This indicates that both acute and chronic effects of ER stress occur in both cell types, but that HT1080 cells had a more consistent expression of stress related proteins. From live cell imaging data, HeLa cells were much more sensitive to tunicamycin induced motility inhibition than the HT1080 cells, which may reflect a state of resistance to stress-induced changes in motility in the HT1080 cells. Genistein decreased the phosphorylation of stress related phosphoproteins slightly.

These findings reveal that consideration of the cell type must be made when devising pharmacological routes to address conditions where endoplasmic reticulum stress is a pathological factor. The differential response of cell lines to pharmacologically induced ER stress could be exploited to create selective therapies specific to individual cell types.

Contents

List of Figures

Abbreviations:

ANOVA	Analysis of variance
AS	Ankylosing spondylitis
ASK1	Apoptosis signal-regulating kinase 1
ATF	Activating transcription factor
ATP	Adenosine triphosphate
BASMI	Bath Ankylosing Spondylitis Metrology Index
BAX	Bcl-2-associated X protein
BCL-2	B-cell lymphoma 2
BIM	BCL-2 interacting mediator of cell death
BiP	Binding immunoglobulin protein
BSA	Bovine serum albumin
CBF	CCAAT-binding factor
CHOP	C/EBP homologous protein
DTT	Dithiothreitol
EDEM	ER degradation-enhancing α-mannosidase-like protein
eIF2α	Eukaryotic translation initiation factor 2
eIF4E	Eukaryotic translation initiation factor 4E
ER	Endoplasmic reticulum
ERAD	Endoplasmic reticulum associated degradation
ERAP	Endoplasmic reticulum aminopeptidase
ERK	Extracellular signal-regulated kinases
ERSE	Endoplasmic reticulum stress response element
GADD34	Growth arrest and DNA damage inducible protein 34
GPT	UDP-N-acetylglucosamine—undecaprenyl-phosphate N-acetylglucosaminephosphotransferase
GRP	Glucose regulated protein
GTP	Guanosine-5'-triphosphate
HLA	Human leukocyte antigen
HSP	Heat shock protein
HO-1	Heme oxygenase-1
HT	HT1080
IL6	Interleukin 6
IRE1α	Inositol requiring enzyme 1

JDP	J-domain proteins
JNK	c-Jun N-terminal kinases
KIR3DL2	Killer cell immunoglobulin like receptor
MAPK	Mitogen activated protein kinase
MAPKK	Mitogen activated protein kinase kinase
MGUS	Monoclonal gammopathy of undetermined significance
MHC	Major histocompatibility complex
MIF	Macrophage migration inhibitory factor
MM	Multiple myeloma
mRNA	messenger ribonucleic acid
NQO	NAD(P)H:quinone oxidoreductase
NF-κB	Nuclear factor kappa beta
NK cells	Natural killer cells
NO	Nitric oxide
NrF2	Nuclear factor-like 2
PCYOX	Prenylcysteine oxidase
PDGF	Platelet derived growth factor
PDGF-R	Platelet derived growth factor receptor
PDI	Protein disulfide isomerase
PERK	protein kinase RNA-like endoplasmic reticulum kinase
PI3K	Phosphoinositide3-kinase
PTEN	Phosphatase and tensin homolog
PTK	Protein tyrosine kinase
RIDD	Regulated IRE1 dependent decay
ROS	Reactive oxygen species
SDS-PAGE	Sodium dodecyl sulfate - polyacrylamide gel electrophoresis
SS	Serum starvation
STAT3	Signal transducer and activator of transcription 3
T	Tunicamycin
TFII-I	Transcription factor II-I
TNF	Tumor necrosis factor
tRNA	Transfer ribonucleic acid
UPR	Unfolded protein response
UT	Untreated
UV	Ultra-violet

XBP1	X-box binding protein 1

Declaration

I declare that the material contained within this thesis is my own and from my own work. This work has not been previously submitted for a higher education degree.

Benjamin Philip Allcock

Acknowledgements

I would like to thank Dr Adam Benham, my supervisor, for his guidance and support throughout this project. I also want to thank the Lab 8 research group for their encouragement and friendliness throughout my time in the laboratory. I would also like to thank Tim and Joanne from microscopy for their assistance and advice in the imaging.

Finally, I would like to thank my family and Meg for everything they have done to help and support me throughout.

Chapter 1: Introduction

1.1 Endoplasmic reticulum stress in context

Endoplasmic reticulum stress (ER stress) is a complex series of reactions that cells undergo when subjected to the specific stress stimulus of misfolded proteins. This introduction will outline the various factors involved in ER stress; from the pathways activated to some diseases involved, and will also outline the rationale of the experiments conducted for this project along with providing information about exactly what the different pharmacological stress inducers do.

ER stress is involved in a plethora of diseases including type II diabetes (Back and Kaufman, 2012), cancer (Urra et al., 2016) and neurodegenerative diseases (Lindholm et al., 2006). ER stress occurs when misfolded proteins accumulate in the ER. Misfolded proteins may arise due to a number of reasons, such as mutations, overloading of protein folding capacity and also due to pharmacological induction using drugs to induce general or specific protein misfolding. Misfolding can contribute to diseases such as AS, and may be a factor affecting disease progression in other diseases such as cancer due to the augmenting effect of ER stress on tumorigenesis, which will be later discussed. The presence of misfolded proteins in the ER activates a cellular stress response called the unfolded protein response or UPR.

Three specific and different pathways are activated in the cell during the UPR (Wang and Kaufman, 2014), and these IRE1α, ATF6α and PERK pathways determine the outcome of a stress response for the cell. These pathways will be discussed molecularly in the following sections. The outcome is either apoptosis or resolution of ER stress through an increase in folding capacity, decreased protein transport and decreased protein synthesis. ERAD (endoplasmic reticulum associated degradation) is increased with the activation of the UPR and this is when the misfolded proteins in the ER are targeted for ubiquitination and degradation. ER stress has attracted attention for the development of new therapies for a range of diseases. For example, if ER stress can be modulated, or if different cell types behave differently under ER stress, then there are implications for creating specific therapies that could target ER stress in selective cells. As the diseases involving ER stress affect a wide range of

bodily functions and areas, it is important to question whether the effects seen in one group of cells will be the same in another cell type, and if differences are seen, then perhaps this could unlock potential areas of investigation to establish why those differences exist, which could in turn reveal potential therapeutic targets.

1.2 Protein Folding

Protein folding is an essential process within the cell, and is closely linked to activation of ER stress and the UPR. Proteins need to be folded into a three-dimensional shape. The protein begins as a random coil and sequence of amino acids, which interact with each other to form covalent bonds that are the basis for a protein's 3D structure. The sequence of amino acids is the primary determinant for its ultimate 3D functional structure (Anfinsen, 1972), but the exact process of how the protein folds is affected by multiple factors. One of the main driving forces behind the folding is related to the hydrophobic nature of specific amino acids such as alanine, isoleucine, leucine, phenylalanine, valine, proline and glycine. In a solvent, the hydrophobic amino acids are repelled by the solvent and therefore a hydrophobic protein core is created, with this core being shielded from the solvent by non-hydrophobic, polar amino acids. These polar amino acids include glutamine, asparagine, histidine, serine, threonine, cysteine, methionine, tryptophan. The process is much more complex than just this though and as the Levinthal paradox demonstrates (Zwanzig et al., 1992), a protein left to fold without any external factors would take a vast amount of time, too long to be biologically viable, due to the huge number of possible folding conformations for the proteins. Kinetics therefore is important for folding, with a bias against locally unfavourable conformations which dramatically reduce the time taken to fold (Zwanzig et al., 1992).

While proteins can fold by themselves, often co-translationally (Fedorov and Baldwin, 1997), an aid to folding often comes in the form of a group of proteins within the cell called chaperones. As the nascent intermediate structures are produced by the ribosome, the chaperones may come to assist the folding as well as helping fold the full length product after release (Fedorov and Baldwin, 1997). Many chaperones reside in the ER as a large amount of protein synthesis occurs here. The chaperones

may aid primarily in protein folding, but others help prevent aggregation of proteins by binding to their intermediate states. These two types of chaperones are classed 'holdases' and 'foldases' (Hoffmann et al., 2004) and help maintain homeostasis in the cell, particularly under times of stress where the need for protein quality control is increased. Under conditions of cellular stress such as elevated temperature or denaturing conditions, chaperones are recruited to help alleviate this stress. Many chaperones are in fact heat shock proteins (HSPs), which primarily act under stressed conditions due to increased temperature for example acting as a protein denaturant. A key protein heavily implicated in ER stress specifically is the HSP70 chaperone, GRP78/BiP (Lee, 2005). This is an ER resident general chaperone, and has multiple functions in both the translocation machinery and maintaining the newly synthesised ER proteins in a stable state for translocation. Once bound to a substrate, BiP is able to aid in protein folding and aggregate prevention. Aggregate prevention is achieved through the combined work of HSP-70 chaperones and their co-chaperones; the J-domain proteins (JDP). The chaperones bind to the hydrophobic regions of the non-native proteins which prevents intermolecular interactions (demonstrating 'holdase' activity) (Mayer and Bukau, 2005). It is also a key component of the unfolded protein response, functioning in the signal transduction for the three pathways involved in the UPR.

ER stress is a term referring to an accumulation of unfolded or misfolded proteins in the ER. The ER has a delicate homeostatic balance between protein load and protein folding capacity (Oslowski and Urano, 2011), and this can be disturbed via pathological and physiological insults which can result in the unfolded and misfolded proteins collecting in the ER and putting pressure on the cell's folding apparatus. Unfolded proteins individually do not pose a strong threat to the cell, however when the unfolded proteins start to aggregate, this can have a cytotoxic effect on the cell so it is essential to clear up the potential threat of unfolded proteins to prevent cytotoxicity and to maintain proper functioning of the ER. The cytotoxicity of the aggregates stems from the excess activation of the ER stress response, and the push towards apoptosis when the stress is unresolvable (Uchio et al., 2007).

1.3 Unfolded Protein Response

The UPR is activated when misfolded and unfolded proteins are present in the ER lumen. There are three signalling pathways in this stress response, all activated through the same first step – sequestration of BiP by unfolded proteins present in the ER. BiP has multiple roles, one of which is maintaining the three transmembrane receptor proteins for each branch of the UPR in an inactive state. When unfolded proteins begin accumulating in the ER, BiP is required for binding to help prevent aggregation and aid in re-folding, and as the free BiP supplies decrease, the BiP bound to the transmembrane receptors dissociates to meet the BiP demand and this subsequently allows activation of the different UPR branches (Wang and Kaufman, 2014). The three pathways start with their respective transmembrane ER sensor proteins: IRE1α, ATF6α and PERK (Wang and Kaufman, 2014). These pathways resolve ER stress through increased folding capacity, increased protein transport out of the ER and increasing the activation of ER associated protein degradation, while preventing further protein synthesis – the adaptive response. If, however, the unfolded protein load exceeds the capacity of the unfolded protein response, then the cells undergo apoptosis (Wang and Kaufman, 2014). The pathways have many downstream signalling cascades (Wang and Kaufman, 2014) - for example IRE1α works via multiple different pathways including JNK signalling, XBP-1 splicing and regulated IRE1 dependent decay, so each branch of the UPR can be regulated individually. Cell fate determination is an important aspect of the UPR, and the balance between the three different pathways is central to deciding whether the cell undergoes apoptosis or survives. If the balance between survival and apoptosis is uneven, then it may lead to diseases such as cancer, and this will be explored in depth later. Over-active apoptosis, for example, could lead to degenerative diseases such as Parkinson's or Alzheimer's (Chen and Brandizzi, 2013). Chronic UPR activation is also closely linked with inflammation via phosphorylation of initiation factor 2 (eIF2α) by PERK; a translation initiation factor 2 kinase (eIF2α kinase) (Hotamisligil, 2010). This phosphorylation leads to translational suppression of inhibitory kappa B (IκB) , which acts as an inhibitor to the pro-inflammatory nuclear factor kappa B (NF-κB). NF-κB then activates due to the regulation of inflammation mediators, resulting in inflammation.

1.4 IRE1α

The IRE1α branch of the UPR is a mammalian pro-survival pathway, but can also cause apoptosis due to the decay of anti-apoptotic micro-mRNAs (Upton et al., 2012). The IRE1α protein has a diverse downstream signalling cascade with two specific pathways contributing towards a decision of cell fate (Chen and Brandizzi, 2013). These pathways consist of unconventional splicing of the transcription factor, x-box binding protein 1 (*Xbp-1*) and regulated IRE1 dependent decay (RIDD).

Originally it was believed that IRE1α signalling was terminated during chronic ER stress to facilitate apoptosis (Hetz, 2012), however it is now debated that IRE1α is persistently involved in UPR signalling and determines cell fate. After BiP dissociates from the IRE1α transmembrane protein, the protein's luminal domain homodimerises, which consequently allows autophosphorylation of the cytoplasmic domains due to close proximity (Ali et al., 2011). The phosphorylation site lies within the central ~10 residues of the kinase segment (720-729), and the putative phosphorylation site is on Ser724. This activates the cytosolic RNase domain which carries out the splicing activity on *Xbp-1* mRNA. By removing a 26 nucleotide intron from the mRNA, the codon reading frame is shifted and this results in the generation of a new COOH-terminal end that is a potent transactivation domain (Hetz et al., 2011). The spliced XBP-1 (sXBP-1) can now activate multiple ER quality control and ER stress genes to help the cell adapt to the stress. Downstream effects of the spliced XBP-1 include upregulation of ER chaperones and ERAD associated genes (Yoshida et al., 2001) including ER resident chaperone genes such as heat shock protein/ chaperone DnaJ (Hsp40/DnaJ), ER Degradation Enhancing α-Mannosidase-like protein (EDEM) and HEDJ (Lee et al., 2003). XBP-1 has a well-documented role in the UPR, and curiously one study purports that the unspliced form may negatively regulate autophagy (Vidal and Hetz, 2013). An alternate pathway to XBP-1 splicing is RIDD, which represses adaptive responses and activates apoptosis (Chen and Brandizzi, 2013) due to IRE1α RNase cleaving multiple other mRNAs as well as XBP-1 (Wang and Kaufman, 2014). These cleaved mRNAs include many ER localised mRNAs encoding secretory cargo proteins and proteins that promote folding (Han et al., 2009). RIDD is also active during the switch between adaption and apoptosis and

during this transition phase, it degrades selective UPR target genes, one of which is BiP, ultimately increasing the ER stress intensity further shifting the balance towards apoptosis. Once a stress intensity threshold is reached, the RIDD degrades anti apoptotic micro-RNAs to induce apoptosis (Upton et al., 2012). These micro-RNAs function as repressors of the translation of *Caspase-2* miRNA. Caspase-2 is a protease that plays an essential role in apoptosis (Vakifahmetoglu-Norberg and Zhivotovsky, 2010). Through inhibiting anti *Caspase-2* miRNA, Caspase 2 is upregulated through IRE1α activation, driving the cell towards apoptosis. This demonstrates how IRE1α acts a molecular switch, able to determine whether the cell undergoes apoptosis, or whether it adapts to the stress.

The cell fate determination through the IRE1α pathway is further affected through cJUN NH_2-terminal kinases (JNKs) during ER stress (Chen and Brandizzi, 2013). The mitogen protein kinase JNK and apoptosis signal regulating kinase 1 (ASK1) form a regulatory part of the IRE1α pathway. JNK along with RIDD, promotes apoptosis in the cell and therefore also plays a role in cell fate determination. ASK1 activates multiple downstream targets including MAPKs and JNK (HAYAKAWA et al., 2012). JNK phosphorylates and activates transcription factors such as cJUN and ATF2 to regulate gene expression levels while also regulating the stability of mRNA (Urano et al., 2000). This pathway works via binding of TNF receptor-associated factor 2 (TRAF2) to the activated IRE1α which recruits ASK1 and JNK. This in turn activates BCL-2 interacting mediator of cell death (BIM) and inactivates BCL-2 (Wang and Kaufman, 2014). BIM is an important pro-apoptotic protein (Gogada et al., 2012) which induces the oligomerisation of the pro-aptotic Bax/Bak on mitochondria (BCL2 associated X, apoptosis regulator). Bax increases the opening of the mitochondrial voltage dependent anion channel, resulting in a loss of membrane potential and a release of cytochrome C. BCL-2 is an anti-apoptotic protein and the inactivation of this protein, coupled with the activation of BIM comprises the pro-apoptotic action of ASK1 and JNK recruitment. **Figure 1.1** highlights the three possible routes that the IRE1α pathway may follow to result in either apoptosis or survival.

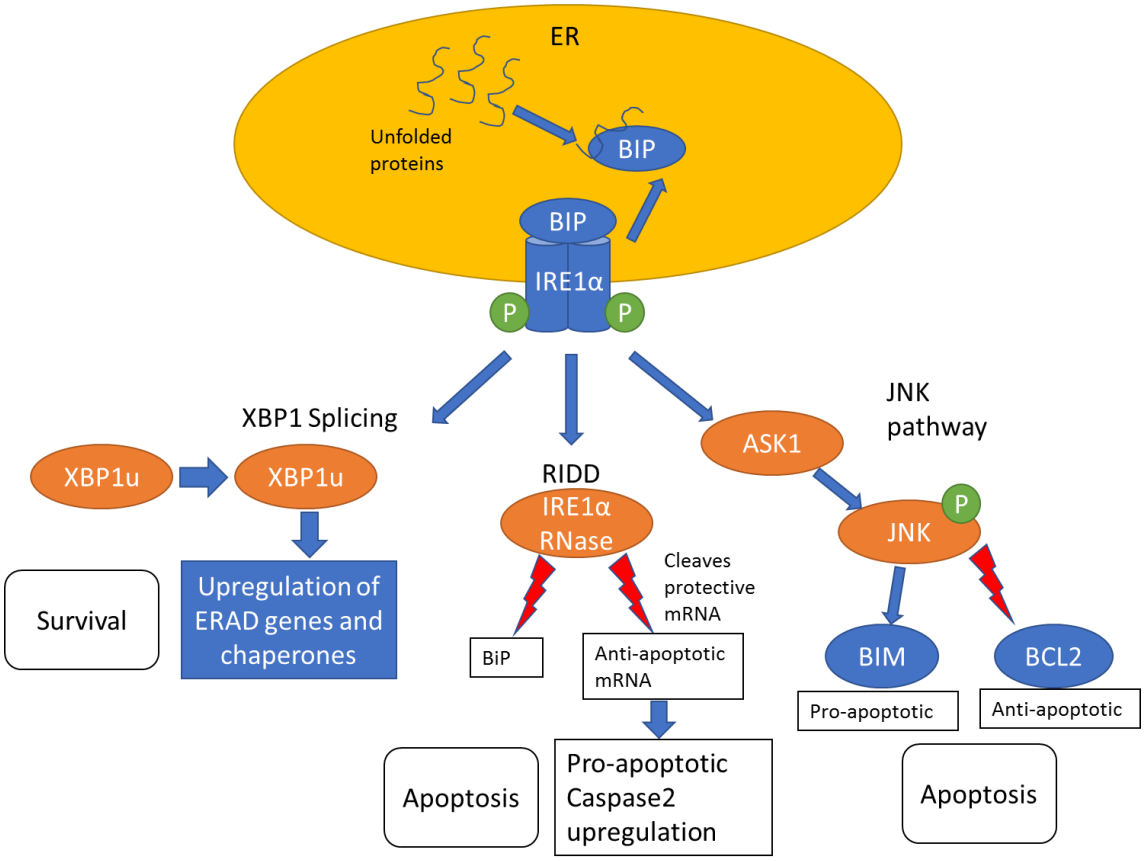

Figure 1.1: The IRE1α pathway can direct cell fate determination.
The transmembrane receptor IRE1α homodimerises and autophosphorylates after dissociation of BiP due to sequestration from unfolded proteins. This may result in XBP1 splicing, which is pro-survival, or may result in the apoptotic outcome of RIDD and the JNK pathway.

1.5 ATF6α

The next UPR pathway to consider is the ATF6α pathway, and this is activated slightly differently to IRE1α. Instead of autophosphorylation once BiP has dissociated, ATF6α translocates from the ER compartment to the golgi apparatus where it is cleaved from a full length protein (90 kDa), releasing a cytosolic fragment (50 kDa) (Zhang and Kaufman, 2004). This process is called regulated intermembrane proteolysis and it is a highly conserved process, whereby information is transferred to the nucleus from the ER in the form of a functionally active protein fragment. There are two steps in the cleavage of the protein, each using a different protease; the first being the cleava

ge of the protein substrate in the extra-cytoplasmic domain, and the second cleavage occurs in the membrane spanning domain (Rawson, 2002). The cytosolic fragment then migrates to the nucleus where it acts as a transcription factor, inducing ER stress genes including the transcriptional induction of XBP-1 (Galindo et al., 2012). Currently, ATF6 is only linked to the adaptive outcome of the UPR and no evidence yet suggests a link between ATF6 signalling and apoptosis.

1.6 PERK

The third branch of the UPR is PERK and this protein is activated in the same fashion as IRE1α. Once BiP disassociates, PERK homodimerises and autophosphorylates (Liu et al., 2000). PERK activates eIF2α via phosphorylation at S51, which attenuates translation initiation through regulation of the translational activity of eIF2. eIF2 creates a ternary complex with GTP and the $tRNA_{met}$ which is the initiator. This complex binds the 40S ribosomal subunit to make a 43S subunit – the preinitiation complex. This binds to the 5' end of mRNA to scan downstream, and once a start codon (AUG) is found, $tRNA_{met}$ binds to the codon, and the GTPase activating protein - eIF5 activates eIF2 hydrolysis of GTP. This results in the release of the eIF2 complex from the ribosome. Translation may then commence after the 60S subunit is recruited and the 80S initiation complex is formed. For a new round of translation initiation to begin, the GDP in eIF2 must be exchanged for GTP, which is achieved with the guanine nucleotide exchange factor eIF2B – a step that is inhibited by eIF5 (Wang and Kaufman, 2014). The eIF2α is part of a heterotrimer that makes up eIF2 along with a beta and a gamma subunit. The phosphorylated eIF2α increases the affinity of eIF2 for GDP greatly and this inhibits the GDP to GTP exchange with eIF2B, instead forming an inactive complex with eIF2 and sequestered eIF2B. There is a low ratio of eIF2B to eIF2, and this means that even small amounts of eIF2α phosphorylation can halt protein synthesis (Harding et al., 2000). **Figure 1.2** shows a simplified version of this signalling pathway and the cellular consequences as discussed below.

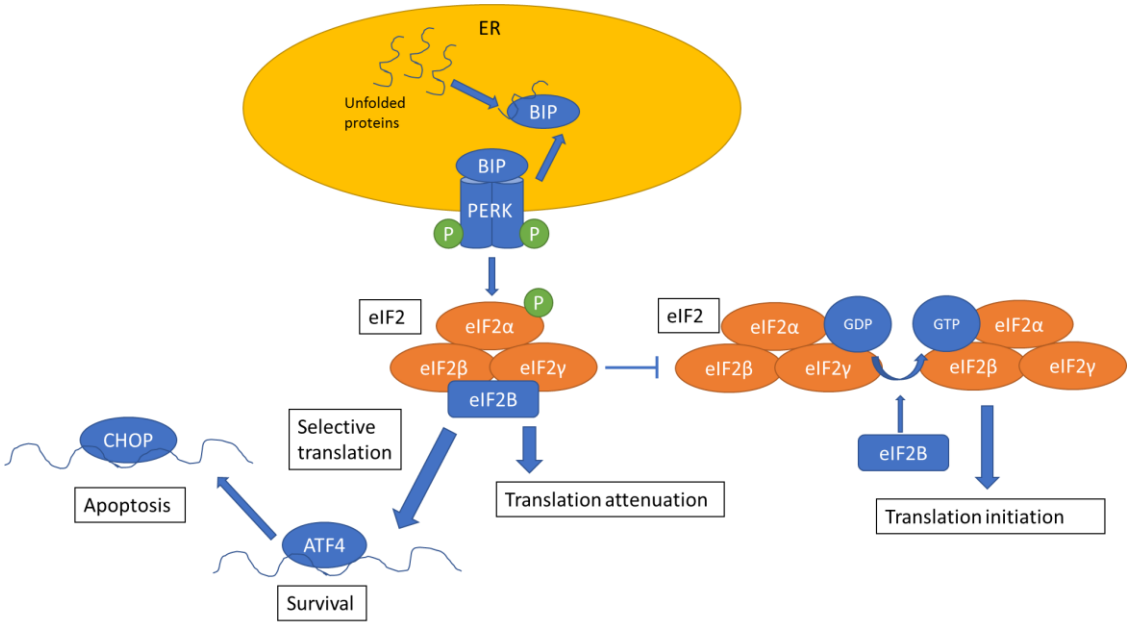

Figure 1.2: PERK activation results in general translational attenuation, but selective pro-apoptotic or pro-survival translation.
Activated PERK phosphorylates eIF2α, preventing eIF2B from initiating translation via exchanging GDP for GTP. This is due to the greatly increased binding affinity of GDP when eIF2α is phosphorylated, so eIF2B is sequestered instead, forming an inactive complex with eIF2. This attenuates translation but selectively translates the mRNA for the transcription factor ATF4 which aids the adaptive UPR. ATF4 in turn transcribes CHOP which is a pro-apoptotic transcription factor.

While the phosphorylation of eIF2α results in a decrease of global mRNA translation, a paradoxical increase in ATF4 mRNA translation amongst other select mRNAs is observed due to selective translation (Harding et al., 2000). ATF4 is a transcription factor that enters the nucleus and upregulates ER stress genes. One target of ATF4 is activating the transcription of the growth arrest and DNA damage inducible protein 34 (GADD34), which in turn promotes de-phosphorylation of eIF2α resulting in restored global translation. The other important transcription target of ATF4 is C/EBP homologous protein (CHOP), which has an important role in promoting apoptosis. CHOP has a similar function to ASK1/JNK in that it can upregulate the pro-apoptotic transcription of BIM (Puthalakath et al., 2007) as well as inhibiting anti-apoptotic BCL-2 expression (McCullough et al., 2001). On top of this, BAX translocation to the mitochondria is promoted by CHOP (Szegezdi et al., 2006). As well as CHOP mediated

apoptosis, eIF2α phosphorylation from PERK in chronic stress also leads to apoptosis due to the attenuation of the two other UPR branches (Rutkowski et al., 2006). To induce apoptosis, a strong chronic activation of PERK is required, namely because of the short half-lives of ATF4 and CHOP (Rutkowski et al., 2006). It is possible that CHOP and ATF4 do not directly induce apoptosis, but instead work through indirect routes. This is supported by chromatin immunoprecipitation of ATF4 and CHOP, which selectively enriches sequences of DNA bound to target proteins, and sequencing of genes directly regulated by these two proteins (Han et al., 2013). This study discovered that there was no enrichment of target genes involved in cell death, by either CHOP or ATF4, when cells were under ER stress. Instead, it was found that CHOP and ATF4 interact and form heterodimers which upregulate protein synthesis and UPR genes. The expression of ATF4 and CHOP increases protein synthesis and consequently protein folding, which can lead to increased reactive oxygen species (ROS) creating oxidative stress and cell death. This data shows that the pro-apoptotic action of these two proteins is not direct, but works instead through increased protein synthesis, with resultant oxidative stress pushing the system towards an apoptotic outcome. The transient phosphorylation of eIF2α after stress halts protein synthesis and the subsequent induction of ATF4 and CHOP acts to restore this synthesis. However, if the protein folding homeostasis is not also restored by this point, then the resulting ROS production will drive the cells to apoptosis (Han et al., 2013). This explains how the PERK pathway and the IRE1α pathway act as molecular switches to help cell fate determination through selective apoptosis of stressed cells. ATF4 also aids in withstanding oxidative stress by interacting with Nuclear factor-like 2 (Nrf2) whose target genes encode antioxidant enzymes such as heme oxygenase-1 (HO-1) and NAD(P)H:quinone oxidoreductase (NQO) which help limit toxicity and further induction of stress (He et al., 2001); however it does not prevent stress from occurring altogether (Clarke et al., 2014). In addition to these antioxidants, the dissociation of the Nrf2/Keap1 complex and activation of Nrf2 by PERK helps alleviate oxidative stress due to Nrf2's function in maintaining glutathione levels, which functions as a buffer against rising ROS levels (Cullinan and Diehl, 2004).

The ER has a delicate redox balance, changes to which can severely perturb protein folding. The ER lumen is particularly sensitive to changes in the redox balance as disulphide bonds form through oxidative protein folding, which is dependent on the redox state of the cell. Under ER stress, the breakage and formation of disulphide bonds may produce ROS which can lead to oxidative stress (Cao and Kaufman, 2014). As well as this, ER stress can lead to mitochondrial dis-function which can result in an increase of mitochondrial ROS too, contributing further to oxidative stress. There is an interaction between ER stress and oxidative stress that acts as a positive feed-forward loop, resulting in pro-apoptotic signalling and disrupted cell function (Cao and Kaufman, 2014).

1.7 ER Stress in Disease

1.7.1 Cancer

ER stress is prevalent in many diseases and this provides a strong reason to continue research on the area. Cancer in particular has had a lot of research undertaken in the context of ER stress and how it affects tumorigenesis. In cancer, it is common for the tumour cores to become hypoxic (starved of oxygen) and consequently the availability of ATP is decreased. This in turn compromises the protein folding ability of the cells in the hypoxic core and thus the UPR is activated (Clarke et al., 2014). Multiple factors of the UPR make a difference to cancer prognosis and tumour progression, with the IRE1α and PERK pathways specifically contributing to tumorigenesis. Splicing of XBP-1 increases the resistance of tumour cells to hypoxia in hypoxic tumours. In XBP-1 deficient cells there was increased apoptosis in hypoxic conditions, and although a different system to tumour cells, this could indicate that XBP-1 splicing leads to a poorer prognosis in tumours (Romero-Ramirez et al., 2004). While XPB-1 knockout cells are not in the same system as tumour cells, there is evidently a link between this component of the UPR signalling pathways and tumour progression.

PERK and IRE1α both have roles in promoting tumour angiogenesis and vascularisation is essential for tumour survival when hypoxia is an issue. Vascular endothelial growth factor, which helps promote angiogenesis, is upregulated by the

PERK-ATF4 branch of the UPR, and proangiogenic transcripts are upregulated in a PERK dependent manner (Blais et al., 2006). PERK also downregulates angiogenic inhibitors during glucose deprivation, and when PERK expression was silenced, the induction of angiogenesis mediators was considerably decreased, resulting in slower tumour growth (Wang et al., 2012). Due to the dual-action nature of the UPR pathways, both pro-apoptotic and anti-apoptotic, the role of IRE1α and PERK signalling is not always as clear-cut. PERK deletion has an effect on oxidative stress also; PERK deficient cells have an increased ROS production as well as a decrease in Nrf2 (Bobrovnikova-Marjon et al., 2010). Nrf2 was identified as a substrate for PERK, and it is a transcription factor whose protein products mediate redox level, including phase II detoxifying enzymes which promote survival under the oxidative stress conditions produced as a side effect of UPR activation (Cullinan et al., 2003). The protective function of PERK against oxidative stress further strengthens the idea that PERK is pro-tumorigenic; however, long term knockout can contribute to tumour susceptibility due to genomic instability (Bobrovnikova-Marjon et al., 2010). Tumour suppressive roles of CHOP have also been proposed, which is seemingly paradoxical considering the pro-tumour activity of the PERK pathway. In a mouse model of K-ras (G12V)-induced lung cancer, CHOP deletion appeared to significantly increase tumour incidence (Huber et al., 2013), illustrating that there is a dichotomy within the PERK pathway on which way it may affect tumorigenesis.

The role of the PERK-ATF4 arm in tumour progression is evidently a complex one and there is a clear link between this branch of the UPR and tumorigenesis. The IRE1α arm also has a role to play, being involved in the upregulation of angiogenic factors and the downregulation of angiogenic inhibitors. Under-expressing IRE1α in a human glioma model, a mouse orthotopic brain model and a chick chorio-allantoic membrane assay demonstrated reduced tumour growth, angiogenesis and invasiveness, as expected (Auf et al., 2010).

The IRE1α pathway has a role in plasma cell differentiation, due to the selective and specific requirement of XBP-1 in terminal differentiation of B cell lymphocytes into plasma cells (Reimold et al., 2001), and consequently, the IRE1α pathway has been the subject of in depth research in relation to multiple myeloma – a cancer of plasma

cells. In transgenic mice engineered to express the spliced isoform of XBP-1 through Eμ directed expression (an Eμ enhancer binds to specific proteins to increase their likelihood of transcription), multiple myeloma (MM) phenotypes were observed, including the premalignant precursor to MM; monoclonal gammopathy of undetermined significance (MGUS). The forced expression of spliced XBP-1 enhanced B-cell proliferative potential and activated known pathways of MM (Carrasco et al., 2007). Interestingly, loss of function mutations in XBP-1 and IRE1α were discovered in multiple myeloma cell lines that showed resistance to proteasome inhibition (Leung-Hagesteijn et al., 2013). Proteasome inhibitors are used as a non-curative therapy for multiple myeloma which extends survival. The failure to cure MM with proteasome inhibitors was partially explained through the discovery of sub-populations of pre-plasmablasts with XBP-1 loss of function that as a result are insensitive to proteasome inhibition. The cells with functioning XBP-1 show sensitivity to the protease inhibitors, which increase the already higher basal levels of ER stress in MM cells due to the inhibition of ERAD. However, in the subpopulations where XBP-1 has a loss of function mutation, the ER load is significantly less, due to a lower production of immunoglobulin (Ig) in these cells, and Ig synthesis plays the most prominent role in the ER of the plasma cells. This means that if less Ig is produced by these mutant plasma cells, they will not be sensitive to the increased ER stress induced by the proteasome inhibitors as they are avoiding the susceptibility to ER stress that arises from constant production of protein. The reason for a de-commitment to Ig production in XBP-1 knockdown is not clear, though this is the effect seen, and provides an explanation for the insensitivity to PIs.

As previously discussed, the UPR has a large role in cell fate determination under stress conditions, and clearly, the active UPR in the hypoxic conditions of tumour cells plays an adaptive and pro-survival role in the disease. Pre-malignant cells harbouring mutations that inhibit the pro-apoptotic outcomes of the UPR may have selective advantages (Wang and Kaufman, 2014) due to irremediable UPR activation allowing constant survival of the tumour cells under stressed conditions. Because of the selective nature of UPR activation in the tumour cells and not in normal cells, targeting UPR activation in cancer could prove useful in selective cancer therapy (X.

Li et al., 2011). The key to potential UPR related therapy in cancer could lie in triggering the apoptotic pathways of the UPR over the adaptive pathways, stimulating cell death in the tumours. The issue with using this therapy is due to whether the selectiveness can be limited to solely cancer cells, and whether the desired apoptotic outcome for the cancer cells can be triggered with minimal downstream effects elsewhere.

1.7.2 Ankylosing spondylitis

Ankylosing spondylitis (AS) is a chronic inflammatory debilitating disease that affects the axial skeleton and often severely impacts the quality of life for sufferers. People with this disease have to cope with many related issues such as pain, functional disabilities and sleep problems (Sieper et al., 2002) amongst other socio-economic factors such as loss of income and additional disease related expenses (Sieper et al., 2002). The prevalence of ankylosing spondylitis varies from region to region with a mean AS prevalence of 23.8 per 10,000 (0.238%) in Europe and 16.7 per 10,000 (0.167%) in Asia (Dean et al., 2014). A main feature of the disease is enthesitis; an inflammation of the area where the tendons, ligaments, capsules and fascia incorporate into the bone (McGonagle, 2009) and along with other factors such as synovitis, subchondral marrow inflammation and osteitis this makes a painful disease that in severe cases can result in complete spinal fusion and rigidity. The role of MHC class I proteins in AS is subject to much research and scrutiny, as there is a clear link between the MHC class I gene HLA-B27*05 and the prevalence of AS. The normal function of MHC class I proteins is to present cytosolic non-self protein fragments to cytotoxic T cells, which elicits a rapid immune response, therefore bringing virally infected cells to the attention of the immune system (Hewitt, 2003).

The pathophysiology of AS is still not fully understood, and there are multiple potential mechanisms that may cause the disease. There is certainly a strong genetic association with certain allotypes of the MHC class I allele HLA-B27 and AS. The MHC genes are encoded on chromosome 6 and the encoded proteins are present on all nucleated cell types (Shamji et al., 2008). The HLA loci are incredibly variable, and thus a different set of subtypes are expressed within each individual (Parham and

Ohta, 1996). Around 90% of ankylosing spondylitis sufferers are positive for HLA-B27; however, amongst HLA-B27 positive populations, only a small number of individuals (1.3% - 13.6%) suffer from AS (van der Linden et al., 1984),(Braun et al., 1998). The risk of developing AS amongst HLA-B27 positive individuals increases 16 fold with HLA-B27 positive relatives (van der Linden et al., 1984), and HLA-B27 positive individuals have a 20 fold higher risk of developing AS compared to negative individuals (van der Linden et al., 1984). The genetic link is clear, however there must be other contributing factors that work with HLA-B27 to cause progression of the disease as the prevalence statistics show that HLA-B27 does not directly cause the disease. A problem with the data from these two papers by Van der Linden et al. and Braun et al. respectively is that the sample sizes are small, and the variance in suggested percentage prevalence between the two papers reflects this. This paints a picture that AS is not present in all HLA-B27 positive individuals but there is an important link between the genotype and the disease that needs to be understood.

Four main theories seek to explain the role of HLA-B27 in the pathogenesis of AS: arthritogenic peptide presentation, aberrant surface chains, protein misfolding and enhanced microbial survival (Shamji et al., 2008). Genetic information is important for understanding AS; for example, the change of the amino acid residue aspartate to histidine means that the allele from the AS associated HLA-B2705 changes to the HLA-B2709 allele which as a result loses the association with AS (Del Porto et al., 1994). This observation is consistent with the arthritogenic peptide presentation theory, which suggests that the differences in peptide binding affinities between different allotypes of HLA-B27 can result in the presentation of unique self-peptides that exhibit molecular mimicry, resembling bacterial antigenic peptides. The mimicry of these peptides can lead to autoimmune cross reactivity due to the action of cytotoxic CD8+ T cells which causes tissue damage and inflammation (Shamji et al., 2008). The aberrant surface chain theory suggests that the HLA-B27 protein has a tendency to form homodimers when the cell surface heavy chains lose β-microglobulin, which occurs during endosomal recycling (Allen et al., 1999). These disulfide bridged homodimers elicit CD4+ T cell and NK cell autoreactivity which is destructive. The theory suggesting that the HLA-B27 phenotype enhances

intracellular microbial survival possibly has the weakest experimental support as there is a lot of conflicting evidence (Shamji et al., 2008). This theory proposes that ineffective peptide loading onto HLA-B27 can cause abnormal immune cell activation, which in turn allows bacteria and viruses to proliferate coupled with decreased clearance of antigenic peptides (Shamji et al., 2008). The final theory is that protein misfolding of HLA-B27 is a causative factor of ankylosing spondylitis. This theory suggests that the cellular ERAD response is exceeded, which results in commonly toxic misfolded aggregates forming inside and outside the cell. Chronic UPR activation here is a contributing factor towards AS, and there is evidence of increased UPR activation in transgenic rats expressing human HLA-B27 (Allen et al., 1999). Prolonged UPR activation increases ERAD and pro-inflammatory NF-kB pathway activation (Shamji et al., 2008), and with the pro-survival arms of the UPR being favoured, the inflammation caused as a result is severe and chronic.

Further effects of prolonged UPR stress on cells were explored in a paper by Lamech (Lamech and Haynes, 2015) which focuses on three stress response pathways in the cells; the heat shock protein response, the UPR and the mitochondrial UPR. This paper suggests there is a cytotoxic effect of continuous UPR stress. Multiple papers have also corroborated the link between misfolded HLA-B27 and UPR stress, including a 2007 study by Lemin et. al. (Lemin et al., 2007). This study demonstrated that the spliced form of XBP-1 is present in lymphocytes with over-expressed HLA-B27. XBP-1 is important in regulating the most conserved branch of the UPR, the IRE1 pathway (Lemin et al., 2007) which, as discussed, is key for cell fate determination. The data showed that XBP-1 was spliced in the HLA-B27+ cells suggesting that the unfolded protein response was active in these cells. Spliced XBP-1 is important for normal cytokine expression, and under ER stress it may be involved in synergistic induction (Colbert et al., 2014). In HLA-B27+ splenocytes from rats, there were higher levels of XBP-1 splicing than in the non-transgenic rats relatively speaking, albeit still with only a low absolute expression of spliced XBP-1 (Turner et al., 2007), further suggesting that a low level of UPR is active in HLA-B27+ cells.

A paper by the Australo-Anglo-American Spondyloarthritis Consortium et al (TASC et al., 2011), demonstrated that other genes are also involved in AS, uncovered from

GWAS (genome-wide association studies). One such gene, ERAP1, acts as a molecular ruler of sorts, trimming polypeptide precursors down to size for presentation as antigenic peptides on MHC class I molecules (Chang et al., 2005). ERAP could play a role in disease, potentially through aberrant peptide trimming. A recent paper by Schittenhelm et al (Schittenhelm et al., 2015) revisited the arthritogenic peptide theory and suggested that conversely to previous beliefs, a potential mechanism is due to a quantitative change in the peptides, not a change in the type of peptides binding. A recent paper by Cortes et al (Cortes et al., 2015) shows that ERAP1 loss of function arising from *Erap* deficiency has a protective effect against ankylosing spondylitis, reducing the presentation of an HLA-B27 immunodominant epitope due to a loss of ERAP1 trimming function. Recently, through these multiple genome wide association studies, 26 risk loci have been identified outside the MHC class 1 (Cortes et al., 2015), and more risk alleles of HLA-B are being discovered including B*07:02, B*13:02, B*40:01, B*40:02, B*47:01, B*51:01 and B*57:01 (Cortes et al., 2015).

In addition to the arthritogenic peptide theory, the aberrant surface chain hypothesis involves specific proteins for example, the role of the KIR3DL2 protein, shown to be expressed on the NK and CD4+ T cells in HLA-B27+ patients. This protein recognises HLA-B27 homodimers (Chan et al., 2005), and therefore is important to the aberrant surface chain hypothesis which suggests that HLA-B27 homodimers are recognised by the autoreactive CD4+ T cells and NK cells. The KIR3DL2 protein therefore is one such receptor responsible for recognising HLA-B27 and contributing to AS. While there has been a large amount of in depth research on AS and the pathogenesis of the disease, there is still much to be learnt.

It is clear that in the pathogenesis of AS, many factors play a role and the importance of cytokines must not be underestimated, specifically relating to the misfolded HLA-B27 theory. The ER resident chaperone BiP/GRP78 is often induced by the signalling pathways invoked by the UPR and this chaperone may promote cytokine production from macrophages which causes inflammation (Zambrano-Zaragoza et al., 2013). Interestingly BiP levels are 2 times higher in transgenic HLA-B27 rat splenocytes (Turner et al., 2007), demonstrating a link to the UPR and AS. Increased and prolonged interaction between BiP and HLA-B27 activates both the ERAD pathway

and the inflammatory NF-kB pathway (Shamji et al., 2008). The pro-inflammatory cytokines involved in AS include TNF-α, IL-1 and IL-6. TNF-α levels are significantly higher in patients with AS (Zambrano-Zaragoza et al., 2013) demonstrated in 143 AS Taiwanese patients (Shiau et al., 2007) and 97 Iranian (Nicknam et al., 2009). Various single nucleotide polymorphisms have been studied of the *TNFA* gene, which shows a relationship between certain polymorphisms and AS. Specifically, the TNF-α polymorphisms at amino acid positions 238 and 308 are significantly decreased in individuals with AS and overrepresented in AS patients as compared to controls (Nicknam et al., 2009). However, these polymorphisms do not seem to have a relation to specific HLA-B27 subtypes. The -238 and -308 polymorphisms have been associated with higher TNF-α levels. and some TNF-α polymorphisms are protective in AS. TNF-α inhibition by etanercept shows an improvement of symptoms in patients with AS (Gorman et al., 2002). This was investigated using a double blind study with a placebo group in which 80% of the treated group showed an improvement in spinal stiffness, enthesitis and quality of life. These improvements were seen in both the treatment time (4 months) and in the longitudinal study (subsequent 6 months). The placebo group only showed a 30% improvement in these indicators (Gorman et al., 2002).

MIF (macrophage migration inhibitory factor) is also a key player in AS. It is believed that this cytokine has an important role in oxidative stress. Stosic-Grujicic et. al. suggested that MIF has an important role in the pathogenesis of autoimmune diseases by inducing the production of NO (nitric oxide) which is an oxidative stress mediator (Stosic-Grujicic et al., 2008). To see if MIF played a role in AS, the levels of MIF were measured in AS patients in a study by Kozaci et al (Kozaci et al., 2009). Though the sample size of this study was small, it was found that the MIF levels were raised in 25 AS patients compared to 18 controls (12.2 ± 7.7 and 7.5 ± 3.7 ng/ml, respectively, $p = 0.01$), and IL-10 levels were lower (210.9 ± 100.4 vs. 527 ± 191 pg/ml; p\0.001) (Kozaci et al., 2009). MIF levels also correlated with BASMI, an index reflecting spinal mobility and disease activity. The authors concluded that MIF could potentially amplify or enhance the existing inflammatory signals in AS rather than actually contributing to the pathogenesis of AS.

While the four theories explaining the role of HLA-B27 in AS (arthritogenic peptides, aberrant surface chains, microbial evasion, and MHC class I misfolding) all have credence individually, it is highly likely that there is a lot of interplay between the various proposed mechanisms of disease. The common factor between the theories is the role of HLA-B27 which is undoubtedly linked to AS. The presence of HLA-B27 alone is not enough to induce AS, and there are many factors that work alongside the MHC class I protein to contribute to the formation of AS. There is undoubtedly a link between UPR activation and AS, which shows that as well as the involvement with cancer with chronic UPR activation contributing to tumorigenesis, the UPR also plays a role in inflammatory diseases. It is clear that some of the key factors that contribute to AS include stress signalling pathways, such as that of XBP-1 which is spliced under ER stress conditions and affects cytokine production. Cytokines are important too in the pathogenesis of AS, as many pro-inflammatory cytokines are involved in enhancing the inflammation encountered in AS. The multiple aspects underlying the pathogenesis of AS demonstrate that one lone therapy may not be enough to eradicate the disease. Instead, a synergistic approach that combines different therapies to target different facets should be employed.

1.8 Stress inducers

The pharmacological stress inducers tunicamycin and DTT both cause ER stress in the cell, however their mechanisms of action are different. Tunicamycin is an ER stress inducer that inhibits the initial steps of glycoprotein biosynthesis. It does this by inhibiting UDP-N-acetylglucosamine-dolichol phosphate N-acetylglucosamine-1-phosphate transferase (GPT) (Oslowski and Urano, 2011). The treatment of cells with tunicamycin results in a build-up of unfolded glycoproteins in the ER, which ultimately triggers ER stress. The primary effect of tunicamycin is to trigger the UPR, which closely mimics the *in vivo* activation of the UPR by unfolded proteins. DTT also induces the UPR. It is a strong reducing agent that reduces disulphide bonds and prevents disulphide bond formation, though this inhibition is not limited to just the ER, making it a non-specific stress inducer (Oslowski and Urano, 2011). Multiple studies have demonstrated the usefulness of these drugs in ER stress induction, with tunicamycin inducing a slower onset of stress over a period of roughly 5 hours

(Oslowski and Urano, 2011), and DTT eliciting a faster response (B. Li et al., 2011). A plethora of studies use tunicamycin as an experimental tool to induce stress, and it has proved very useful in mimicking the environment of misfolded proteins in the ER that is prevalent in many ER stress linked diseases.

While tunicamycin is the main stress inducer used in the investigations in this thesis, it is important to note that there are other ER stress inducers. Thapsigargin, for example, is also commonly employed as a stress inducer (Iurlaro and Muñoz-Pinedo, 2016; Sano and Reed, 2013; Zhang et al., 2014). Thapsigargin specifically inhibits the endoplasmic/sarcoplasmic reticulum Ca^{2+}-ATPase, which results in a decrease of calcium inside the endoplasmic reticulum. This means that calcium dependent chaperones in the ER like calnexin lose their chaperone activity (Oslowski and Urano, 2011), resulting in an increase of unfolded proteins and consequently ER stress. MG132 is another stress inducer, which specifically inhibits proteasome activity resulting in decreased ERAD, therefore indirectly causing a build-up of unfolded proteins in the ER.

1.9 Genistein

Genistein is an isoflavone found in soy based foods (Spagnuolo et al., 2015) and a tyrosine kinase inhibitor, currently employed as a drug for use in chemotherapy trials on animals and *in vitro* to target cancers. Tyrosine kinases transfer phosphate from ATP to protein substrates. When functioning normally, tyrosine kinases have a role in enhancing sensitivity to apoptosis and regulating cell growth by preventing uncontrollable proliferation (Paul and Mukhopadhyay, 2004). Tyrosine kinases also have an important role in cancer; for example, cancers often harbour mutations that cause constitutive activation of tyrosine kinases. The consequence of this is a constant activation of pathways that disrupts the normal regulation of cell growth and apoptosis, and will push the cells towards uncontrollable proliferation, resulting in the development of cancers. Genistein is of interest as an anticancer agent because it can inhibit protein tyrosine kinase (PTK) signalling to attenuate cancer development (BANERJEE et al., 2008). Tyrosine kinases are manifold, and another target of interest is the MAPK pathway, which is also involved in ER stress. MAPK

(ERK, JNK and p38) can induce NF-κB and drive cells toward survival under stress stimuli (Seger and Krebs, 1995). P38 MAPK is tyrosine phosphorylated by the MAP kinase kinases MKK3 and MKK6 (Zarubin and Han, 2005). Inhibition of these tyrosine kinases with genistein could result in an inhibition of the MAPK pathway, which may promote apoptosis due to inhibition of MAPK phosphorylation.

The high pleiotropy of genistein means it can alter apoptosis, the cell cycle and angiogenesis via a synergistic effect on multiple biochemical pathways involved in the development on cancer (Spagnuolo et al., 2015). However, many of its downstream effects are not fully understood. Apoptosis induction by genistein was achieved by downregulating the anti-apoptotic B cell lymphoma 2 (BCl2) protein and upregulating the pro-apoptotic BAX in gastric cancer cells (Zhou et al., 2004). Epidemiological studies have demonstrated that the intake of isoflavines through a soy based diet appears to lower the incidence of breast cancer in Asian women in particular (Wu et al., 2008). The particular type of soy food consumed may change the relative risk, but when 15 epidemiological studies on soy consumption and 9 studies on isoflavines were compiled, it was found that intake of soy based products also reduced prostate cancer in men, with a relative risk of 0.74 (95% CI: 0.63, 0.89; P = 0.01). The protective effect of isoflavines was more prominent in Asian men, with a relative risk of 0.52 (95% CI: 0.34, 0.81; P = 0.01) compared to 0.99 (95% CI: 0.85, 1.16; P = 0.91) for Western populations (Yan and Spitznagel, 2009).

Previous studies have found that genistein can inhibit the induction of GRP78/BiP during ER stress (Zhou and Lee, 1998a). This may be due to the importance of tyrosine kinase signalling in the pathways that lead to the production of chaperones such as GRP78. TFII-I is a multifunctional transcription factor that binds to the ER stress response element (ERSE) which is highly conserved across the promoters for ER stress related genes, under ER stress conditions (Hong et al., 2005a). The GRP promoters that promote transcription of essential chaperones, for example, contain multiple copies of the ERSE. The TFII-I protein exhibits enhanced binding to the ERSE of the GRP promoters under ER stress conditions. Specifically, a conserved GGC motif is required for optimal binding and this is located in a 9 bp CG rich region of the ERSE (Parker et al., 2001). The activity of TFII-I is mediated by phosphorylation, and TFII-I

is phosphorylated at specific serine and tyrosine sites. The tyrosine kinase phosphorylation of tyrosine residues Tyr^{248} and Tyr^{611} is dependent on the kinase c-Src (Cheriyath et al., 2002). Genistein has been shown to inhibit GRP78 production (Zhou and Lee, 1998a), and the known inhibitory action of genistein on tyrosine kinases may explain GRP78 inhibition due to the importance of tyrosine kinase signalling in TFII-I signal transduction. Indeed, it has been shown that genistein inhibits tyrosine kinase phosphorylation of two specific tyrosine residues on TFII-I linked to ER stress; Tyr^{248} and Tyr^{249}, and that genistein can act as a general inhibitor of ER stress induction (Hong et al., 2005a) due to its inhibition of thapsigargin and tunicamycin induced GRP78 expression. Another possible mechanism by which genistein inhibits GRP78 production is via interference with the key transcription factor CBF/NF-Y (Zhou and Lee, 1998a), which also regulates the ERSE, binding to the closest CCAAT site closest of the GRP78 promoter. The treatment of cells with genistein does not appear to disrupt GRP78 already produced, and therefore genistein is likely just to inhibit further production of the chaperone. Genistein-mediated inhibition of GRP78 transcription works through the ERSE, and highlights one particular role of tyrosine kinase activity in ER stress. **Figure 1.3** shows how tunicamycin induces stress in the cell, and the possible effect of genistein on the stressed cell.

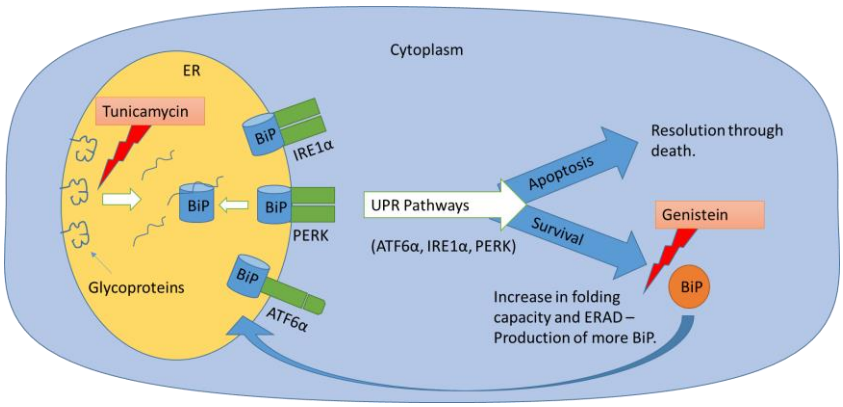

Figure 1.3: The action of tunicamycin and the possible consequence of genistein treatment on the stressed cell.
Tunicamycin blocks N-linked glycosylation and therefore causes a build up of unfolded glycoproteins which leads to the sequestration of BiP, activating the three possible UPR pathways (IRE1α, PERK, and ATF6α). Genistein is known to inhibit the production of more BiP, which could possibly push the cell to an apoptotic fate due to an inability to adapt to the stress.

Previous research in the laboratory has suggested that genistein can modulate ER stress (Lemin, 2007). In the fibrosarcoma HT1080 human cell line, insufficient tunicamycin induced ER stress could be overcome by genistein, allowing the reactivation of stress signalling pathways and resolution of the cellular stress. In contrast, the cervical cancer HeLa cell line exhibited a robust response to tunicamycin and there was less of an obvious effect of genistein. The different outcome of tunicamycin-induced stress responses in the two cell types could be in part explained by genetic differences in the cells. If irremediable stress can be resolved by the addition of genistein, then there are certainly therapeutic implications in addition to the already known effect of genistein on cancer. For example, in the chronic inflammatory disease AS, there is clear evidence of UPR activation, and while this is not the complete picture, genistein could prove to be useful as a therapeutic agent if used in conjunction with other drugs targeting other aspects of the disease.

1.10 Hypotheses and aims

Through these investigations, the aim is to investigate the differential cell specific responses between HeLa and HT1080 cells to tunicamycin induced ER stress, and whether genistein could modulate this to any extent. These differences will be measured through investigating changes in expression of ER stress related proteins through western blotting, and through changes in cellular phenotype and cell motility via the use of live cell imaging.

It is hypothesised that there will be specific differences in how both cell lines respond to tunicamycin induced stress, with protein expression levels changing in different ways for each cell line, as well as possible variances in how cell motility is affected. It is hypothesised also that genistein will rescue the effect of tunicamycin induced cell stress, though it is unknown whether this will occur in both cell lines.

Chapter 2: Methods

2.1 Cell Culture

Three cell lines were used throughout this study: human neonatal dermal fibroblasts (HDFs) isolated from neonate foreskin, cervical cancer HeLa cells and fibrosarcoma HT1080 cells. The HT1080 and HDF cell lines were grown in Dulbeco's Modified Eagle Medium (DMEM, GibCo, Thermofisher Scientific) and the HeLa cell line was grown in Minimum Essential Medium (MEM, GibCo, Thermofisher Scientific). Both types of medium were supplemented with 100 units ml^{-1} of penicilin, 100 µg ml^{-1} of streptomycin, 2 mM glutamax (all GibCo, Thermofisher Scientific), and 8% foetal bovine serum (Sigma). To keep the cells alive, they were passaged twice a week on Mondays and Fridays, providing that they had reached 90% confluence. Confluency was assessed by observing how many cells were adherent to the surface of the flasks. To passage the cells, they were first washed in phosphate buffered saline (PBS) (Sigma) twice before adding 0.05% trypsin (GibCo Thermofisher Scientific) to the surface of the culture flasks. The cells were left to trypsinise for 2 – 5 minutes (the sensitivity of the cells varied), and once the cells had detached from the surface of the flask (ascertained by light microscopy), they were re-suspended in fresh medium, warmed to 37^{o}C. The medium containing the cells was added to fresh media in new flasks at the dilutions of 1:2 for HDFs, 1:10 for HeLa cells, and 1:10 for HT1080s. All cell lines were culture in T75 flasks (Techno plastic products).

2.2 Chemical Treatment of Cell Lines

Cells were subjected to chemical treatments to induce or modify an ER stress response. For western blotting experiments, the cells were treated using different drugs for different time frames and for the spinning disc experiemnts all treatments were for 6 hours. The treatments were either the addition of dithiothreitol (DTT) at 5 mM or tunicamycin at 1 µg ml^{-1}. These treatments were applied both on their own and also in conjunction with genistein at 140 µM. For serum starving experiments, serum free MEM and DMEM was applied to the cells in the place of serum containing media for the duration of the chemical treatments. After washing the cells twice in PBS, medium containing the chemicals was added to fresh medium in 6 cm plates for lysis or 35mm µ-Dishes (Ibidi) for the spinning disc experiments.

2.3 UV treatment of cell lines

To induce UV related stress, both HeLa and HT1080 cells were exposed to UV-C, 40 J/m^2 UV over 5 seconds, using an 8 watt bulb.

2.4 Cell lysis

Two different lysis buffers were used to lyse the cells, MNT lysis buffer and RIPA lysis buffer. MNT buffer is a general lysis buffer for protein extraction, however RIPA buffer is versatile as it enables extraction of cytoplasmic, membrane and nuclear proteins; the latter of which MNT lysis buffer cannot retrieve. MNT lysis buffer was composed of 20 mM MES, 30 mM Tris-HCl, 100 mM NaCl, 1% (v/v) Triton x100; supplemented with 1 µg/ml of the protease inhibitors: cystatin, leupeptin, antipain and pepstatin A (Sigma Aldrich) and 20 mM NEM to inhibit disulphide bonds reforming. RIPA buffer was composed of 1% (v/v) Triton x100, 50 mM Tris-HCl pH 8, 150 mM NaCl, 0.5 % Na-deoxycholate, 0.1% SDS, supplemented with 1 µg/ml of the protease inhibitors: cystatin, leupeptin, antipain and pepstatin A (Sigma Aldrich) and 1% Phostop (Roche) which contains a cocktail of phosphatase inhibitors. Prior to lysis, the cells were washed twice with PBS before being placed on a tray of ice. To start with, two hundred µl of lysis buffer was applied and the cells in the dishes scraped to encourage lysis. The sample lysates were then centrifuged for 10 minutes at 4 ^{o}C and 16,100 g to separate the nuclear pellet from the rest of the lysate. The supernatant was then be removed and flash frozen to be used later on for SDS-PAGE and Western Blotting.

2.5 BCA Assay

The BCA assay (Thermofisher Scientific) was used to quantify protein concentration in cell lysates. A colour change from green to purple is seen in the assay, which works through the highly selective sensitive colorimetric capability of the cuprous cation (Cu^{+1}). This uses the bicinchoninic acid (BCA) contained in the working reagent, in combination with the biuret reaction; the reduction of Cu^{+2} to Cu^{+1} by protein when in an alkaline medium. The colour change to purple is seen because two BCA molecules are chelated with a cuprous ion. This colour change shows a linear

relationship with protein concentration and was therefore a suitable method to use ("Pierce BCA Protein Assay Kit - Thermo Fisher Scientific,").

For a typical protein determination assay, nine BSA protein standards of increasing concentrations (0, 25, 125, 250, 500, 750, 1000, 1500, 2000 µg/ml of BSA) were prepared. The working reagent consists of working reagent A and B and these were mixed using 50 parts of reagent A and 1 part of reagent B (50:1). The standards were made with different dilutions of the same lysis buffer that was used to lyse the cells, along with a 2 mg ml^{-1} albumin standard. Once made, 50µl of the standards and samples were placed into appropriately labelled Eppendorf tubes along with 1 ml of the mixed working reagent. These were then incubated for 30 minutes at 37°C and afterwards removed and cooled to room temperature. Once cooled, a spectrophotometer set to the BCA setting (562 nm) was used to measure the absorbance, starting by blanking the machine to the standard I (which contains no protein) and reading the rest of the standards first before measuring the samples. Then using graphical software, a standard curve was plotted and the protein concentration of the samples was measured.

2.6 Sample preparation

To prepare the samples for gel electrophoresis, frozen lysates were thawed slowly on ice to reduce protein degradation, and fresh lysates on ice were used straight away. For each lysate, the protein concentration was used to calculate the volume of lysate needed in each sample to achieve a uniform final protein concentration. This was calculated for every sample using the standard curves obtained from the BCA assays. Gel electrophoresis samples were then prepared using 2× Laemmli sample buffer (4% (w/v) SDS, 20% glycerol, 120 mM Tris-Cl, 0.02% (w/v) bromophenol blue (BioRad)) and 50 mM DTT (to reduce disulphide bonds) and the lysate plus lysis buffer if required to equalise protein concentrations. Samples were boiled for 5 minutes at 95°C in a heating block, then centrifuged for 5 minutes at 16,100 g. The samples were either loaded onto SDS-PAGE gels, or were flash frozen for subsequent analysis.

2.7 SDS-PAGE

To analyse proteins by Western blotting or Coomassie staining, the proteins in the samples were separated out by SDS-PAGE, which allows separation of the proteins according to size. This is achieved by running a voltage through a gel, causing negatively charged proteins to migrate away from the negative electrode (cathode) and towards the positive electrode (anode). The proteins are separated out by size due to smaller proteins being able to migrate more easily though the pores in the gel. The proteins become negatively charged through the addition of sodium dodecyl sulphate (SDS) into the gel mixture, which disrupts covalent bonds in the proteins and denatures them.

A Hoefer mighty small dual gel caster was set up with glass and ceramic plates to cast 10% SDS-PAGE gels. **Table 1** shows the quantities of each chemical needed for 10% resolving gels, with a quantity enough to cast 2 gels.

Table 2.1: Volumes of solutions used to cast 10% SDS-PAGE gels.

	10% resolving gel	stacking gel
H2O	4.8 ml	2.2 ml
40 % Acrylamide	2.5 ml	0.4 ml
1.5 M Tris (pH 8.8)	2.5 ml	0.4 ml
10% SDS	0.1 ml	0.03 ml
10% APS	0.1 ml	0.023 ml
TEMED	0.004 ml	0.002 ml

Once set, the gels were taken out of the casting kit and moved to the electrophoresis apparatus (Hoefer mighty small basic unit 8 × 7 cm). Pre-chilled running buffer (25 mM Tris, 192 mM Glycine, 0.1 % (w/v) SDS; BioRad) was then poured into the central chamber of the apparatus and into the bottom reservoir, ensuring that there was buffer in the wells of the gel. After taking the comb out, 6 µl of molecular weight marker (Precision Plus Protein™ Dual Color Standards, BioRad) containing a mixture of 10 recombinant proteins (10 – 250 kDa)) was loaded alongside the samples. For the 10-well comb gels, 20µl of sample was loaded and for the 15-well comb gels, 10µl of sample was used.

Once loaded, the gel was run at 40 mA for ~1 hour, until the dye front reached the bottom of the gel. The gels were then removed from the plates for use in either Western Blotting or Coomassie staining.

2.8 Coomassie Staining.

Coomassie brilliant blue staining was used to visualise the proteins after SDS-PAGE. The coomassie dye binds to the proteins, which stabilises the anionic (negatively charged) form of the dye which results in the production of a blue colour (Chial et al., 1993). For the coomassie staining process, the gels were placed in a tray containing fixating solution (7% acetic acid and 40% methanol, made to 50 ml with dH_20) and rocked for 10 minutes in a fume hood. After this, the gels were transferred to a tray containing the coomassie stain (80% brilliant blue G colloidal (Sigma) made to 50 ml with dH_2O) and left on a rocker to stain overnight. Because the coomassie stains the polyacrylamide gel as well as the proteins, destaining was required. This was done by leaving the stained gels in destain solution (10% acetic acid, 25% methanol, made to 50ml with dH_2O) for 10 minutes and then leaving the gel overnight in a secondary destain (25% methanol made to 50ml with dH_2O). Once destained, the gel could be removed and scanned onto a computer using a CANON LiDE 120 scanner.

2.9 Western Blotting

Western blotting was used to transfer the proteins from an SDS-PAGE gel to a PVDF (polyvinylidine difluoride) membrane, which was then probed for the expression of proteins of interest. The transfer step of the western blotting works through electroblotting, which uses an electrical current to pull the proteins in the gel onto the PVDF membrane. After transfer, non-specific membrane binding was blocked by incubating the membranes in a 5% milk solution. Then the proteins on the membrane were probed with a primary antibody, specific for a target protein or group of proteins. To visualise the protein expression, a secondary antibody conjugated to horseradish peroxidase (HRP) was applied to the membrane, and this binds to a species-specific region on the primary antibodies attached to the protein of interest.

The horseradish peroxidase catalyses a chemiluminescent ECL reaction, which luminesces in proportion to the antigenic protein concentration. A strip of photographic film was laid over the membranes once they had been incubated with the ECL solution and the exposure was made for different times according to protein expression levels. **Figure 1** highlights the key features and principals behind SDS-PAGE and western blotting.

For every gel, 4 pieces of filter paper and 1 piece of PVDF membrane (pore size 0.45 µm (Millipore)) were cut to the same size as the gel. Ten minutes before transfer, the PVDF membrane was primed in methanol for 30 seconds, and then placed in a tray containing pre-chilled transfer buffer (25 mM Tris-base, 190mM glycine, 20% methanol, made to 1 litre with dH_2O), where it was soaked for 10 minutes. When ready for transfer, a transfer cassette was prepared with two sponges (one on each side), four pieces of filter paper (two on each side) and the PVDF membrane (towards the anode). The membranes were soaked in transfer buffer before placing the washed gel on top of the PVDF membrane. The cassette was closed and loaded into the transfer kit (Mini Trans-Blot®; BioRad) which was filled with transfer buffer and kept cold with an ice pack. The transfer was carried out for 2 hours at 150 mA or overnight at 30 V and 4^{o} C.

After transfer, the PVDF membrane was removed from the transfer apparatus and blocked by incubating it in 5% dry, nonfat milk in 1×TBS-T (0.1% v/v) Tween, 150 mM NaCl, 2.68 mM KCl, 10 mM Tris base) for one hour. Depending on the antibody, the membrane was washed in TBS-T three times before incubating in the primary antibody. The primary antibody was diluted to the required amount (see **Table 2.2**) in either 1 ml of 5% milk and 2 ml of TBS-T, or 5% BSA in 1× TBS with 0.1% Tween. After the first incubation, the primary antibody mix was removed and the membranes washed 5 times in TBS-T, allowing 5 minutes on a roller for each wash. The secondary antibody dilution was then prepared, using GAMPO (goat anti-mouse peroxidase; DAKO) if a murine monoclonal primary antibody was used, or SARPO (swine anti-rabbit peroxidase; DAKO) if a polyclonal rabbit primary was used. The secondary antibodies were both diluted to 1:3000 in 1 ml of 5% milk and 2 ml of TBS-T, and the membranes incubated for another hour. Once this incubation step was

complete, the membranes were washed 5 times in 5 ml of TBS-T for 5 minutes each, then they were removed from the tubes and placed in a tray of TBS for 10 seconds before being dabbed on tissue paper and placed onto saran wrap. An ECL solution was made by mixing 250 µl of detection reagent 1 and 250 µl of detection reagent 2 (Amersham ECL Prime Western Blotting Detection Agent) to make 500 µl of ECL per membrane, which was spread over the membrane by folding over the saran wrap and smoothing the mix out over the membrane. The membranes were then removed, the excess ECL dabbed off and the membranes placed on fresh saran wrap. A phosphorescent sticker was attached to the corner to allow alignment of the blot after development. The wrap was then cut to the size of the membrane, placed in a cassette and exposed to photographic film (Kodak) in a darkroom. Common exposure times were 30 seconds, 2 minutes and 5 minutes, though this varied according to the antibody and experiment. The photographic film was then processed using an X-OMAT developing machine.

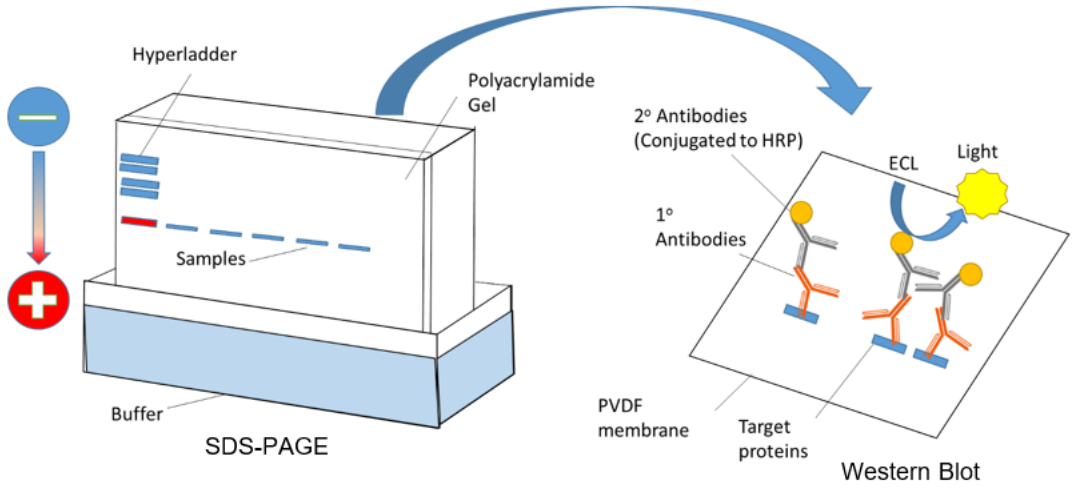

Figure 2.1: Simplified diagram showing the process of SDS-PAGE (left) and Western blotting (right). The samples are run through a gel alongside a molecular weight marker, and they migrate towards the positive anode. Once the proteins are separated they are transferred to a PVDF membrane (step not shown), which is probed for a target protein using primary and secondary antibodies.

2.10 Antibodies

Multiple primary antibodies were used for protein detection in the western blots. **Table 2.2** shows detailed information about the antibodies used.

2.11 Live Cell Imaging Microscopy

To study cell morphology and the response to ER stress, cellular behaviour was monitored using live cell imaging. Time lapse movies of HT1080 or HeLa cells were taken over an extended period of time to investigate cellular behaviour e.g. motility and ER morphology. Cells were grown on 35 mm µ-dishes with glass bottoms (Ibidi) and were washed twice with PBS, before applying the lipid staining ER-Tracker Blue-White DPX (Thermofisher) dye at a 1:800 dilution in fresh DMEM or MEM medium. The cells were incubated with the dye for 1 hour. The dye is specific for the endoplasmic reticulum.

Table 2.2: Table showing all the antibodies used in this thesis.
The manufacter, the dilution of primary and secondary antibody, used, the incubation time, and the medium required for incubation are also shown.

Antibody	Manufacturer	Dilution	Secondary	Incubation time	Incubation medium
STAT 3	Cell Signalling Technology	1:2000	GAMPO	Overnight	5% BSA in 1× TBS with 0.1% Tween
Phospho STAT 3	Cell Signalling Technology	1:2000	SARPO	Overnight	5% BSA in 1× TBS with 0.1% Tween
ASK 1	Cell Signalling Technology	1:1000	SARPO	Overnight	5% BSA in 1× TBS with 0.1% Tween
Phospho ASK 1	Cell Signalling Technology	1:1000	SARPO	Overnight	5% BSA in 1× TBS with 0.1% Tween
Phospho JNK	Cell Signalling Technology	1:1000	SARPO	Overnight	5% BSA in 1× TBS with 0.1% Tween
P-Tyrosine	Cell Signalling Technology	1:2000	GAMPO	Overnight	5% BSA in 1× TBS with 0.1% Tween
PDGFR (MAPK) - PathScan	Cell Signalling Technology	1:2000	SARPO	Overnight	5% BSA in 1× TBS with 0.1% Tween
PYCOX	Abcam	1:10000	SARPO	Overnight	5% BSA in 1× TBS with 0.1% Tween
HC10	(Stam et al., 1986)*	1:200	GAMPO	1 Hour	5% milk in 1× TBS with 0.1% Tween
W632	(Barnstable et al., 1978)*	1:200	GAMPO	1 Hour	5% milk in 1× TBS with 0.1% Tween
1B5	*	1:1000	GAMPO	1 Hour	5% milk in 1× TBS with 0.1% Tween
BiP	Santa Cruz Biotechnology	1:500	GAMPO	1 Hour	5% milk in 1× TBS with 0.1% Tween
GRP94	Cell Signalling Technology	1:1000	SARPO	Overnight	5% milk in 1× TBS with 0.1% Tween
B-Actin	Abcam	1:10000	GAMPO	1 Hour	5% milk in 1× TBS with 0.1% Tween
PDI	(Benham et al., 2000)	1:1000	SARPO	1 Hour	5% milk in 1× TBS with 0.1% Tween

* A gift from Prof. J. Neefjes, Netherlands Cancer Institute, The Netherlands

After a 1 hr incubation, the cells were again washed twice with PBS before treating them with ER stressors as described in **section 2.2.** The CO_2 levels of the incubation chamber were set to 5% at 3 litres per hour and the temperature was set at 37.4^{o}C. An Andor Revolution XD spinning disc confocal microscope was used to image the cells. The microscope was set to an exposure of 60 ms, a laser exposure intensity of 25, and an EM gain of 300.

The absorbance and emission spectra of ER-Tracker Blue-White DPX can be seen in **Figure 2** and the 405 nm laser was selected to visualise the dye with the microscope. The imaging was carried out for 6 hours, with a photograph of the cells being taken every minute, resulting in a time-lapse movie composed of 360 frames.

2.12 Data Analysis

To track the movement of the cells, the ImageJ plugin MTrack2 was used which allowed tracking of individual cells by moving through each frame of the time-lapse movie and creating a path for each cell by clicking on its location for each frame. Every visible cell was tracked, and once the scale had been set, it was possible to view the Len values (length in μm) for each cell's pathway.

These values were then inputted into Graphpad's Prism software, where the 1-way ANOVA T-test was used to determine if there were any significant differences between the conditions, and Tukey's test was used to individually compare each condition to all other conditions and determine which treatments had significant differences with others.

The parametric one-way ANOVA T-test was used due to its ability to compare significance between multiple groups at once. The one-way ANOVA T-test assumes that the data is normally distributed, and to test for this, the D'Agostino and Pearson normality test was used on the data. This test demonstrated that the data was normally distributed and therefore the one-way ANOVA T-test was applicable.

Chapter 3: Results

3.1 Investigation into the change of downstream protein expression between HeLa and HT1080 cells after induced ER stress.

3.1.1 Initial investigation into the action of tunicamycin and DTT on the expression of UPR associated chaperones and MHC class I glycosylation.

The preliminary experiments were designed to investigate the effect of DTT and tunicamycin on the stress response of HT1080 and HeLa cells (**Figure 3.1.1)**. The cells were treated with medium supplemented with either DTT for 30 minutes or tunicamycin for 6 hours, based on previous research in the laboratory. It has been shown that induction of XBP1 processing by DTT was effective in both cell lines after 30 minutes of 5 mM DTT treatment; however, the induction of XBP1 processing by 1 µg/ml tunicamycin was efficient in HeLa cells but not HT1080 cells, indicating that the two cell types differ in their response to dysregulation of N-linked glycosylation (Lemin et al FEBS Lett and unpublished). Cell lysates were analysed by SDS-PAGE followed by immunoblotting to ascertain the expression of MHC class I molecules, and two heat shock proteins, GRP78/BiP and GRP94 (Hsp90). β-actin expression was used as a control to demonstrate the equal loading of protein across the samples. Antibodies raised against GRP94 and BiP/GRP78 were used to investigate chaperone expression in the cells. BiP and GRP94 are ER resident chaperones, and both are heavily linked to ER stress, with roles in assisting ERAD and interacting with ER folding proteins (Eletto et al., 2010).

GRP94 could be detected in both cell lines, whereas the detection of BiP was variable, and reproducible results with the santa-cruz anti-BiP antibody (catalogue number sc-13539) could not be achieved. The GRP94 expression was slightly raised in DTT and Tun treated HT1080 cells, but this was not significant when compared to the actin control (**Figure 3.1.1**, compare lanes 1 and 3). It is also possible that the expression of GRP94 even went down slightly in the HeLa cells with the DTT and tunicamycin treatments, however the small fluctuations were not reproducible in subsequent experiments. MHC class I expression was detected with the HC10 antibody, raised against HLA-B heavy chains (Stam et al., 1986). MHC class I was detected in both cell

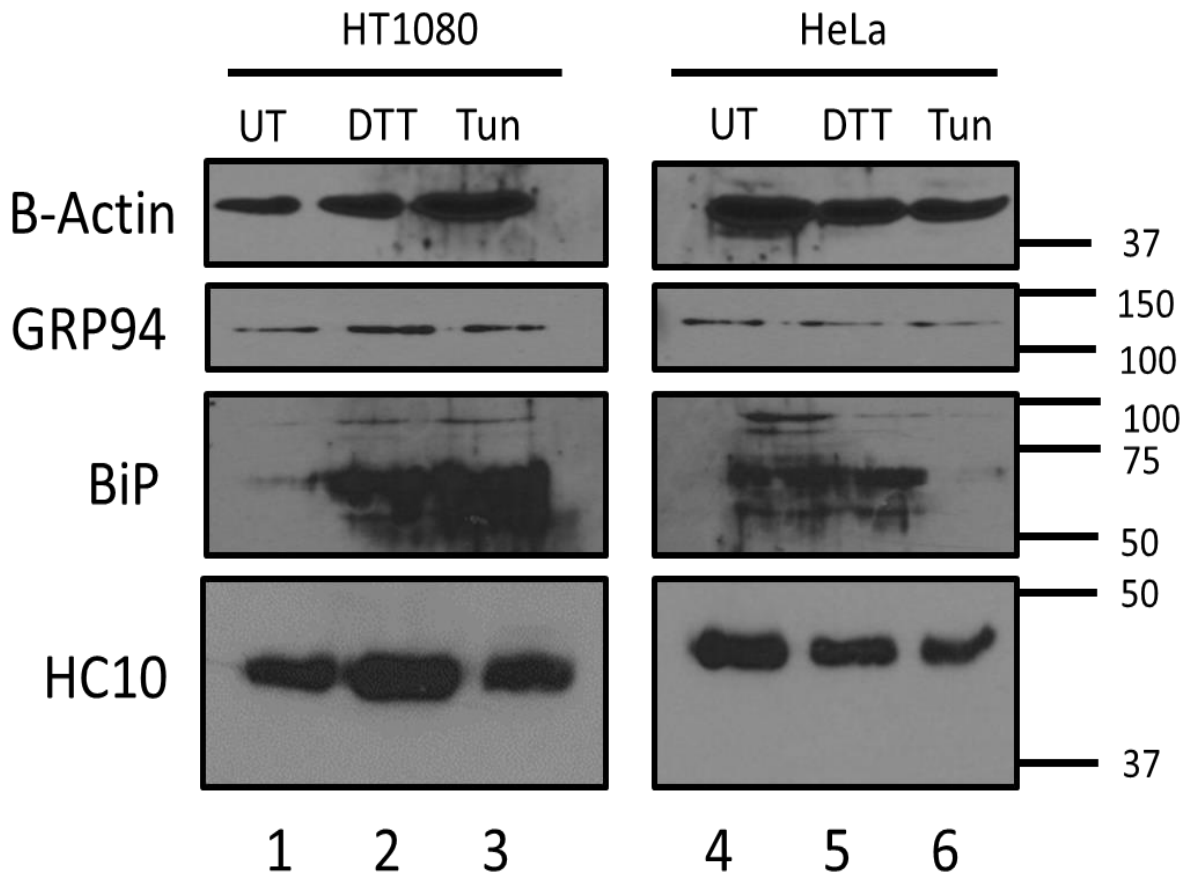

Figure 3.1.1: The effect of Tunicamycin and DTT on GRP94, BiP and MHC class I glycosylation.

Western blot of HT1080 and HeLa cell lysates from cells treated with either DTT (lanes 2 and 5) or tunicamycin (lanes 3 and 6) or untreated (lanes 1 and 4) to detect B-Actin (first panels), GRP94 (second panels), BiP (third panels) and MHC class I heavy chains (fourth panels). UT = Untreated, Tun = 6 hours 1 µg/ml tunicamycin, DTT = 30 minutes 5 mM DTT. GRP94 is observed at a molecular weight of around 125 kDa, BiP at around 75 kDa, and HC10 at about 48 kDa.

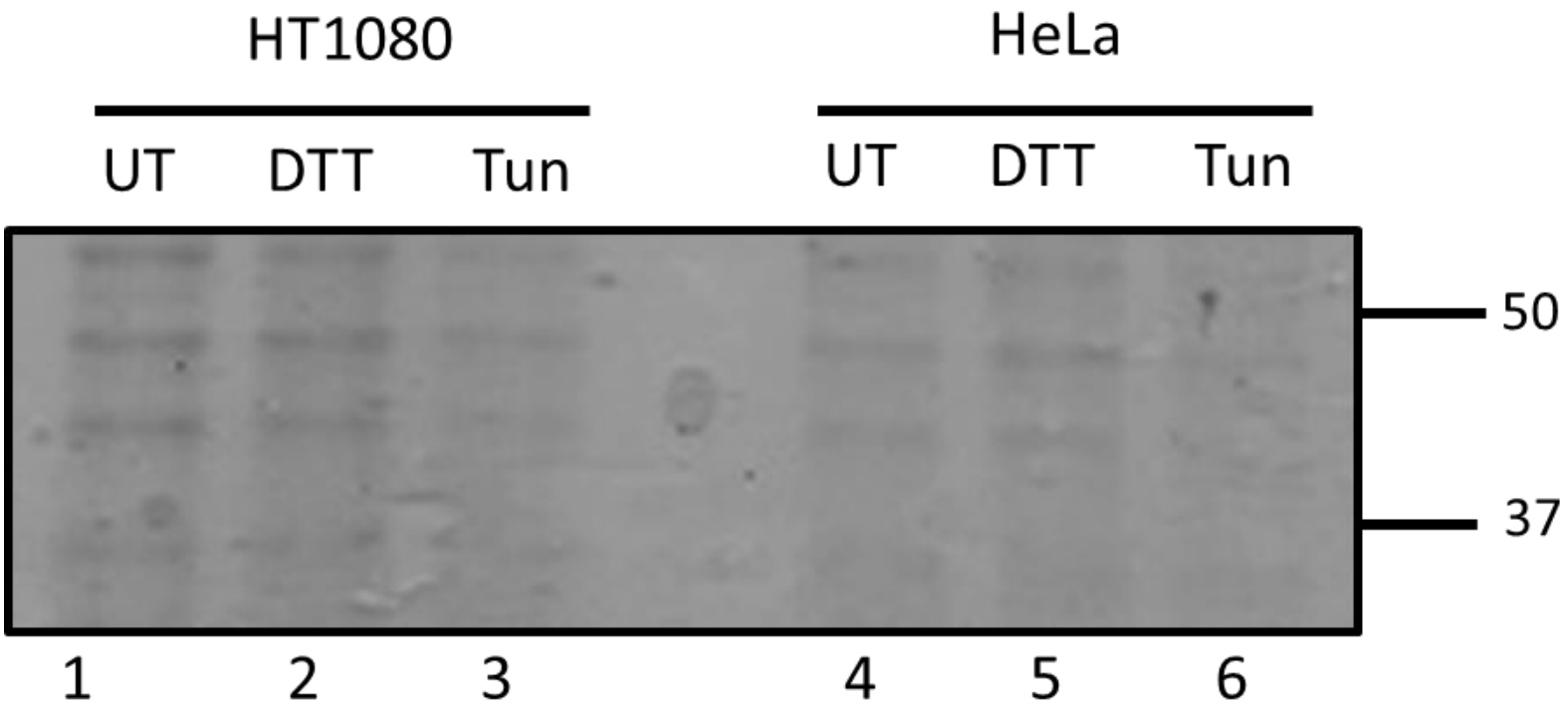

Figure 3.1.2: Initial DTT and Tunicamycin treated cell lysates are loaded in equal concentrations.
Coomassie Brilliant Blue stain of gels loaded with HT1080 and HeLa cell lysates treated with either DTT (lanes 2 and 5) or tunicamycin (lanes 3 and 6) or untreatd (lanes 1 and 4). UT = Untreated, Tun = 6 hours 1 µg/ml tunicamycin, DTT = 30 minutes 5 mM DTT.

lines as expected. It was hypothesised that the addition of tunicamycin might decrease the molecular weight of a subset of immature heavy chains, since tunicamycin inhibits the early stages of N-linked glycosylation. No decrease in molecular weight could be visualised, probably because of the heterogenous nature of the total MHC heavy chain pool. However, there was a small and reproducible decrease in the total class I pool from tunicamycin treated cells when compared with DTT treated cells (see also **Figure 3.1.3**). The samples shown in Figure 1 were also analysed by Coomassie staining (**Figure 3.1.2**). This acted as an extra control to demonstrate consistent loading. While faint, the Coomassie confirmed that the samples had been loaded equally, and that the BCA assay used to equalise protein concentration was accurate.

3.1.2 Investigation into the effect of ER stress on downstream tyrosine phosphorylation and Stat3 expression.

Previous research in the laboratory suggested that DTT and tunicamycin induce different downstream stress responses in HT1080 and HeLa cell lines. Preliminary evidence suggested that changes in tyrosine phosphorylation could be involved (Masose and Benham, unpublished results). To investigate this further, HT1080 and HeLa cells were Mock treated, treated for 30 minutes with DTT, treated for 30 minutes with tunicamycin and treated for 6 hours with tunicamycin **(Figure 3.1.3)**. In addition to these treatments, both the HT1080 and HeLa cells were UV treated (UV-C, 60 J/m^2) to induce a stress response as a positive control (Tournier et al., 2000). β-Actin was used as a loading control (**Figure 3.1.3**, first panel) and demonstrates equal loading of the samples. The expression of MHC class I heavy chains diminished somewhat after 6 hours of tunicamycin treatment, most noticeably for the HT1080 cells (consistent with **Figure 3.1.1**). The status of Stat3 was assessed, because Stat3 is a cell cycle regulator that controls autophagic responses in stressed cells, and induces pro-inflammatory cytokines (Meares et al., 2014). Blotting with an antibody raised against Stat3 revealed two bands in both HT1080 and HeLa cells: a strong band at around 86 kDa and a weaker shadow band at around 79 kDa (**Figure 3.1.3**, lanes 3 and 7). These are likely to be two isoforms of Stat3; the upper - Stat3α (86kDa) and the lower - Stat3β (79kDa).

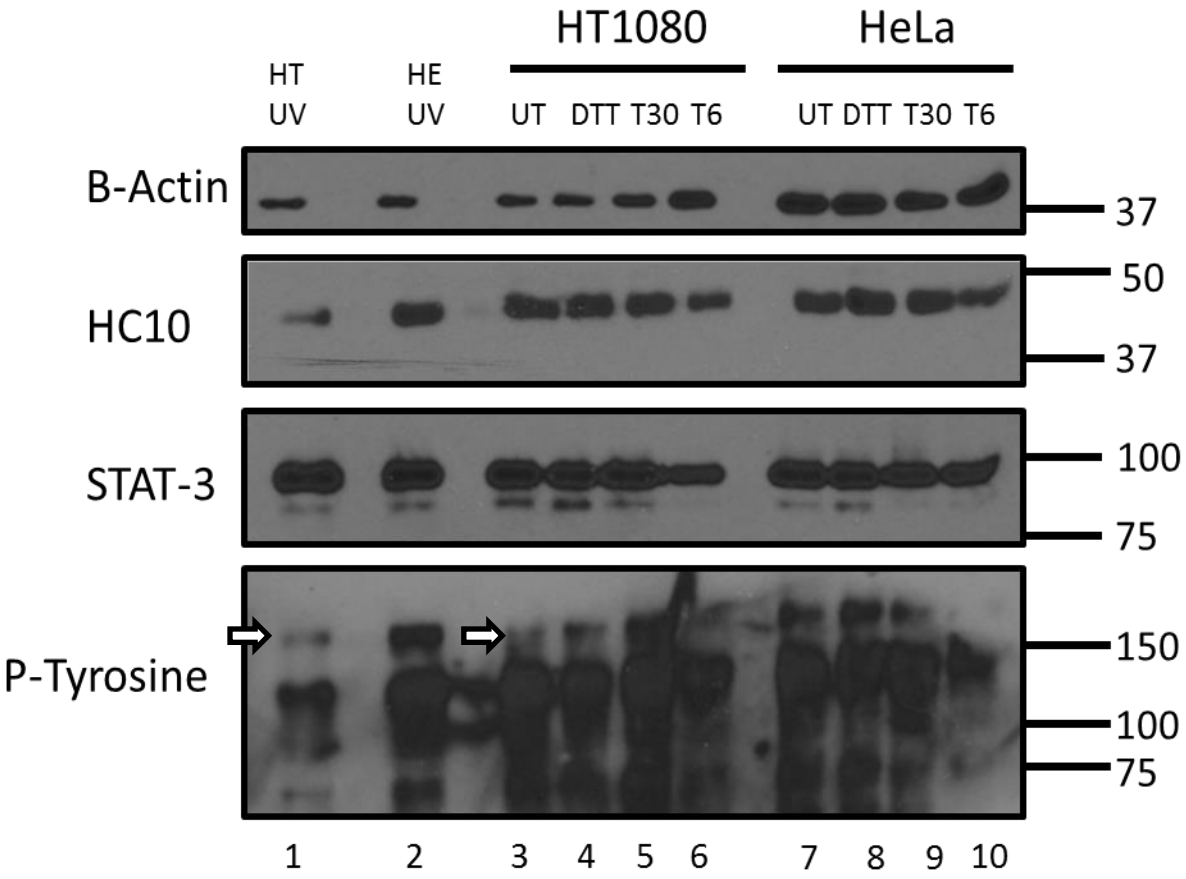

Figure 3.1.3: Stat3 expression dips in the 6 hour tunicamycin treatment for both cell lines. Western blot of HT1080 and HeLa cell lysates from cells treated with either UV light (lanes 1 and 2), DTT (lanes 4 and 8) or tunicamycin (lanes 5,6 and 9.10) to detect B-Actin (first panel), MHC class I heavy chains (second panel), Stat3 (third panel) and P-Tyrosine (fourth panel). UT = Untreated, UV = UV-C, 60 J/m^2, T30 = 30 minutes 1µg/ml tunicamycin, T6 = 6 hours 1 µg/ml tunicamycin, DTT = 5 mM DTT. HC10 is observed at a molecular weight of around 48 kDa, STAT-3 at about 96 kDa.

The difference in function between these isoforms is unknown. Both are produced from the same gene product via alternate splicing. However Stat3β has prolonged nuclear retention compared to Stat3α (Huang et al., 2007). Figure 3 suggests that the Stat3β isoform decreased after 6 hour tunicamycin treatment in the HT1080 cells and decreased after 30 minutes and 6 hours of tunicamycin treatment in the HeLa cells. In the HT1080 cells, the Stat3α isoform expression seemed to decrease after 6 hours of tunicamycin treatment. The levels of Stat3α were elevated in the UV controls indicating a differential stress response to tunicamycin compared to UV stress. It would appear that the Stat3β isoform is more susceptible to stress related suppression of expression, and this seems to be specific to tunicamycin due to the absence of any effect with DTT. Further experiments will be required to determine the functional significance of this change in expression.

Next, tyrosine phosphorylation was investigated using a pan phospho-tyrosine antibody that detects all phosphorylated tyrosine kinases. This was performed to examine if there were any changes in the level of tyrosine phosphorylated proteins between stress treatments and cell lines. The pan-Tyr100 antibody gave variable results, though when comparing the untreated HT1080 cells with the UV control, there seemed to be induction of a protein at around 200 kDa (**Figure 3.1.3 white arrow**) after UV induced stress. In the HeLa cells, there was already a higher level of expression of this protein. Due to inefficient transfer at the top right hand corner of this blot, it was not possible to conclude whether this protein was expressed after the 6 hour tunicamycin treatment in the HeLa cells. **Figure 3.1.4** shows a Coomassie gel of the lysates analysed in **Figure 3.1.3** as an additional loading control. The band that seems to increase in prominence may be due to residual BSA in the media.

3.1.3 Genistein

Previous experiments in the laboratory have suggested that the isoflavone genistein can potentiate the effect of tunicamycin-induced ER stress in HT1080 cells (Lemin, Masose, Benham, unpublished observations). To assess whether the changes in Stat3 and GRP94 expression could also be modulated by genistein, HeLa and HT1080 cells were subjected to 30 minutes mock treatment, 30 minutes 5 mM DTT, 10 minutes 1

µg/ml tunicamycin, 30 minutes 1 µg/ml tunicamycin, and 6 hours 1 µg/ml tunicamycin, all with or without 140 µM genistein (+/-). The cells were lysed after treatment and the lysates subjected to western blotting (**Figure 3.1.5**). The β-actin control shows that protein recovery and loading was equal in all lanes for these samples (**3.1.5**, first panel). The chaperone GRP94 was examined and the blot suggests that genistein may reduce the expression of this chaperone to some extent (lanes 2,8,10,14,18 and 20). In the HT1080 cells, the genistein treatment on its own (UT+) seemed to result in less GRP94 expression than the mock without genistein, and though this could be an air bubble (lane 2), that pattern is reflected in the 30 minute (lane 8: T30+) and 6 hour tunicamycin (lane 10: T6+) with genistein when compared to those treatments without genistein, albeit to a lesser extent. The HeLa cells treated for 30 minutes and 6 hours with tunicamycin also show the same pattern as the HT1080 cells, with the addition of genistein seemingly decreasing the amount of GRP94 present. This corroborates with the fact that genistein regulates the DNA binding affinity of CBF/NF-Y; a transcription factor that binds to the promoter of GRP78 as well as GRP94 (Zhou and Lee, 1998b). GRP94 production has also been shown to be dependent on the presence of the transcription factor TFII-I, which is also a possible target for the inhibitive effects of tunicamycin (Hong et al., 2005b). The inverse of this pattern seems to be the case however in the other HeLa conditions with genistein increasing GRP94 expression in the untreated (lane 12: UN+) and 10 minute tunicamycin timepoint (lane 16: T10+).

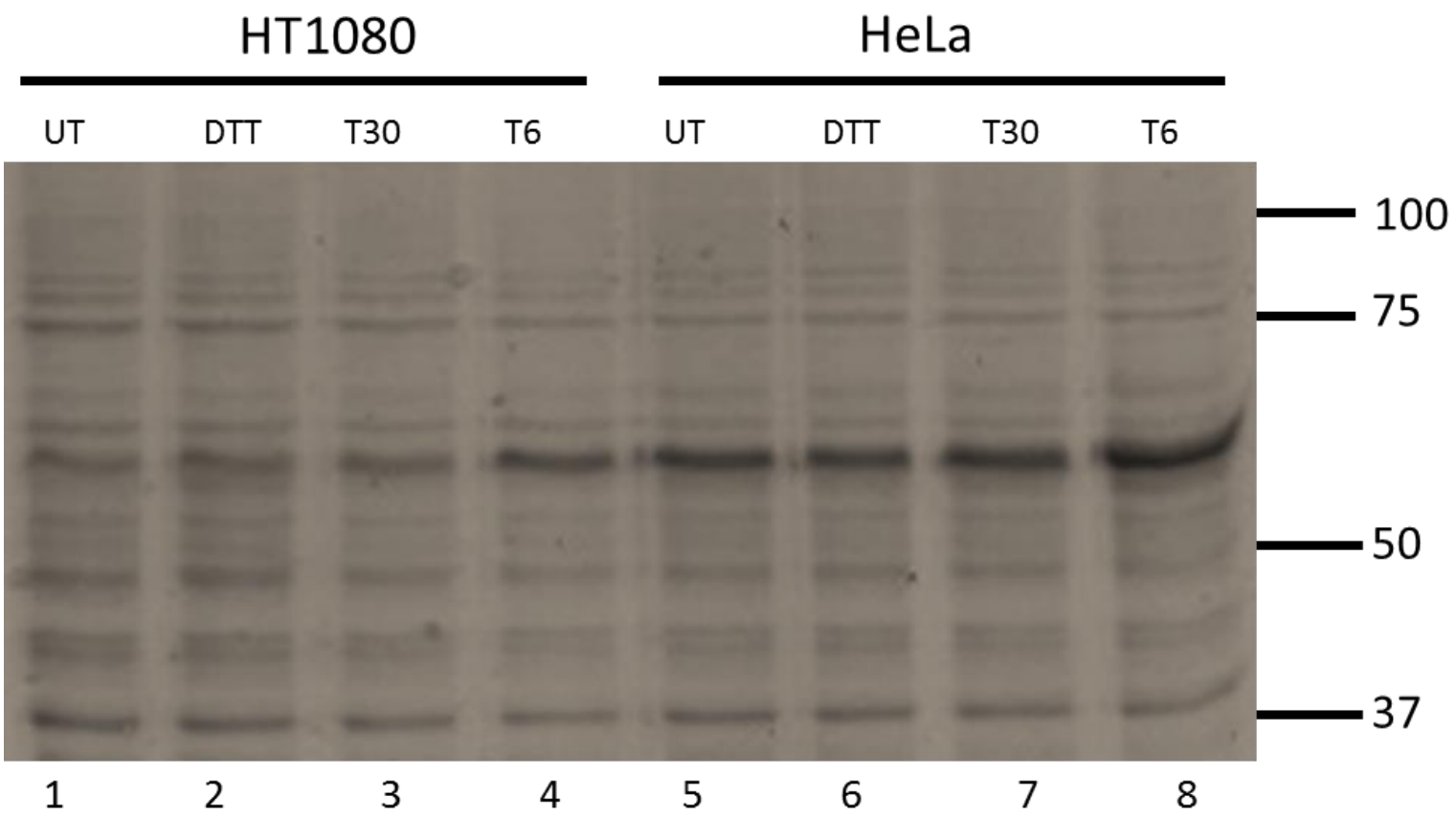

Figure 3.1.4: Coomassie stain acts as a loading control for HT1080 and HeLa cell lysates using different lengths of tunicamycin treatment. Coomassie Brilliant Blue stain of gel loaded with HT1080 and HeLa cell lysates from cells treated with either DTT (lanes 2 and 6) or tunicamycin (lanes 3,4 and 7,8) or untreated (lanes 1 and 5). UT = Untreated, T30 = 30 minutes 1 µg/ml tunicamycin, T6 = 6 hours 1 µg/ml tunicamycin, DTT = 5 mM DTT.

In the Stat3 blot, the two isoforms of Stat3 were present, and in the HeLa cells, the shadow band – Stat3β again decreased slightly in the 6 hour tunicamycin treatment (lanes 19, 20: T6+/-), however there was not an observable decrease in the 30 minute tunicamycin which contrasts with the decrease seen in the first Stat3 blot. The HT1080 cells did not seem to show any noticeable decrease; however, due to the high intensity of the bands, it is difficult to make this a certain conclusion. Interestingly, there was an additional band seen in the HeLa cells that was not seen in the first Stat3 blot. This band appears just below 150 kDa (labelled with the white arrow) and acted as a useful control in subsequent experiments, however there was not enough time to fully explore the identity of this band.

Given that tunicamycin-induced changes in glycosylation were difficult to visualise with the MHC class I antibody HC10, PCYOX was investigated as a putative indicator of immature N-linked glycosylation status, as PCYOX is lysosomal oxidoreductase with 3 N linked glycans. The PCYOX antibody (**Figure 3.1.5,** fourth panel) did not detect a major difference in the molecular weight of PCYOX when comparing untreated cell lysates with tunicamycin treated cell lysates (compare lanes 1 and 2 with 5-10 and 11 and 12 with 15-20). There may have been a small decrease in the migration of the protein upon treatment with DTT (due to reduction; compare lanes 11 and 12 with lanes 13 and 14). Pulse-chase experiments and experiments using lower percentage polyacrylamide gels would be required to explore this further. With the HeLa cells, there does seem to be an increase in migration after 6 hours of tunicamycin treatment (lanes 19,20: T6+/-). This could indicate a lower molecular weight which is possibly due to inhibition of glycosylation. A coomassie stained gel of the lysates shown in Figure **3.1.6** showed equal protein recovery and loading of proteins after the various treatments.

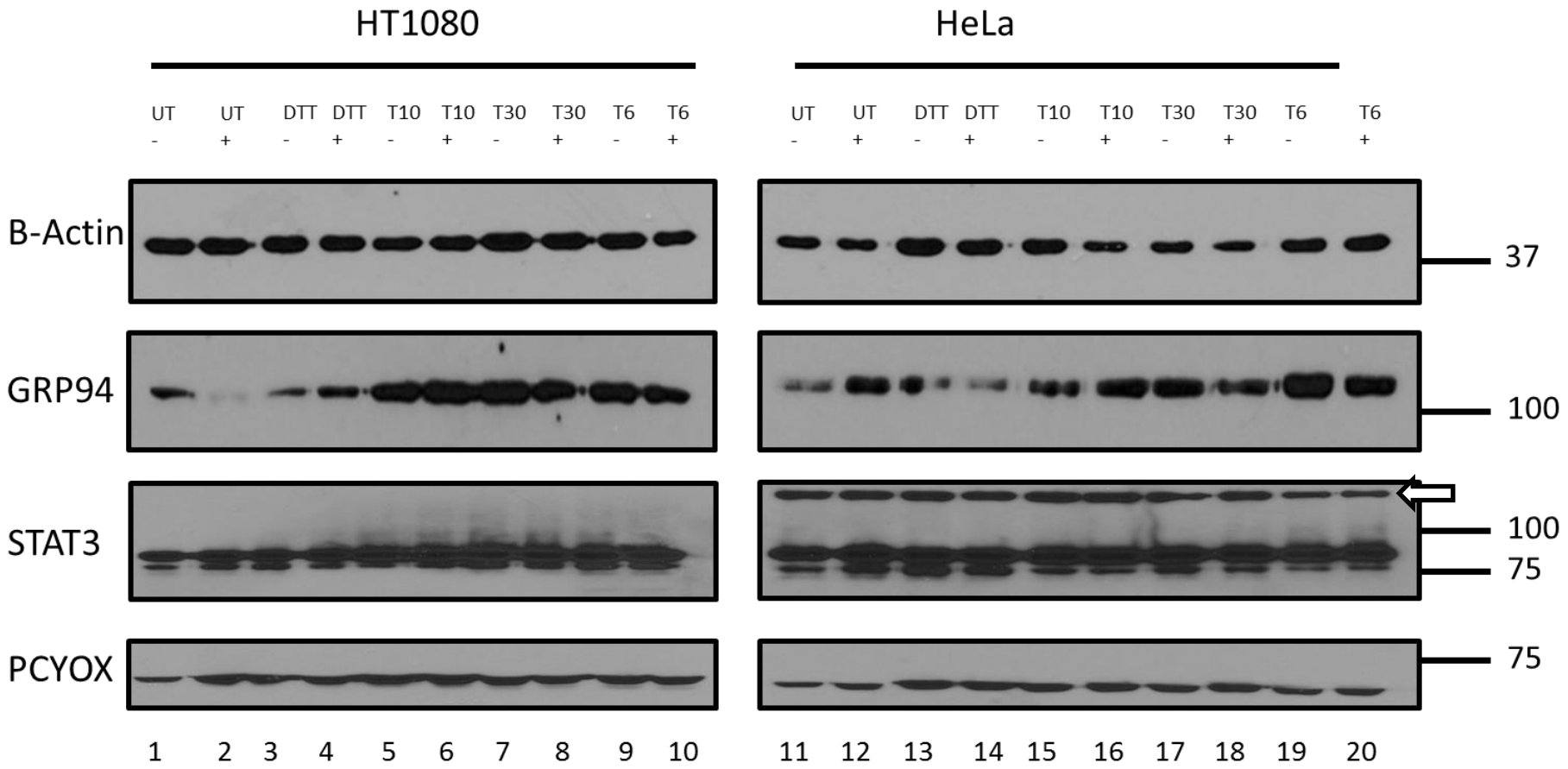

Figure 3.1.5: Tunicamycin and Genistein treated HT1080 and HeLa cells exhibit different expression profiles of GRP94 and Stat3.
Western blot of HT1080 and HeLa cell lysates from cells treated with either DTT (lanes 3,4 and 13,14), tunicamycin (lanes 5-10 and 15-20) or genistein alone or in combination with the previous treatments (lanes 2,4,6,8,10,12,14,16,18,20) to detect B-Actin (first panel), GRP94 (second panel), STAT3 (third panel) and PCYOX (fourth panel). UT = Untreated, T10 = 10 minutes 1 µg/ml tunicamycin, T30 = 30 minutes 1 µg/ml tunicamycin, T6 = 6 hours 1 µg/ml tunicamycin, DTT = 5mM DTT, - = without genistein, + = 140 µM genistein. GRP94 is observed at a molecular weight of around 125 kDa, Stat3 at around 80 kDa and PCYOX at around 70 kDa.

Having observed some changes in the appearance of STAT3 isoforms after stress treatments, the phosphorylation status of STAT 3 was examined in HT1080 and HeLa cells that had been treated with tunicamycin (**Figure 3.1.7**). Firstly, the Stat3α isoform (86 kDa) followed a similar pattern to the first Stat3 blot, with the HT1080 cells particularly showing a decrease in Stat3α expression after the 6 hour tunicamycin time point (lane 8: T6). The HeLa cells also showed a decrease in Stat3 expression after 6 hours of tunicamycin treatment (lane 7: T6) but possibly to a lesser extent. This result shows that the decrease in the expression of the Stat3α isoform in the HT1080 cells particularly, is reproducible. The Stat3β isoform also showed a reproducible decrease in expression in both cell lines after the 6 hour tunicamycin treatment (lanes 7,8: T6) but the HeLa cells did not show a noticeable decreased expression of the Stat3β isoform after the 30 minute tunicamycin timepoint (lane 5: T30) which was seen in the first Stat3 blot. The unidentified ~150 kDa band appeared in all the HeLa lysates, but not the HT1080 lysates (**Figure 3.1.7**, second panel, compare lanes 1, 3 , 5 and 7 with lanes 2, 4, 6 and 8). This result acted as a control to demonstrate correct loading. The Stat3 result again showed a decreased expression of the shadow band, this time both in the HeLa cells and HT1080 cells.

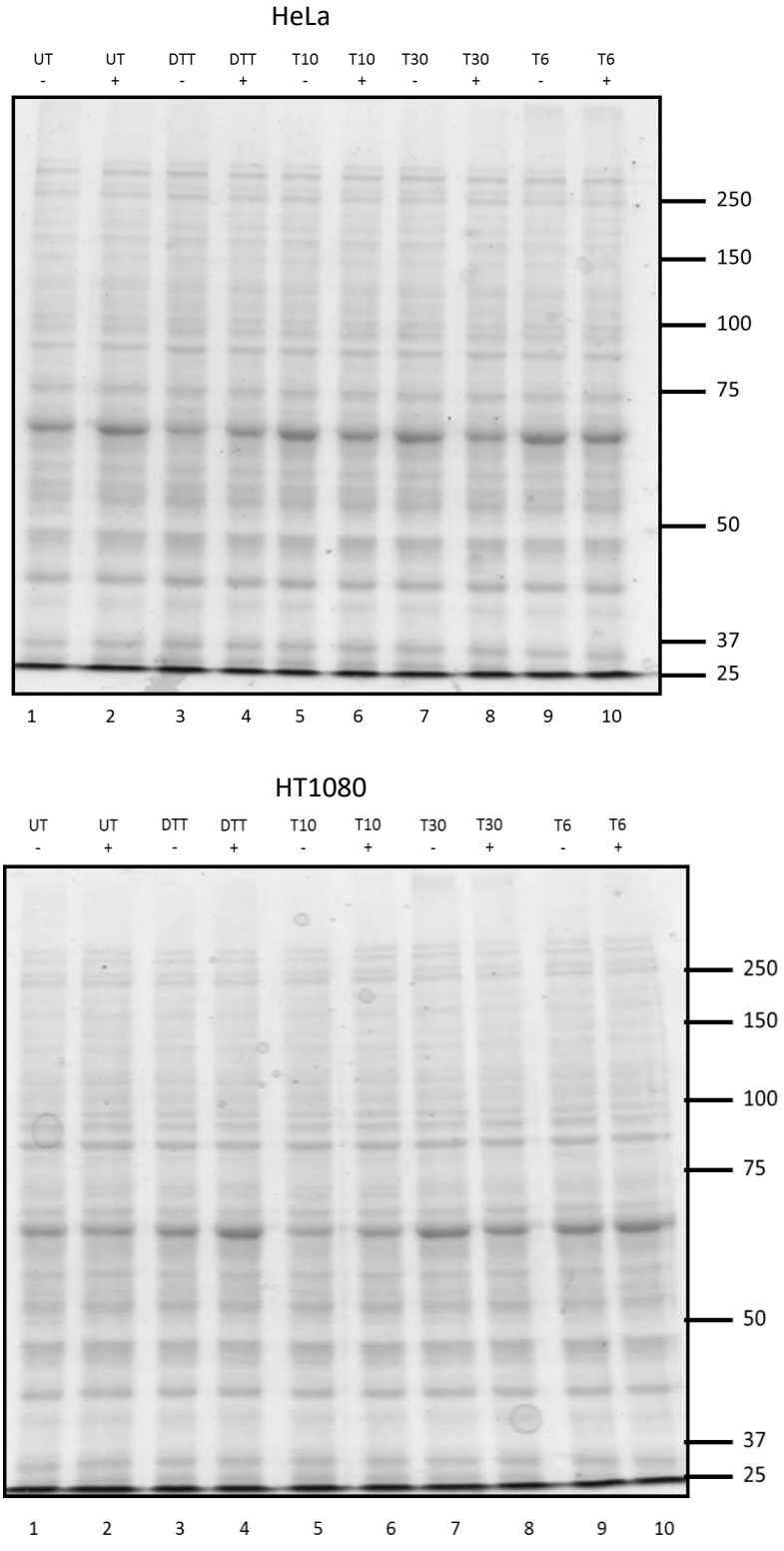

Figure 3.1.6: Coomassie gels loaded with lysates created from Genistein, DTT and Tunicamycin treated Hela and HT1080 cells.

Coomassie Brilliant Blue stain of gels loaded with HeLa (first panel) and HT1080 (second panel) cell lysates from cells treated with DTT (lanes 3,4) and tunicamycin (lanes 5-10). UT = Untreated, T10 = 10 minutes T1 µg/ml tunicamycin, 30 = 30 minutes 1 µg/ml tunicamycin, T6 = 6 hours 1 µg/ml tunicamycin, DTT = 5mM DTT, - = without genistein, + = 140 µM genistein.

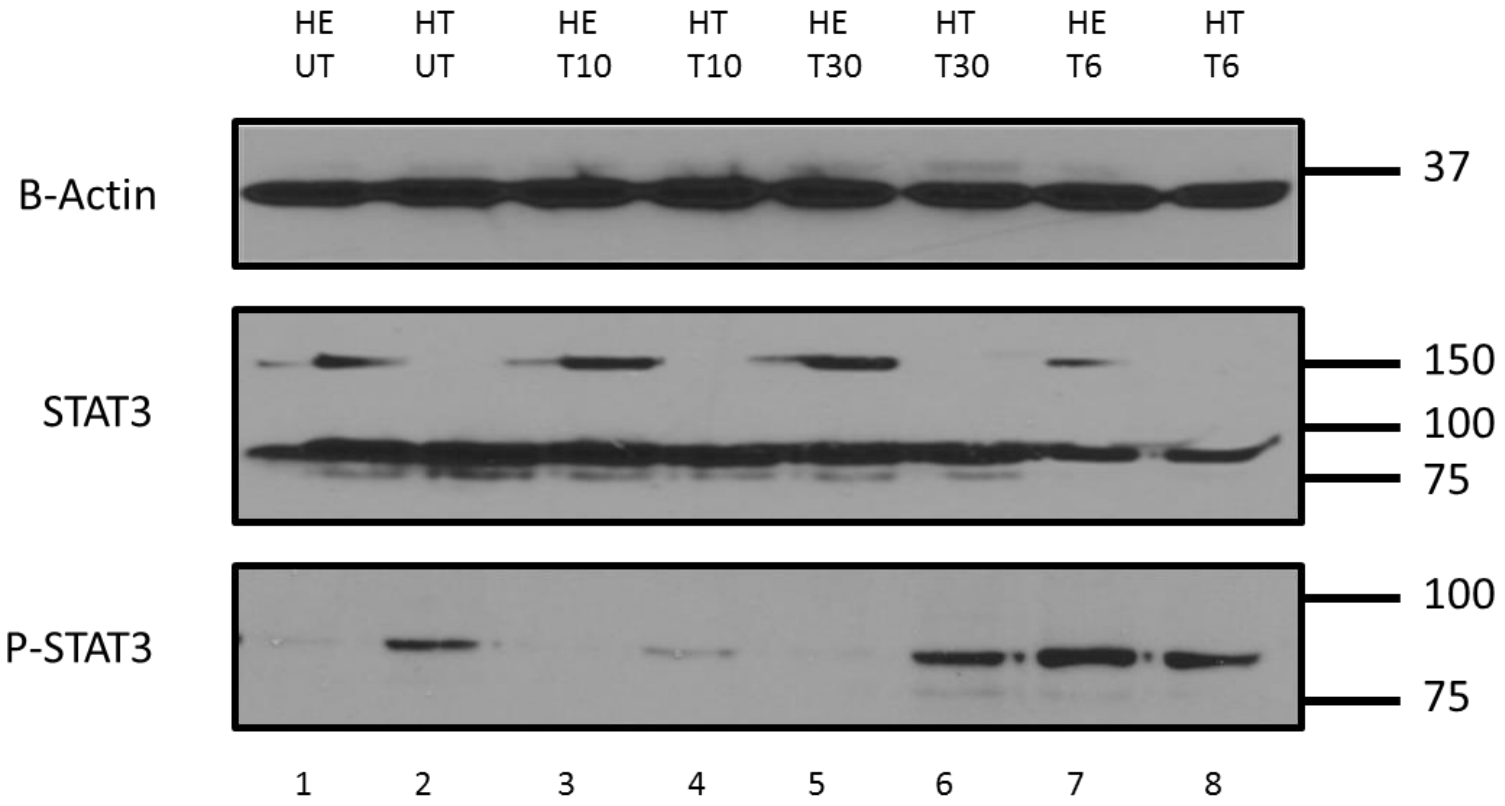

Figure 3.1.7: The expression of phosphorylated Stat3 differs between HeLa and HT1080 cells after exposure to tunicamycin.
Western blot of HT1080 and HeLa cell lysates from cells treated with tunicamycin (lanes 3-8) to detect B-Actin (first panel), Stat3 (second panel) and phosphorylated-Stat3 (third panel). UT = Untreated, T10 = 10 minutes T1 µg/ml tunicamycin, T30 = 30 minutes 1 µg/ml tunicamycin, T6 = 6 hours 1 µg/ml tunicamycin, HT = HT1080 cell lysates, HE = HeLa cell lysates. STAT3 is observed at a molecular weight of around 80 kDa, and P-STAT3 at around the same MW; 80 kDa

The P-Stat3 blot did not seem to reflect the Stat3 pattern, with an unexpected appearance of P-Stat3 expression in the HT1080 cells, showing induction of P-Stat3 in the HT1080 untreated sample and then a dip in expression in the 10 minute tunicamycin sample. Another rise of expression was seen in the 30 minute and 6 hour tunicamycin samples. This seemed to indicate that there was a baseline expression of P-Stat3 in the mock HT1080 cells that then undergoes an immediate dip and subsequent rise over time. In contrast, the HeLa cells showed a delayed induction of P-Stat3 in the 6 hour tunicamycin sample. It is possible that HT1080 cells have an elevated baseline expression of P-Stat3 and Stat3 in general compared to HeLa cells, and that tunicamycin has the immediate effect of reducing these expression levels, with a resurgence of P-Stat3 occurring later on. This indicates a potential build-up of irremediable stress after an initial UPR adaption of the cell. It appears that the UPR is already active to an extent in the HT1080 cells but it may be the case that it is in a chronic state of UPR activation, as seen by the high baseline level of P-Stat3. A previous study on the induction of P-Stat3 in astrocytes using the pharmacological stress inducer thapsigargin seemed to indicate a peak of P-Stat3 expression at around 2 hours (Meares et al., 2014). It is possible that these results reflect both acute and chronic effects of P-Stat3 induction, particularly in the HT1080 cells. The HT1080 cells contain an endogenous N-Ras mutation that may be causing constitutive P-Stat3 activation, which could account for the signal seen in the untreated HT1080 cell lysates (Gupta et al., 2000). This will be discussed further in the discussion.

3.1.4 Phosphorylated MAPK p44/42 expression is transiently increased after tunicamycin induced stress.

The same lysates were analysed by western blot using the PathScan® PDGFR activity assay **(Figure 3.1.8)**. This cocktail of antibodies detects the activation of multiple pathways including phospho-p44/42 MAPK, phospho-SHP2 and phospho-Akt. These cells were not stimulated with the addition of PDGF and therefore phosphorylation of PDGFR was not detected. The results suggest that DTT and tunicamycin treatment do not result in the non-specific induction of the PDGFR receptor. Interestingly, downstream signalling molecules were detected; with a

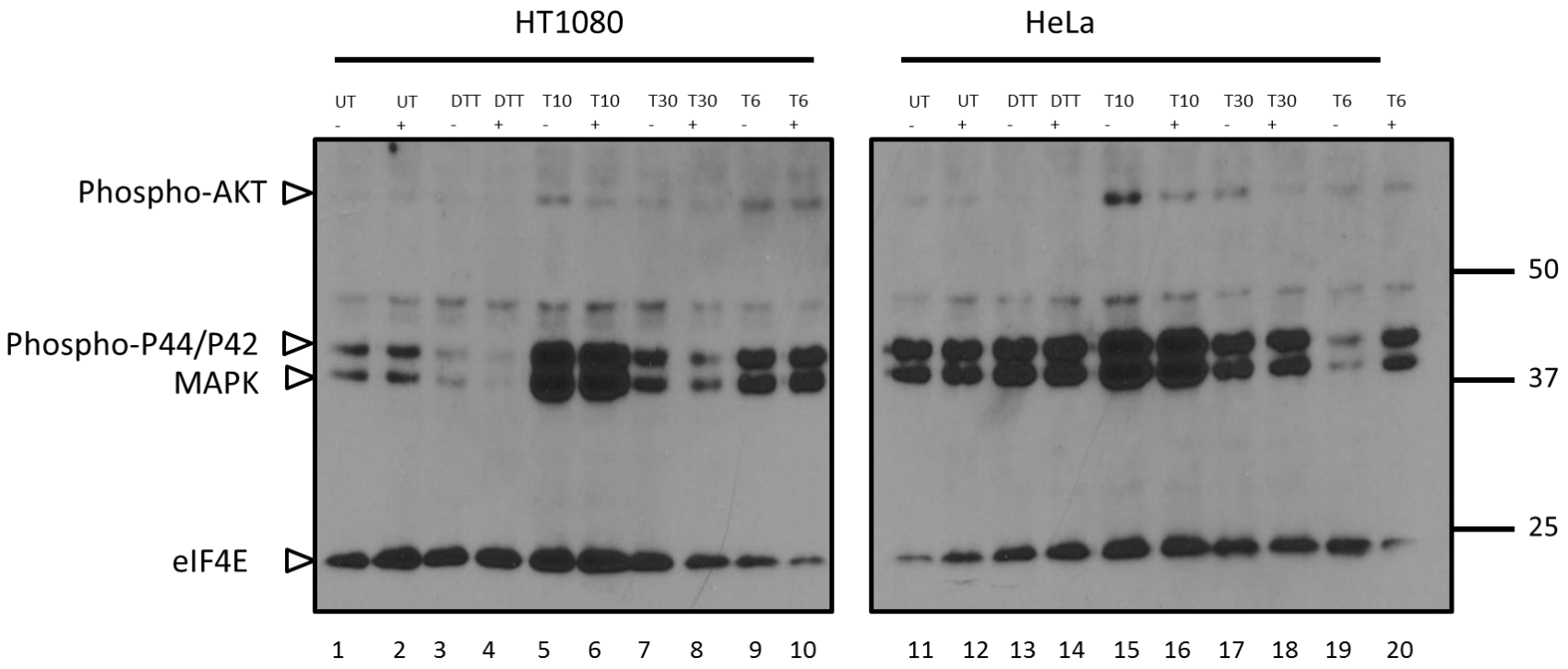

Figure 3.1.8: The expression of phosphorylated p44/42 MAPK differs between HeLa and HT1080 cells after exposure to tunicamycin and genistein, but peaks in both cell lines after 10 minutes.

PathScan® western blot of HT1080 and HeLa cell lysates from cells treated with DTT (3,4 and 13,14), tunicamycin (lanes 5-10 and 15-20) and genistein on its own or in combination with the previous treatments (2,4,6,8,10,12,14,16,18,20) to detect multiple proteins including Phospho-AKT, Phospho-p44/42 MAPK, and the loading control eIF4E. UT = Untreated, T10 = 10 minutes T1 µg/ml tunicamycin, T30 = 30 minutes 1 µg/ml tunicamycin, T6 = 6 hours 1 µg/ml tunicamycin, DTT = 5mM DTT, - = without genistein, + = 140 µM genistein.

very clear peak of phosphorylated p44/42 MAPK expression in both cell lines after 10 minutes of tunicamycin treatment (**Figure 3.1.8**, lanes 5,6 and 15,16: T10+/-). The 10 minute tunicamycin treatment was included because through other work in this laboratory, it was found that tunicamycin induced a peak of phosphorylated MAPK/p44/42 expression at 10 minutes, and therefore this time point was included to see if a short-term ER stress response was occurring. This blot indicated that there was a baseline activation of P44/P42 MAPK in the untreated samples in both cell types. Even with this baseline MAPK phosphorylation, the peak signal in the 10 minute tunicamycin treatment was very clear in both cell types. Both cell lines seemed to exhibit a dip in MAPK phosphorylation after the 10-minute peak, with the 30 minute tunicamycin treated HT1080 cell signal (lanes 17,18: T30+/-) falling to a similar level of phosphoprotein expression as the untreated cells (lanes 11,12: UT+/-). Another smaller rise in MAPK and P44/P42 activation was observed in the 6 hour tunicamycin treated HT1080 cells. The Hela cells, on the other hand, had a smaller reduction in phosphorylated p44/42 expression in the 30 minute tunicamycin lysates (lanes 17,18: T30+/-), with the expression at 6 hours of tunicamycin treatment (lanes 19,20: T6+/-) less than the level of expression observed in the untreated lanes (lanes 11,12: UT+/-).

The HT1080 and HeLa cells exhibited slightly different patterns in phosphorylated p44/42 expression within the tunicamycin treatments **(Figure 3.1.8)**, and with the 30 minute DTT treated samples there seemed to be a difference too, with the HT1080 cells dropping in phospho-p44/42 expression but the HeLa cell signal rising slightly. When comparing the effect of the addition of genistein to the cells, it had little effect on phosphorylated p44/42. The only exception to this would appear to be after 6 hours of tunicamycin treatment, where the addition of genistein to HeLa cells induced an increase in phospho-p44/42 expression compared to the 6 hour tunicamycin sample without genistein. The internal eIF4E loading control was detected in all the samples, with the only potential difference being in the samples in lanes 10, 11 and 20, which could be due to uneven protein transfer to the membrane. If the loading was normalised, it would appear that the HT1080 6 hour tunicamycin sample with genistein showed an increased expression of MAPK.

A component of the pro-survival pathway, PI3K/AKT (Dai et al., 2010) was visible in this blot due to the probe for the phosphorylated AKT protein. Observation of the phosphorylation pattern of this protein could suggest whether genistein potentiates the ER stress response and pushes the cells towards a particular fate (e.g. apoptotis). The phospho-AKT protein can be seen in this blot, however it is fainter than MAPK, and the phospho-P44/P42 bands are thus harder to interpret. As seen from the phospho-P44/P42 bands, the 10 minute tunicamycin treatment seemed to induce a similar peak of expression in the phospho-AKT in both cell lines. Genistein did seem to have an effect in this case, with the phospho-AKT expression decreasing in both cell lines with the addition of genistein to the 10 minute tunicamycin treated samples (lanes 6, 16: T10+) as opposed to the 10 minute tunicamycin treated samples without genistein (lanes 5,15: T10-). The effect was more pronounced in the HeLa cells as the peak of phospho-AKT at 10 minutes was higher than in the HT1080 cells and hence the subsequent decrease in signal with genistein was larger. Aside from the 10 minute tunicamycin treated samples, the phospho-AKT bands did not seem to appear, precluding further analysis.

To further understand the role of MAPK kinases in the cellular response to ER stress, the HT1080 cells and HeLa cells were serum starved and treated with or without tunicamycin **(Figure 3.1.9)**. The process of serum starving was used to induce cell cycle arrest, which may lead to increased sensitivity to tunicamycin treatment as well as controlling for possible unknown effectors of the MAPK pathway contained in the FBS. The first point of interest from this data comes from the untreated samples from both cell lines. The untreated samples from this experiment (lanes 1,2 and 7,8) were dissimilar to the MAPK and phospho-P44/P42 expression seen in the untreated samples from the previous experiment (lanes 1,2 and 11,12). All of the PDGFR pathway blots exhibited reproducible results for the treated cells, but the first experiment shows inconsistency with mock treated cells. Subsequent experiments showed similar p44/42 expression in the untreated samples as this blot.

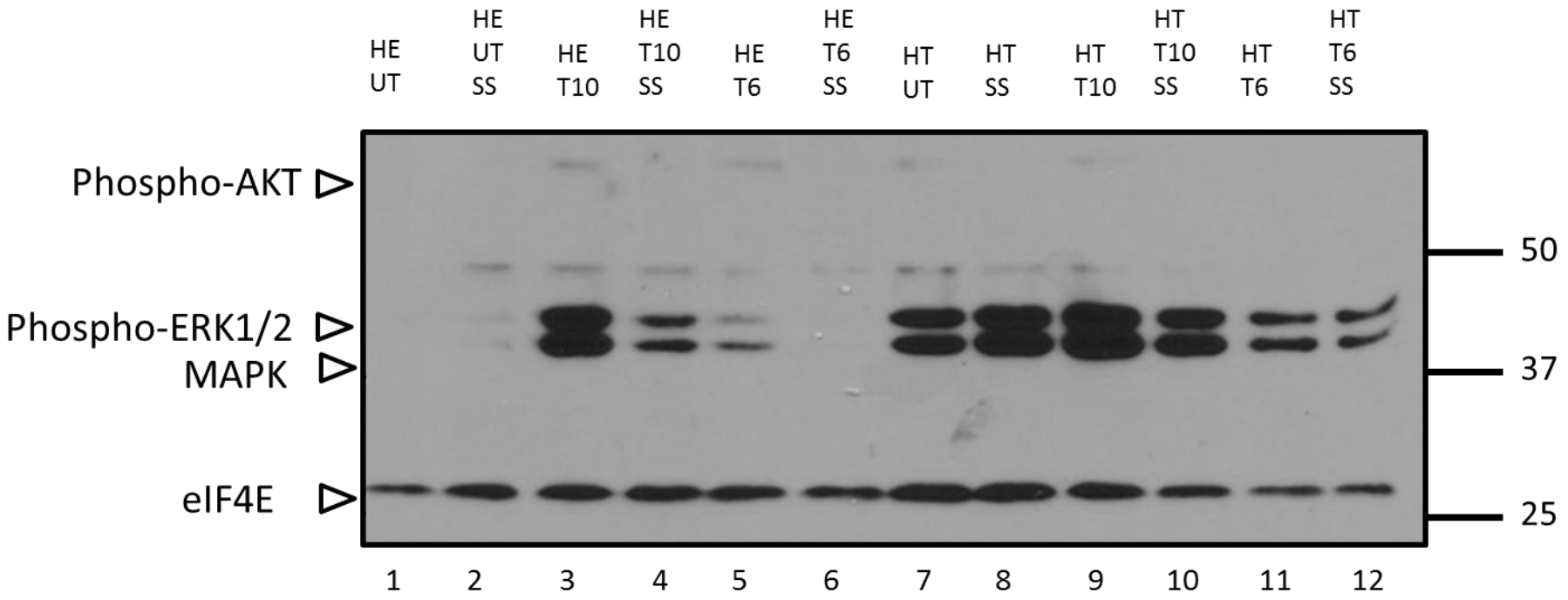

Figure 3.1.9: Serum starvation decreases the effect of tunicamycin on the induction of phosphorylated p44/42 MAPK in HeLa and HT1080 cells.
PathScan® western blot of HT1080 and HeLa cell lysates from cells treated with tunicamycin (lanes 5-10 and 15-20) and serum starvation (2,4,6,8,10,12) to detect multiple proteins including Phospho-AKT, Phospho-p44/42 MAPK, and the loading control eIF4E. UT = Untreated, T10 = 10 minutes T1 µg/ml tunicamycin, T6 = 6 hours 1 µg/ml tunicamycin, SS = serum starvation, HE = HeLa cell lysates, HT = HT1080 cell lysates.

It is possible that the HT1080 cells showed a similar expression of phospho-p44/42 MAPK to the previous experiment (which used cells grown in media containing 8% FBS); however, the HeLa cells exhibited a noticeably lower expression in these bands than previously. Aside from the untreated samples, the phospho-P44/P42 expression profile is similar to what was observed previously, with a clear peak occurring in the 10 minute tunicamycin treatment for both cell lines with a subsequent dip in expression for the 6 hour tunicamycin treated samples. The 6 hour tunicamycin treatment resulted in a relatively low expression of phospho-p44/42 MAPK for the HeLa cells, and a slightly higher expression for the HT1080 cells. Serum starving the cells seemed to have a clear effect on the HeLa cells, specifically with the 10 minute tunicamycin treatment and at the 6 hour timepoint. Strangely, this showed the converse of what was expected, with a pronounced reduction in activation of the phospho-P44/P42 expression in the 10 minute tunicamycin treated, serum starved HeLa cells (compare lanes 3 to 4). The difference that serum starving makes to phospho-p44/42 MAPK expression in HT1080 cells is not pronounced, however there does still seem to be a minor decrease in expression in the 10 minute tunicamycin serum starved lane (compare lanes 9 to 10). The eIF4E loading controls indicated even loading. The phospho-AKT bands were very faint in these blots however there does seem to be a slight increase in phospho-AKT expression in the non-serum starved 10 minute tunicamycin lanes for both cell lines; more so in the HeLa cells, which was also the case in the previous experiment.

The Coomassie brilliant blue stain of the gels containing serum starved lysates **(Figure 3.1.10)** acted as a control for lysis and sample recovery. One distinct ~50 kDa band was absent in all the serum starved lysates, and this band is likely to be residual albumin.

After seeing the discrepancy of phospho-p44/42 MAPK expression between the untreated samples in different experiments on the same gel, lysates from both sets of MAPK experiments were loaded next to each other to observe whether phosphorylation patterns differed within what should be the same treatments **(Figure 3.1.11)**. The genistein and serum starved treatments were excluded, and just the untreated, 10 minute tunicamycin and 6 hour tunicamycin treatments were used.

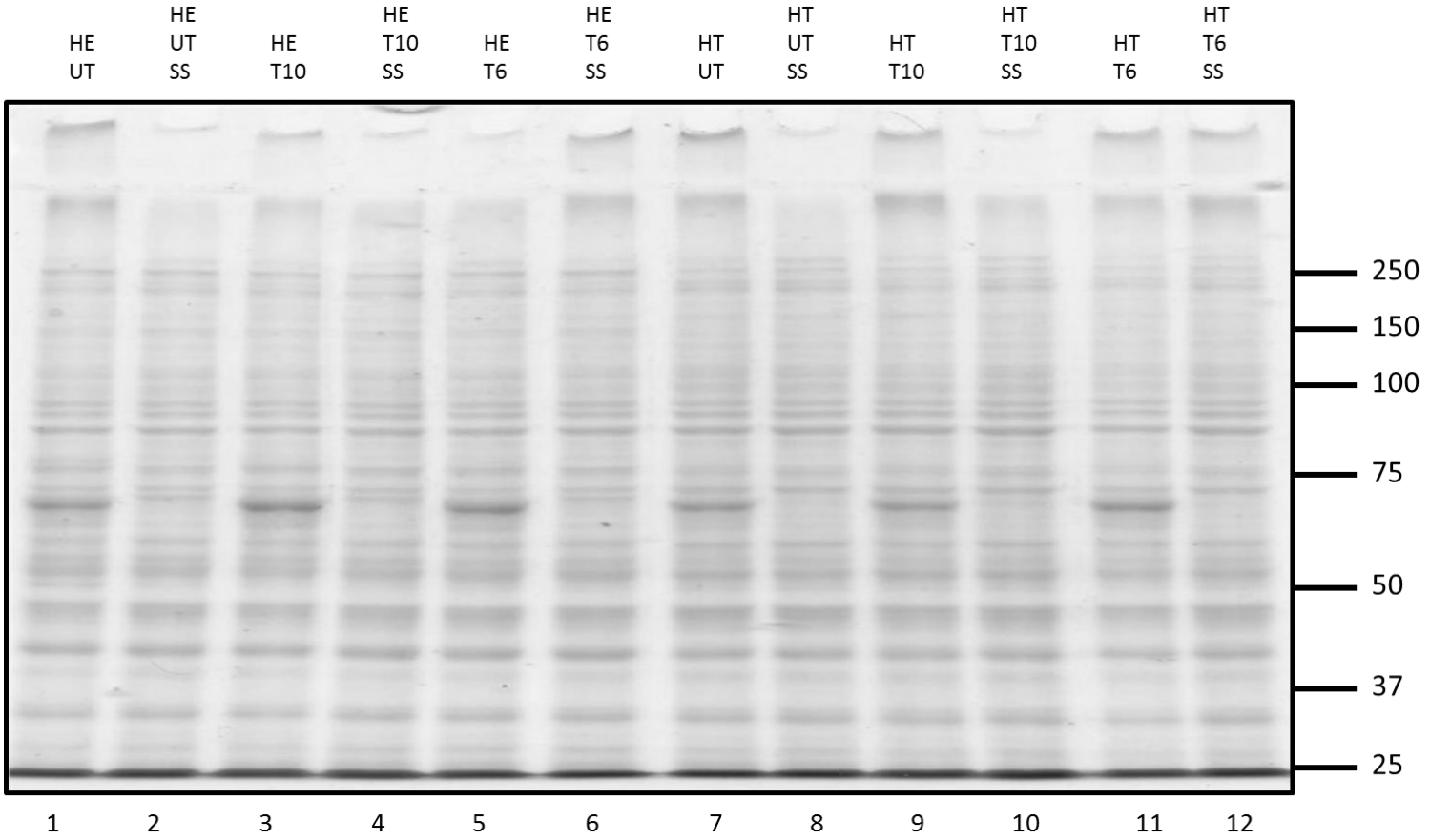

Figure 3.1.10: Coomassie stain of gel containing lysates created from serum starved HeLa and HT1080 cells acts as a loading control.

Coomassie Brilliant Blue stain of HeLa and HT1080 cell lysates from cells treated with tunicamycin (lanes 2-12), and serum starving (2,4,6,8,10,12). UT = Untreated, T10 = 10 minutes T1 µg/ml tunicamycin, T6 = 6 hours 1 µg/ml tunicamycin, HE = HeLa cell lysates, HT = HT1080 cell lysates, SS = serum starved.

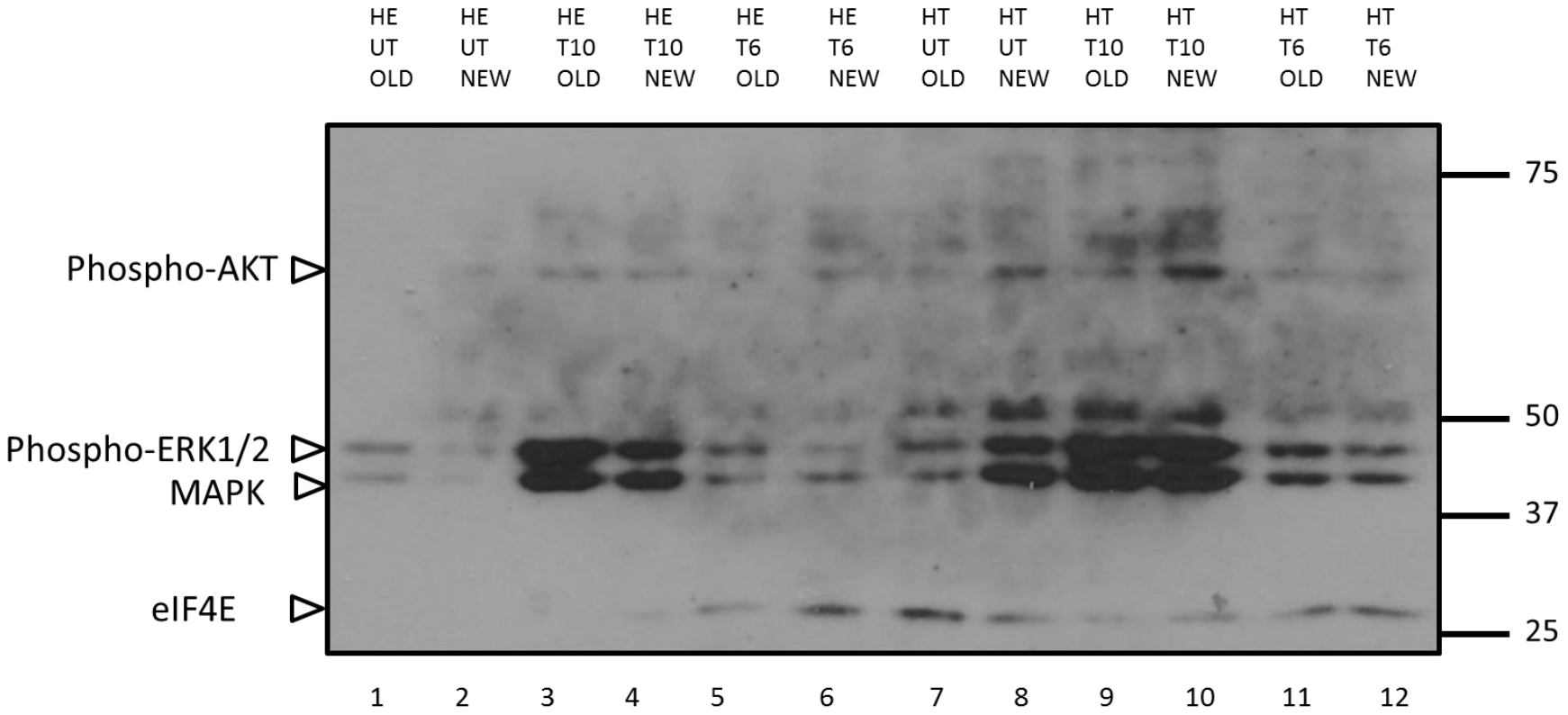

3.1.11: Comparison between two sets of lysates (old and new) created from HT1080 and HeLa cells acts a control for differences in phosphorylated p44/42 MAPK expression between two experiments.

PathScan® western blot of HT1080 and HeLa cell lysates from cells treated with tunicamycin (lanes 3-12), comparing older and newer lysates to detect multiple proteins including Phospho-AKT, Phospho-p44/42 MAPK, and the loading control eIF4E. This was used to detect if there were any differences in phospho-p44/42 MAPK expression between experimental repeats. UT = Untreated, T10 = 10 minutes T1 µg/ml tunicamycin, T6 = 6 hours 1 µg/ml tunicamycin, HE = HeLa cell lysates, HT = HT1080 cell lysates, OLD = initial lysates, NEW = experimental repeat.

Both cell lines having the older (genistein experiment) and newer (serum starved experiment) samples loaded next to each other for each treatment. The results show that between the experiments, the phosphorylated p44/42 is weak but consistent apart from the HT1080 untreated samples where the MAPK and phospho-P44/P42 expression is clearly stronger in the newer sample generated for the second experiment. The 10 minute tunicamycin exhibited the clear peak of phospho-p44/42 MAPK expression here which demonstrates that across all experiments, there is an early, reproducible and almost immediate effect of tunicamycin on MAPK pathways. The subsequent dips in expression are the same, with the HeLa cells showing a very weak signal in the 6 hour tunicamycin treatment compared to the 10-minute treatment. The HT1080 cells again show a dip in expression in the 6 hour tunicamycin but it is stronger than the expression in the HeLa cells.

3.2 Live cell imaging of cells subjected to ER stress

3.2.1 The effect of tunicamycin on the motility of HeLa and HT1080 cells

In order to assess the effect that tunicamycin had on the morphology and the motility of the two cell lines (HT1080 and HeLa), a series of live cell imaging studies were performed. Using a spinning disc microscope allowed motility assays to be performed on the cells, but also provided useful qualitative information about how the cells responded to the treatments in general. In these experiments, HT1080 cell and HeLa cells were either mock treated, tunicamycin treated (1 µg ml^{-1}), genistein treated (140 µM) or a combination of genistein and tunicamycin treated to assess whether genistein either potentiated or reduced the effect of tunicamycin. The cells were then stained with ER tracker blue-white DPX which enabled visualisation of the endoplasmic reticulum. The cells were then imaged using the Andor Spinning Disc microscope for 6 hours with an image of the cells being taken every minute to create a time-lapse movie of 360 frames. The data was then analysed using image J and the Mtrack2 plugin was used to track each individual cell's movement. In multiple conditions, some cells disappeared from the field of view and therefore these were excluded from analysis as they may skew the results due to truncated measurements.

Panels from typical microscope images are shown in **Figures 3.2.1** to **3.2.4. Figure 3.2.1** shows the mock and tunicamycin treated HeLa cells. The beginning of the 6 hour imaging session for the mock treated HeLa cells is shown in panel **A** of **Figure 3.2.1**, and the morphology of the endoplasmic reticulum appeared varied, however in each cell the ER was mainly perinuclear. After 6 hours of mock treatment (**Figure 3.2.1B)**, the cell tracking lines suggest that each cell has moved a considerable distance; with an average distance travelled of 0.139 µm, with the direction of migration appearing random. The majority of tunicamycin treated HeLa cells appear morphologically normal at the beginning of the 6-hour measurement (**Figure 3.2.1C**), apart from cell number 7, for example, which seems to have an enlarged ER with what could be described as a bubbly appearance. After the 6 hours of tunicamycin treatment (**Figure 3.2.1D**), it is evident that multiple cells have migrated much less in comparison to the 6 hours of mock treatment, with an average distance of 0.0676 µm. **Figure 3.2.2** shows the genistein and the tunicamycin + genistein treated HeLa cells. **Figure 3.2.2A** shows the genistein treated HeLa cells at the beginning of the 6-hour treatment, and the morphology of the ER seems similar to the mock treated HeLa cells; with clear ER staining. **Figure 3.2.2B** shows the HeLa cells after 6 hours of genistein treatment. While the staining was faded (likely due to photobleaching), the morphology still seemed normal, and the migration of the cells appears to be high with an average distance of 0.109 µm. The first frame of the genistein + tunicamycin treated cells is shown in **Figure 3.2.2C**, and there were a few cells with shrunken ERs compared to the previous conditions (cells 15,14,2). After 6 hours of the genistein + tunicamycin treatment (**Figure 3.2.2D**), the migration did not appear to be noticeably lower than the genistein treated HeLa cells, with mean migration distances of 0.065896552 µm and 0.051852941 µm respectively. Due to photobleaching, it is difficult to comment on the comparative morphology here.

Figure 3.2.3 shows the mock and tunicamycin treated HT1080 cells, and the mock cells at the first frame (**Figure 3.2.3A**) seem very similar morphologically to the HeLa cells. In terms of migration, the HT1080 cells did not seem to have migrated as much as the HeLa cells after 6 hours of mock treatment, with an average distance of 0.0958 µm (**Figure 3.2.3B**). The tunicamycin treated HT1080 cells do not show any

differences in morphology at the beginning (**Figure 3.2.3C**) and were photobleached considerably after 6 hours (**Figure 3.2.3D**). It is noticeable here that the cells migrated a lot after 6 hours, with an average distance of 0.189 µm, and have travelled in more extended distances compared to the mock HT1080 cells which moved in a more restricted area despite being seeded at a similar density. The genistein and genistein + tunicamycin treated HT1080 cells are shown in **Figure 3.2.4**, and **Figure 3.2.4A** shows the genistein treated HT1080 cells at the beginning of the 6-hour treatment. The morphology here was very similar to the both the HeLa cells and the HT1080 cells analysed at the start of other treatments, as expected. After 6 hours of genistein treatment (**Figure 3.2.4B**), the HT1080 cells did not appear noticeably affected in terms of migration with mean migration distances of 0.073961538 µm and 0.074821429 µm for 6 hour mock and 6 hour mock with genistein respectively. The morphology of the genistein + tunicamycin treated HT1080 cells at the first frame (**Figure 3.2.4C**) was not different. After 6 hours of genistein + tunicamycin treatment, the cells' migration was not inhibited with a mean migration of 0.06562069 µm.

3.2.2 Statistical analysis shows that HeLa cells are sensitive to motility inhibition after treatment with tunicamycin.

The different ER stress treatments had visible effects on the behaviour of the cells but the magnitude of the effect differed between the two cell lines. HeLa cells were much more sensitive to the addition of tunicamycin, resulting in a visible reduction of movement which was quantitatively demonstrated through the significantly reduced movement seen in the tunicamycin treated HeLa cells in comparison with the mock condition **(Figure 3.2.1,3.2.5 and Table 3.2.1)**, with the mock treated HeLa cells moving on average 0.0616 µm more than the tunicamycin treated HeLa cells.

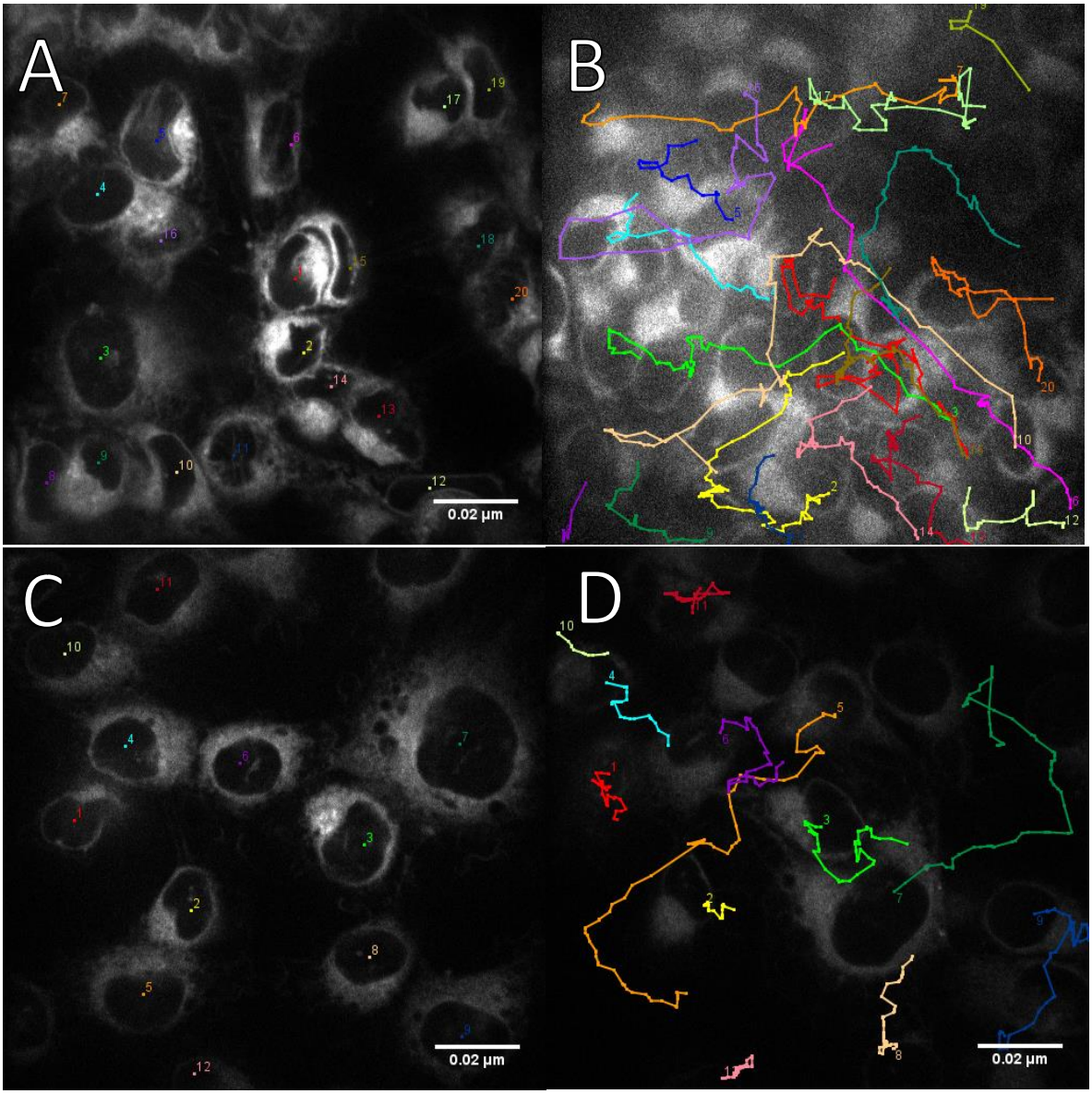

Figure 3.2.1: Live cell imaging of HeLa cells shows that tunicamycin treatment decreases motility.

Live cell imaging pictures taken of mock treated (A,B) and tunicamycin treated (C,D) HeLa cells all stained with ER tracker dye DPX. Panels A and C represent the first frame taken from the 6 hour time-lapse movie of the cells. Panels B and D represent the last frame from the 6 hour time-lapse movie. The coloured lines and dots represent the tracking of individual cells. Tunicamycin treatment = 1 µg/ml. While the laser power remained consistent between conditions, photo-bleaching can be observed in panel B and this may be because of inefficient washing, meaning more residual dye in the media, resulting in the noisier image. In the future, the use of different ER tracker dyes could be explored that may be less susceptible to photo-bleaching.

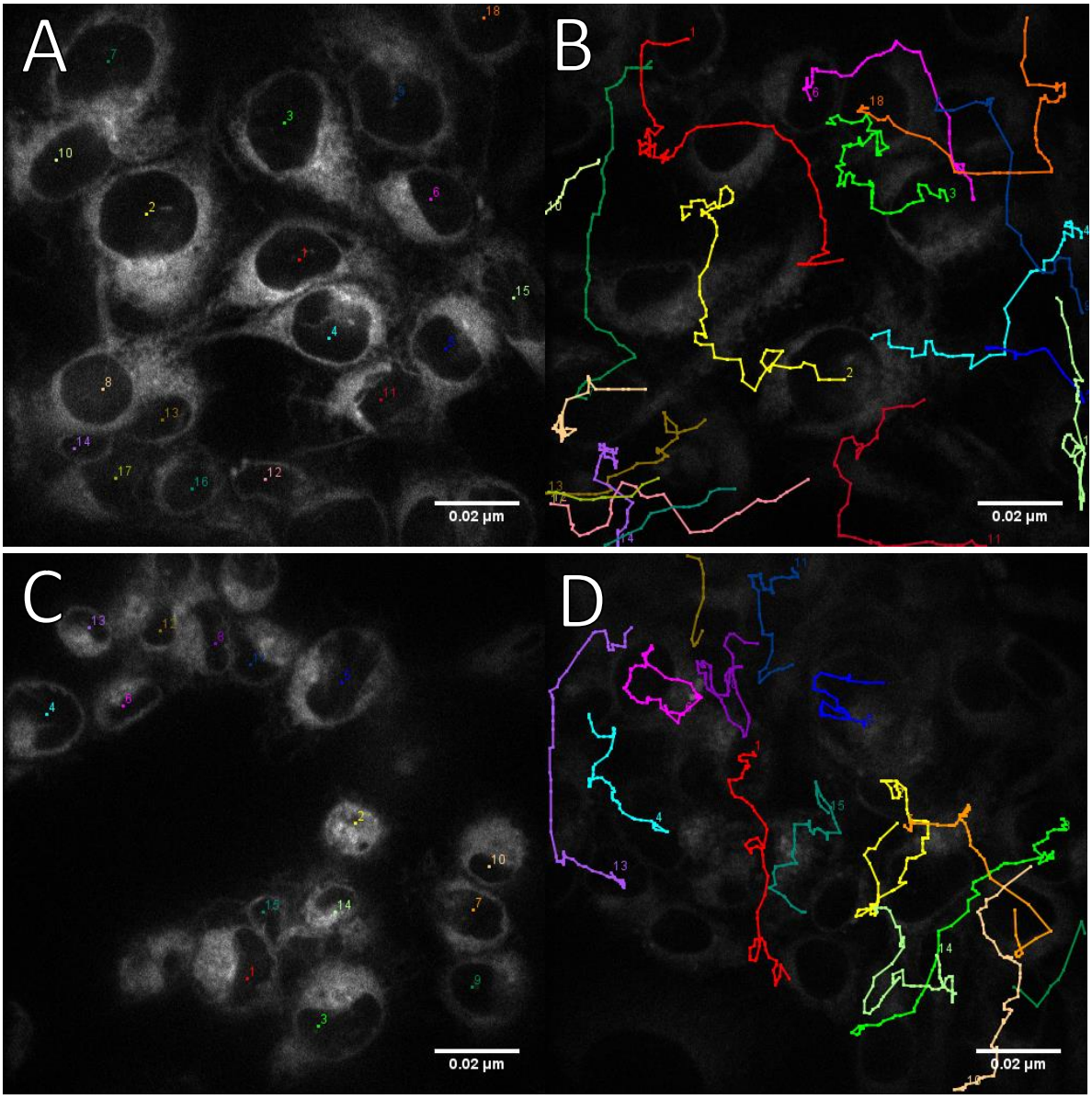

Figure 3.2.2: Live cell imaging of HeLa cells shows that genistein does not appear to affect motility when combined with tunicamycin.

Live cell imaging pictures taken of genistein treated (A,B) and tunicamycin + genistein treated (C,D) HeLa cells all stained with ER tracker dye DPX. Panels A and C represent the first frame taken from the 6 hour time-lapse movie of the cells. Panels B and D represent the last frame from the 6 hour time-lapse movie. The coloured lines and dots represent the tracking of individual cells. Tunicamycin treatment = 1µg/ml, Genistein treatment = 140 µM

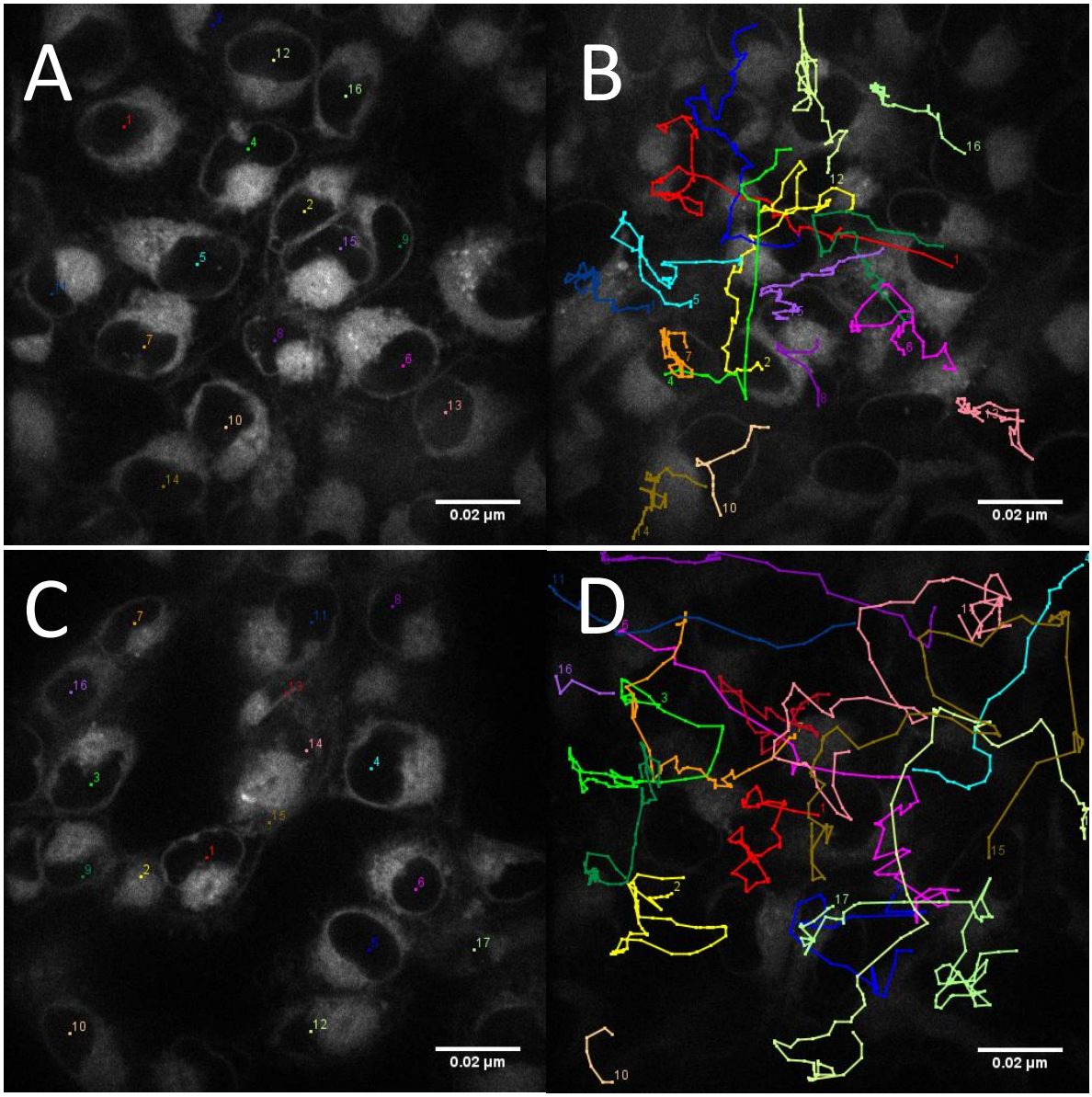

Figure 3.2.3: Live cell imaging of HT1080 cells shows that tunicamycin treatment seems to increase motility.

Live cell imaging pictures taken of mock treated (A,B) and tunicamycin treated (C,D) HT108 cells all stained with ER tracker dye DPX. Panels A and C represent the first frame taken from the 6 hour time-lapse movie of the cells. Panels B and D represent the last frame from the 6 hour time-lapse movie. The coloured lines and dots represent the tracking of individual cells. Tunicamycin treatment = 1 µg/ml

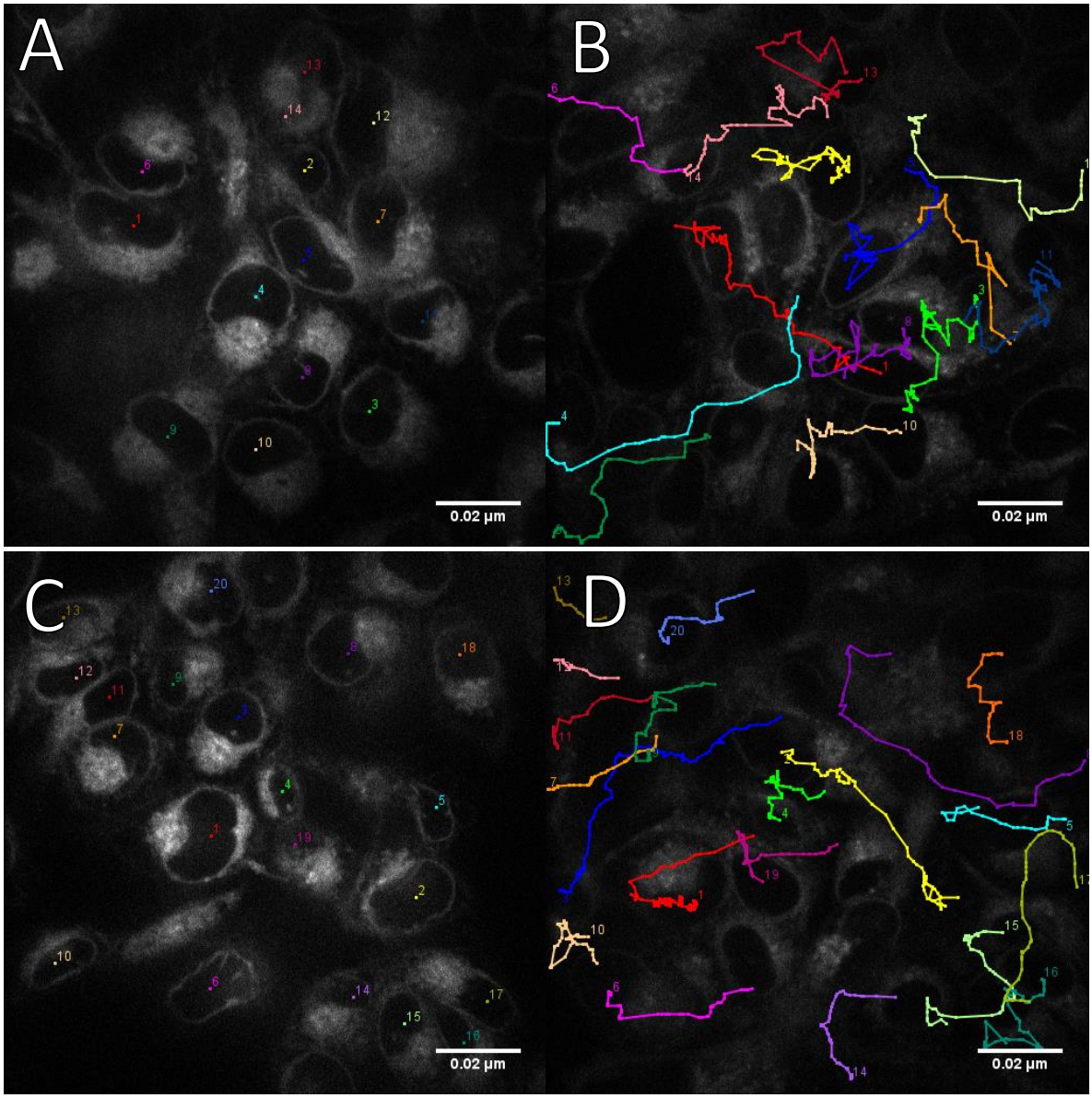

Figure 3.2.4: Live cell imaging of HT1080 cells shows that genistein does not appear to affect motility when combined with tunicamycin.

Live cell imaging pictures taken of genistein treated (A,B) and tunicamycin + genistein treated (C,D) HT1080 cells all stained with ER tracker dye DPX. Panels A and C represent the first frame taken from the 6 hour time-lapse movie of the cells. Panels B and D represent the last frame from the 6 hour time-lapse movie. The coloured lines and dots represent the tracking of individual cells. Tunicamycin treatment = 1µg/ml, Genistein treatment = 140 µM

The response of HeLa cells to the treatments was reproducible in repeat experiments (microscopy images not shown**, Figure 3.2.5**), with the mock (untreated) HeLa cells exhibiting the highest level of motility and the most noticeable difference being between the untreated and the tunicamycin treated cells. Overall, the genistein treatment on its own did appear to inhibit migration significantly (**Table 3.2.1**) – with an average motility reduction of 0.0483 µm, but the error bar for the combined result is quite high, as in the individual experiments it was not as clear cut. The genistein + tunicamycin condition resulted in a marginally lower motility than the genistein treatment only in both HeLa experiments, however the average motility is still slightly higher than that of the tunicamycin on its own in both experiments. There was an example in the genistein + tunicamycin treatment of the HeLa cells where the cells appeared to be shrinking drastically and blebbing (**Figure 3.2.2C,D**). This could be indicative of possible apoptosis, although this cannot be concluded with certainty without direct analysis of apoptotic markers.

The HT1080 cells on the other hand were more variable **(Figure 3.2.3,3.2.4,3.2.6 and Table 3.2.2)**. The tunicamycin treated HT1080 cells elicited a strong and significant increase in motility in the first experiment with an average increase of 0.0936 µm, but only a slight increase in the repeat, with an average increase of 0.00525 µm. In fact the repeat had no significant changes between the treatments. On one hand this does show that tunicamycin did not decrease motility in the HT1080 cells and confirms that HeLa and HT1080 cells respond differently to tunicamycin induced ER stress. The genistein treated HT1080 cells showed no significant change in motility compared to the mock treatment in either experiment, however the genistein + tunicamycin treated cells exhibited a significant decrease in motility compared to the tunicamycin treatment on its own, suggesting that genistein rescues the effect of tunicamycin. The combined data indicates that tunicamycin significantly increased migration in the HT1080 cells, however the error bar is very wide indicating a lot of variability. It is clear though that tunicamycin does not inhibit migration in the HT1080 cells as opposed to the clear inhibition seen in the HeLa cells.

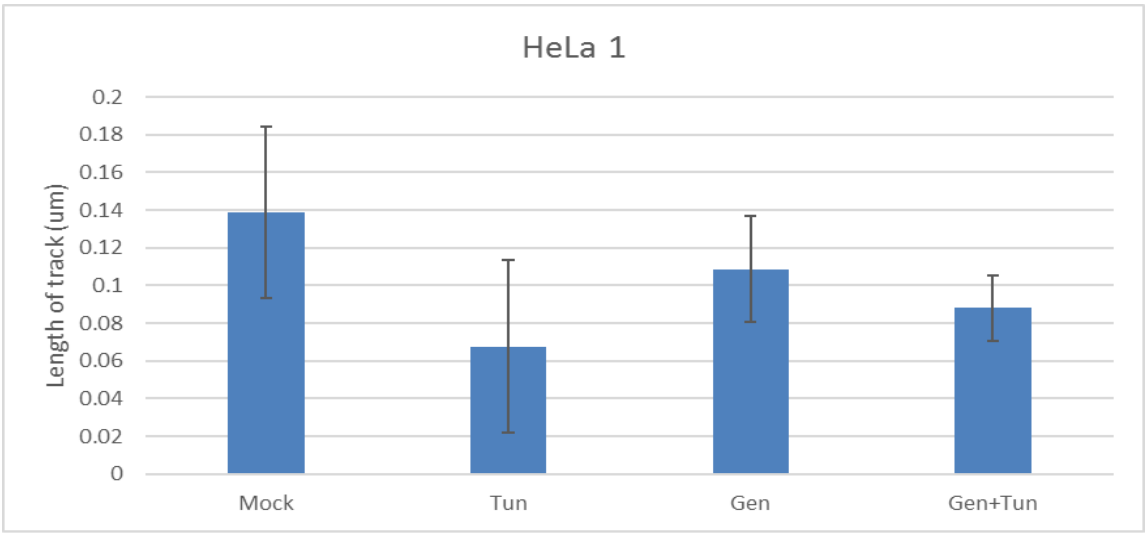

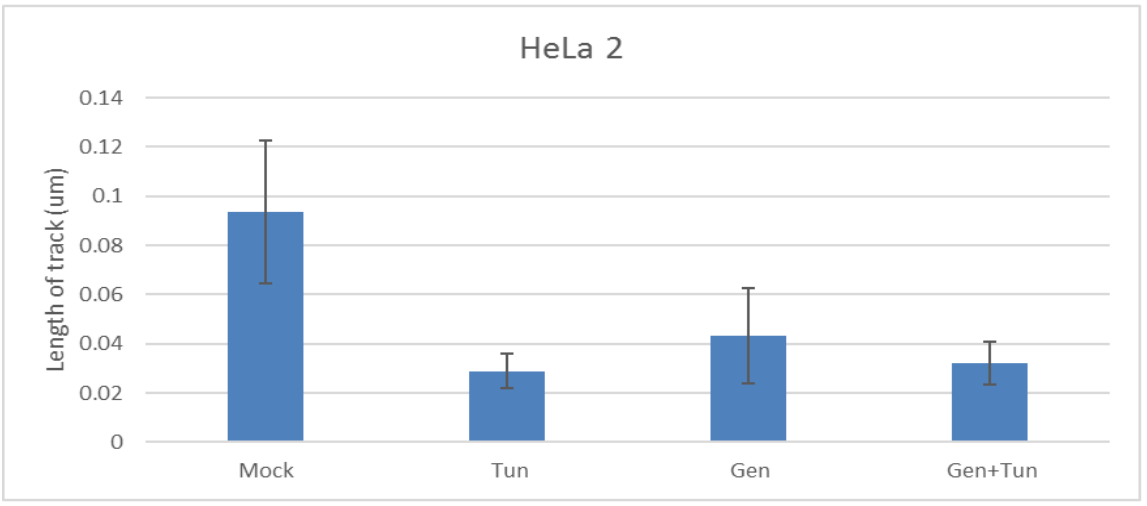

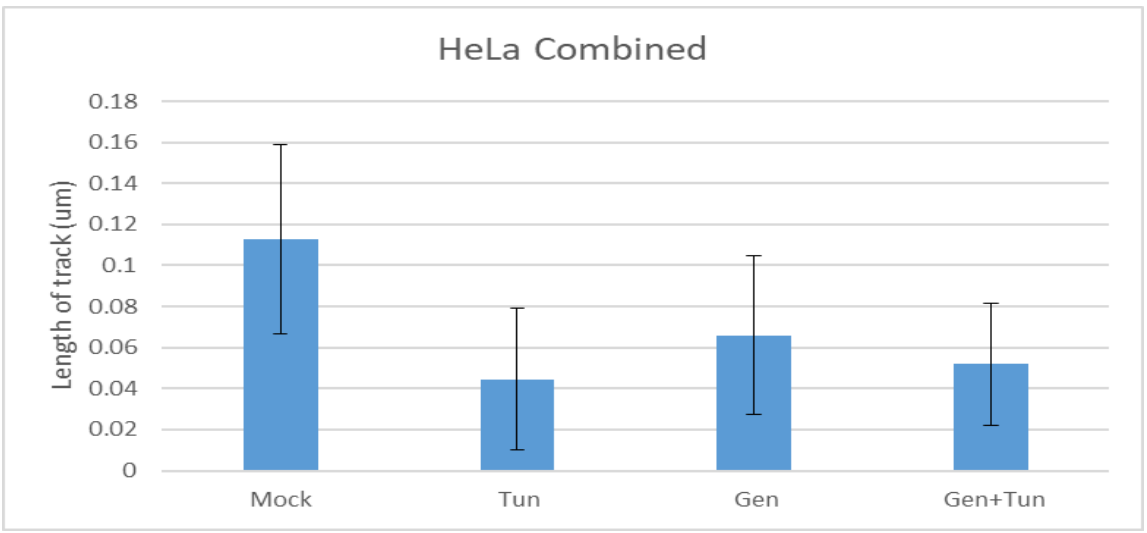

Figure 3.2.5: Graphs showing the migration of HeLa cells shows that tunicamycin inhibits migration in this cell line.

Graphs from the two live cell imaging experiments (1,2) with the combined data (combined) showing the mean distance (µm) travelled by HeLa cells under the different treatments: Mock = untreated, Tun = 1 µg/ml tunicamycin, Gen = 140 µM genistein. Standard deviation is shown in the error bars

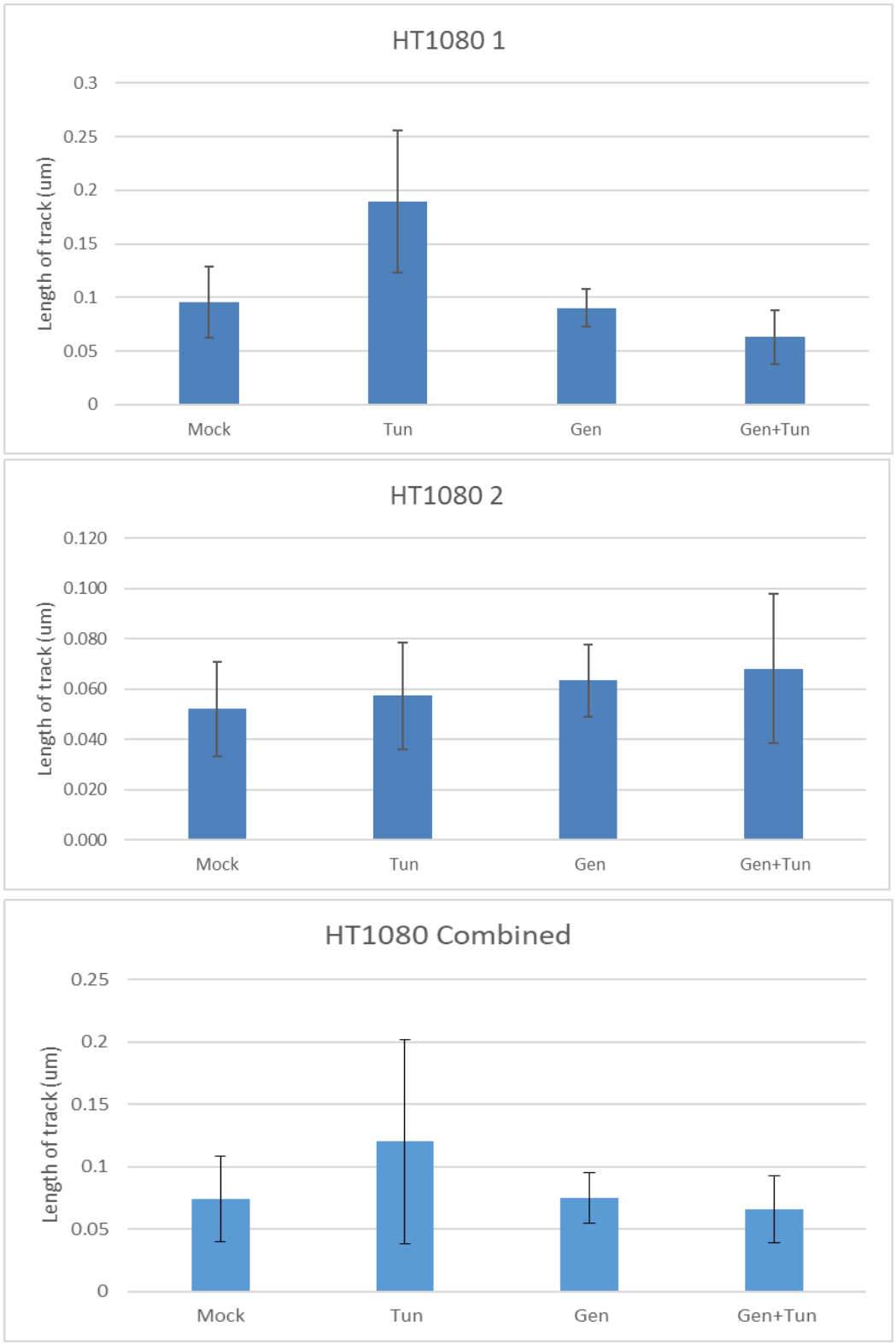

Figure 3.2.6: Graphs showing the migration of HT1080 cells shows that tunicamycin does not inhibit migration in this cell line.

Graphs from the two live cell imaging experiments (1,2) with the combined data (combined) showing the mean distance (µm) travelled by HT1080 cells under the different treatments: Mock = untreated, Tun = 1 µg/ml tunicamycin, Gen = 140 µM genistein. Standard deviation is shown in the error bars

Table 3.2.1: Statistical analysis reveals that tunicamycin significantly decreases migration in HeLa cells.

Tukey's test (parametric) table showing all comparisons between treatments for the HeLa live cell imaging experiments and the combined results.

Compared Treatments (1)	Significance	Mean Difference
Mock vs. Tunicamycin	***	0.07109
Mock vs. Genistein	ns	0.02949
Mock vs. Genistein Tun	**	0.05053
Tunicamycin vs. Genistein	ns	-0.0416
Tunicamycin vs. Genistein Tun	ns	-0.02057
Genistein vs. Genistein Tun	ns	0.02103

Compared Treatments (2)	Significance	Mean Difference
Mock vs. Tunicamycin	****	0.05783
Mock vs. Genistein	****	0.04359
Mock vs. Genistein Tun	****	0.05465
Tunicamycin vs. Genistein	ns	-0.01424
Tunicamycin vs. Genistein Tun	ns	-0.003179
Genistein vs. Genistein Tun	ns	0.01106

Compared Treatments (Combined)	Significance	Mean Difference
Mock vs. Tunicamycin	***	0.06833
Mock vs. Genistein	***	0.04680
Mock vs. Genistein Tun	***	0.06084
Tunicamycin vs. Genistein	ns	-0.02154
Tunicamycin vs. Genistein Tun	ns	-0.007493
Genistein vs. Genistein Tun	ns	0.01404

ns $P > 0.05$
* $P \leq 0.05$
** $P \leq 0.01$
*** $P \leq 0.001$
**** $P \leq 0.0001$ (For the last two choices only)

Table 3.2.2: Statistical analysis reveals that tunicamycin does not inhibit migration in HT1080 cells.

Tukey's test (parametric) table showing all comparisons between treatments for the HT1080 live cell imaging experiments and the combined results.

Compared Treatments (1)	Significance	Mean Difference
Mock vs. Tunicamycin	****	-0.09356
Mock vs. Genistein	ns	0.005769
Mock vs. Genistein Tun	ns	0.0325
Tunicamycin vs. Genistein	****	0.09933
Tunicamycin vs. Genistein Tun	****	0.1261
Genistein vs. Genistein Tun	ns	0.02673

Compared Treatments (2)	Significance	Mean Difference
Mock vs. Tunicamycin	ns	-0.005246
Mock vs. Genistein	ns	-0.01128
Mock vs. Genistein Tun	ns	-0.01599
Tunicamycin vs. Genistein	ns	-0.006038
Tunicamycin vs. Genistein Tun	ns	-0.01074
Genistein vs. Genistein Tun	ns	-0.004705

Compared Treatments (Combined)	Significance	Mean Difference
Mock vs. Tunicamycin	**	-0.04593
Mock vs. Genistein	ns	-0.0008599
Mock vs. Genistein Tun	ns	0.008341
Tunicamycin vs. Genistein	**	0.04507
Tunicamycin vs. Genistein Tun	***	0.05427
Genistein vs. Genistein Tun	ns	0.009201

ns P > 0.05
* P ≤ 0.05
** P ≤ 0.01
*** P ≤ 0.001
**** P ≤ 0.0001 (For the last two choices only)

Within the first experiment on the HT1080 cells there is no observable apoptosis of cells in the areas viewed, however in the repeats, the genistein + tunicamycin does seem to show some cells shrinking and blebbing. This could indicate the effect of genistein 'rescuing' ER stress in the cells; removing the barrier to the stress, and allowing a typical stress reaction to occur which may lead to apoptosis, due to the mechanisms of genistein mentioned earlier in the introduction. It is clear however from these live cell imaging experiments that HeLa cells and HT1080 cells have a different response to tunicamycin induced stress, with inhibition of motility occurring within HeLa cells, indicating sensitivity to tunicamycin, whereas the HT1080 cells did not display not any significant sensitivity to tunicamycin in terms of motility inhibition.

Chapter 4: Discussion

4.1 Discussion overview

The aim of this project was to investigate differences between two human cell lines, HeLa cells and HT1080 cells, in their responses to pharmacological or chemically induced stress. This was investigated in combination with the effect of the tyrosine kinase inhibitor genistein, which previously showed promise in modulating ER stress.

4.2 Differential protein expression as a result of pharmacologically induced ER stress in HT1080 and HeLa cells.

4.2.1 The effect of ER stress on the expression of heat shock proteins and glycosylation in HT1080 cells and HeLa cells.

The western blot experiments for expression of GRP94 and HC10 (**Figure 3.1.1, Figure 3.1.3** and **Figure 3.1.5**) were undertaken to investigate whether the protein pool of heat shock proteins changes as a result of chemically induced ER stress, and whether ER stress affects the expression or glycosylation of MHC class I molecules. GRP94 is known to be upregulated under ER stress (Marzec et al., 2012, p. 94), and for the experiments here it was intended for use as an ER stress indicator. Previous findings have demonstrated that MHC class I plasma membrane expression on the cell surface is significantly decreased when the cells are exposed to chemically induced stress from both tunicamycin and thapsigargin (Ulianich et al., 2011). This was also shown in a previous study, but the decreased surface expression was induced by palmitate instead (Granados et al., 2009). This study also indicated that the overall intracellular protein levels of MHC class I were not altered with the induction of ER stress. It would seem from these papers that the processing of MHC class I proteins is perturbed but the expression remains unaffected. The experiment undertaken for this thesis investigated whether the overall expression would differ according to cell type, and while it does not measure surface expression, observing any change in glycosylation could indicate impaired processing.

The GRP94 showed a clearer result in **Figure 3.1.5** compared to **Figure 3.1.1**, after using lysates with multiple tunicamycin treatment time points and in combination with genistein. With this result, the HT1080 cells certainly showed an increase in

GRP94 with the tunicamycin treatments, but the HeLa cells less so at the earlier time points - at least in the 10 minute tunicamycin treated lysates. The blot showed an interesting effect of genistein on GRP94 expression in the HeLa cells, with an increase of GRP94 expression when genistein is added in both untreated and 10 minute tunicamycin conditions. With DTT and the 10 minute tunicamycin timepoint, the GRP94 expression is slightly decreased when genistein is added. Inversely, in the HT1080 cells a pronounced reduction of GRP94 expression is seen in the untreated + genistein condition, with an increase in expression seen in DTT and 10 minute tunicamycin in the presence of genistein. This pattern is the opposite of what is seen in the HeLa cells, however in the 30 minute and 6 hour tunicamycin time points, there is a reduction of GRP94 expression with genistein which is similar to the HeLa cells. The different expression patterns of the stress indicator GRP94 between the cell two cell lines highlights cell specific differences in the reaction to genistein. The raised expression of GRP94 does point towards activation of stress pathways in both cell lines, with an increase in the chaperone GRP94 indirectly indicating an increase in ERAD and protein folding. The difference seems to lie in the time point of stress activation with the HT1080 cells surprisingly expressing an increase in GRP94 earlier than the HeLa cells. The HeLa cells do have a higher expression of GRP94 than the HT1080 cells at the 6 hour tunicamycin treatment point. There is a bell-shaped curve type stress response with the HT1080 cells, which could explain the potential reason a 'barrier' to stress was seen by previous research in this lab as it is possible the stress response is activated earlier in the cells and earlier time-points are needed to highlight this. It could be that the ER stress response decreases to a small extent in the HT1080 cells towards the later time points perhaps due to an adaption to the stress in the cellular machinery after the initial high response. In the HeLa cells, however it is possible that the stress pathways activate more slowly in comparison to the HT1080 cells, and instead reach a peak at the 6 hour tunicamycin treatment. The use of GRP94 as readout was intended to show differences in UPR induction between the cell lines, and although the effect on the overall protein pool were not as clear as if RT-PCR analysis of gene expression was used, this still hinted at a temporal difference in the activation of stress pathways between the cells.

For both cell lines, the initial results indicated a reproducible decrease in the overall protein expression in the tunicamycin treated cells when compared to DTT treatment. No change in glycosylation was observed however. This result was seen at the 6 hour tunicamycin treated timepoint in subsequent experiments suggesting that the overall protein pool does decrease after 6 hours of treatment. This longer treatment of tunicamycin was not included in the aforementioned paper (Ulianich et al., 2011), which had not seen a decrease in overall expression of GRP94 but only with a 30 minute tunicamycin treatment. The findings suggest some avenues for further exploration, particularly when coupled with previous research produced by this laboratory. Looking further into the effects of tunicamycin on glycosylation and the expression of MHC class I molecules between cell lines may reveal some interesting differences.

A further test for the ability of tunicamycin blocking glycosylation was performed in the blot for PCYOX1 or prenylcysteine oxidase 1 (**Figure 3.1.5**, bottom panel). Prenylcysteine oxidase has three N-glycosylated sites at positions 196, 323 and 353 (Liu et al., 2005), and therefore disruption of N-glycosylation by tunicamycin could be potentially be seen in the western blots. This blot did not show any strong differences in glycosylation between timepoints or treatments in either of the cell types. A known effect of tunicamycin is the inhibition of N-glycosylation (Esko and Bertozzi, 2009), and therefore an expected result would be increased migration due to less glycosylation and a lower molecular weight. This was not entirely clear from the experiments in this thesis. Therefore, it is possible that the minimal changes seen are due to a pre-existing high number of PCYOX glycoproteins, which masks any change in glycosylation states for newly synthesised proteins due to a stronger expression. These data could indicate that tunicamycin is not effective at blocking glycosylation for proteins with longer half lives.

4.2.2 P-STAT3 - A role for STAT3 in differential ER stress responses?

The role of STAT3 in the UPR is not entirely clear. There is however evidence of STAT3 signaling downstream of the PERK UPR branch, via JAK-1 phosphorylation of PERK which then goes on to recruit and activate STAT3 via phosphorylation, allowing it to

carry out its function as a transcription factor inducing pro-inflammatory cytokines including the ER stress linked interleukin 6 (IL6) (Meares et al., 2014). The activation of the STAT3 signaling pathway is therefore dependent on PERK (Meares and Benveniste, 2013), and this suggests that the presence of STAT3 may useful as an indicator of PERK pathway activation, particularly when looking at the phosphorylated form. Interestingly one study showed that obesity related ER stress inhibited STAT3 phosphorylation in mice hepatocytes (Kimura et al., 2012), by comparing the induction of STAT3 phosphorylation by interleukin 6 (IL6) in combination +/- tunicamycin. The fact that this was studied *in vivo*, with tunicamycin administered intraperitoneally 8 hours before analysis, and on a different cell type may explain the differences between the results seen here, but it is interesting nonetheless that tunicamycin induced ER stress seems to inhibit phosphorylation induction. It also is notable that tunicamycin appeared to have no effect on STAT3 phosphorylation when applied on its own in this study either.

The P-STAT3 (**Figure 3.1.7**) blot indicates a late tunicamycin induced increase in phosphorylated STAT3 with the HeLa cells after 6 hours of tunicamycin treatment. The HT1080 cells however show a pre-existing expression of P-STAT3 in the untreated samples, which then declined after 10 minutes of tunicamycin treatment, and rose again for 30 minutes and 6 hours of tunicamycin treatment. Due to the untreated samples exhibiting P-STAT3, it is possible that the phosphorylation of STAT3 may not just be reflecting pharmacologically induced ER stress. For example, HT1080 cells contain an endogenous N-Ras mutation (Gupta et al., 2000) and Ras may be an upstream component of the STAT3 signalling pathway. The activity of Ras was shown to be important in the mediation of p38 and JNK signalling in the transcriptional activation of STAT3 (Turkson et al., 1999), and therefore if there is a mutation causing constitutive activation of Ras in the HT1080 cells, then it is likely that the P-STAT3 baseline activity would be raised.

The STAT3 phosphorylation is a valid reflection of Stat-3 activation and when coupled with the inherent mutations in HT1080 cells, it is highly likely that the presence of P-STAT3 in the untreated HT1080 cells is indicative of constitutive Stat-3 activation. However, this activation seems to become lower when exposed to tunicamycin, and

rise back up after longer exposures of cells to the drug. Therefore, it is possible that with HT1080 cells, stress induction interferes with the constitutive phosphorylation of STAT3 via an unknown mechanism. But equally, this could reflect published data on the inhibition of STAT3 phosphorylation seen in mouse hepatocytes treated with tunicamycin (Kimura et al., 2012). It is possible that the acute tunicamycin induced ER stress inhibits phosphorylation, but chronic tunicamycin induced ER stress promotes it. Thus, either by the accumulation of stress or through a restoration of the constitutive phosphorylation, the STAT3 becomes active again. Either way, it appears that the HT1080 results may not indicate ER stress alone, and this consideration means that further study would be needed to differentiate the effects of inherent mutations and pharmacological inducers on the presence of P-STAT3, and whether there is any synergistic effect between the two.

The STAT3 results seem to show a consistent pattern of fading of the shadow band – STAT3β – at the later timepoints, though this fading occurs more readily in the HeLa cells. This lower band at around 75 kDa disappears at the 6 hour tunicamycin treatments in both the HeLa cells and HT1080 cells, but is also decreased in the 30 hour tunicamycin treatments in HeLa cells indicating a possible difference to HT1080 cells (**Figure 3.1.3).** A reduction in either isoform of STAT3 may be indirectly indicative of phosphorylation. While the upper STAT3α band does not seem to change, a reduction in STAT3β expression could show sequestration of the available non-phosphorylated STAT3β due to a higher amount of phosphorylated Stat-3. If this were the case, however, the expected result would most likely show lower STAT3 expression in both the untreated and 30 minute tunicamycin treated HT1080 samples, but this is not the case. It is possible that the expression of STAT3 is not directly related to the levels of P-STAT3. It is worth noting that in the HeLa cells, there is an unusual band consistently expressed at around 150 kDa which currently eludes explanation.

4.2.3 The MAPK/ERK/Akt pathway and the stress responses of HeLa and HT1080 cells.

The PDGF-R signalling pathway analysis is particularly interesting due to the patterns seen in the phospho-P44/P42 MAPK bands. The p44/42 MAPK (or Erk1/2) can be activated downstream of the active Ras-GTP, which activates Raf1 via translocation to the plasma membrane from the cytosol (Marais et al., 1995). This then proceeds to activate the MEK1 and MEK2 MAPKs which in turn activates the p44/42 MAPKs seen in the experiments presented here. The p44/42 MAPKs are translocated to the nucleus where they activate a variety of transcription factors through phosphorylation. These transcription factors regulate cell growth and proliferation (Plattner et al., 1999). These results (**Figures 3.1.8, 3.1.9** and **3.1.11**) were of interest both because of how ER stress may affect the phosphorylation of p44/42 MAPK and because of the endogenous N-Ras mutation present in HT1080 cells resulting in constitutively active Ras-GTP in the cells (Gupta et al., 2000). The differing effect of pharmacologically induced stress between the HT1080 cells and the HeLa cells may reveal how this mutation affects the stress related MAPK response.

The pattern of phosphorylation in the untreated samples across both cell lines was unfortunately inconsistent between the different experiments. It seems however from **Figure 3.1.11**, which compares two sample sets, that the HeLa cells exhibit a low baseline of phospho-P44/P42 expression in the untreated samples, and the HT1080 cells demonstrate a slightly higher expression to start with. Both cell lines demonstrate a peak of MAPK activity at the 10 minute tunicamycin treatment, however the HeLa cells seem to show a bell-shaped curve, with a tailing off of MAPK activity in the 6 hour no genistein tunicamycin treatment. The HT1080 cells on the contrary still demonstrate some MAPK activity in the 6 hour tunicamycin treatment, suggesting a continuous, unresolved stress response. There is a definite link between short term tunicamycin activity and the activation of MAPK p44/42 pathways, with a possible attenuation of activity towards the later stages.

An important pro-survival pathway in cells is PI3K/AKT, which is involved in inhibiting apoptosis by promoting stability of the GRP78 protein, especially during endoplasmic reticulum induced stress (Dai et al., 2010). Inhibition of this pathway has been shown to induce the pro-apoptotic CHOP and promote ER stress induced apoptosis in cells (Hyoda et al., 2006; Dai et al., 2010), and therefore it may help indicate what fate the

tunicamycin treated cells here will be pushed towards. Both in the HeLa cells and HT1080 cells, there is a visible increase of phospho-AKT at the 10 minute tunicamycin treatment, and a slight induction at the 6 hour tunicamycin treatment in the HT1080 cells more so than the HeLa cells. This could be indicative of active pro-survival pathways in the cells during these treatment points, suggesting that while there is clearly a potent immediate effect of tunicamycin; the cells compensate by AKT phosphorylation which in turn promotes GRP78 recruitment to help compensate for the stress and keep the cells alive.

The activation of MAPK is not necessarily an exclusive indicator of ER stress, but it is a downstream signalling component in ER stress pathways (Ron and Walter, 2007). The activity of MAPK signalling as a consequence of stress in the cell was seen in a study by Wei et al. who discovered that mice brain cells under ER stress induced by heart failure showed higher levels of phosphorylated p44/42 MAPK, and the upregulation of excitatory and inflammatory mediators (Wei et al., 2016a). Enhanced ERK (p44/42) activity was found to mediate cyto-protective effects in cells pre-conditioned with ER stress (Usuki et al., 2013), alongside inhibition of p38/JNK pathways. This could suggest that a higher phosphorylation of p44/42 in the HT1080 cells at the 6 hour timepoint compared to the HeLa cells is indicative of both an eventual attenuation of the pro-survival pathways in the HeLa cells, and a continuous push towards survival in the HT1080 cells. It is also possible that MAPK signalling – while downstream of ER stress – may work as a feed forward mechanism to further induce ER stress, possibly through the production of pro-inflammatory cytokines. This possible mechanism of MAPK signalling was discovered through the observation that ER stress is decreased when MAPK signalling is inhibited (Wei et al., 2016b). This may add credence to the possibility that treated HT1080 cells are maintained in a state of prolonged ER stress, which could be unresolvable due to a consistent push towards survival.

The known induction of p44/42 under ER stress correlates nicely with these results (**Figures 3.1.8, 3.1.9** and **3.1.11**) which clearly indicate a potent effect of the pharmacological stress inducer tunicamycin on the activity of p44/42 MAPK, therefore indirectly suggesting that the tunicamycin induces ER stress in these cells.

Discounting the inconsistent untreated samples, HT1080 cells perhaps have an earlier and prolonged signalling response after induced ER stress in comparison with the HeLa cells, which is also seen in the P-STAT3 results. It is possible that the HeLa cells are more sensitive to induced ER stress than the HT1080 cells, possibly due to a pre-existing low level ER stress response active in the HT1080 cells. With the HeLa cells showing a decrease in both the phosphorylation p44/42 MAPK at the 6-hour mark, but an increase in the phosphorylation of STAT3, it may be that the activation of p44/42 MAPK has some consequent effect on the phosphorylation of STAT3. It has been detailed that induction of the c-src - p44/42 MAPK cascade leads to phosphorylation of STAT3 (Tkach et al., 2013), which provides context to the link between the P-STAT3 and MAPK blots. This suggests that when phosphorylation of p44/42 MAPK is seen, the phosphorylation of STAT3 may follow, and certainly this could concur with the results seen in these blots. Again, with the N-Ras mutation in the HT1080 cells, the higher baseline activity of both p44/42 and STAT3 makes biological sense when compared to HeLa cells, which carry wild type Ras genes (Leblanc et al., 1999).

Serum containing media is optimal for cell growth however in experimental situations, the poorly defined makeup of serum in formats such as foetal bovine serum may present unwanted variables (Krämer et al., 2005). Serum contains many growth factors and cytokines (Pirkmajer and Chibalin, 2011) that could feasibly influence the signalling pathways under scrutiny in cell biology. In addition to this, a side effect of serum starvation can be cellular stress responses and apoptosis due to a lack of necessary growth factors and cytokines (Pirkmajer and Chibalin, 2011). Serum starvation is thus commonly used as a means to induce a form of physiological cellular stress (Arrington and Schnellmann, 2008). Serum starvation also helps create a more homogenous cell population due to the induced G_0/G_1 cell cycle stage quiescence in the starved cells.

The serum starvation experiment (**Figure 3.1.9**) shows an interesting pattern in that it seems to decrease the expression of phosphorylated p44/42 MAPK in comparison to non-serum starved blots. This is possibly due to the absence of extra growth factors that may trigger the MAPK pathway. What it does show is that the induced

p44/42 MAPK activation seen in these experiments is attributable to the action of tunicamycin and not other cytokines present in the serum that may have affected signalling. Due to the untreated serum starved samples still exhibiting less phosphorylated p44/42 than the serum starved tunicamycin samples, this does show that it is not just serum starved induced stress acting on the cells, and that tunicamycin does potentiate p44/p42 activation. Comparing the untreated to the untreated serum starved samples in both HeLa cells and HT1080 cells, there may be a slight rise in phosphorylated p44/42 MAPK expression which could indicate a small increase in cellular stress due to the serum starvation itself.

4.2.4 Does genistein potentiate ER stress signalling responses.

In Figure 5, the action of the tyrosine kinase inhibitor genistein on p44/42 activity (**Figure 3.1.8**) is more potent than its action on GRP94 (**Figure 3.1.5**). With the HeLa cells particularly, it appears to induce a higher activity of p44/42 in the 6 hour tunicamycin treated timepoint. This could suggest that genistein makes the HeLa cells more susceptible to prolonged ER stress. If genistein inhibits GRP78/BiP, then an exaggerated stress response would make sense, as an adaptive resolution to the stress via increased protein folding is not as readily achievable. Interestingly, the HT1080 cells show little cell specific effect of genistein, which was unexpected as it was hypothesised that genistein may rescue the HT1080 cells from the continuous low level stress response seen in the other experiments (**Figure 3.1.7**). However, both the HT1080 cells and HeLa cells did show a clear effect of genistein on the induction of the pro-survival phospho-AKT in the 10 minute tunicamycin timepoint. The genistein seemed to decrease the expression of phospho-AKT in the presence of tunicamycin which could indicate that the known action of genistein inhibiting GRP78 could be exerted indirectly via inhibiting the PI3K/AKT pathway, and it is possible that the drive towards the apoptotic cell fate is happening here with the genistein.

4.2.5 Summary

From the experiments in **Figures 3.1.1 to 3.1.11**, there are obvious differences in the reactions of the two cell lines to pharmacologically induced stress. The STAT3 activation is interesting due to reflecting a possible constitutive STAT3

phosphorylation in HT1080 cells, while still showing a compounding effect of tunicamycin on the phosphorylation. In the HeLa cells, a late appearance of P-STAT3 indicates later activation of stress-related signalling pathways compared to the HT1080 cells. The difference may be due to the pre-existing STAT3 phosphorylation in HT1080 cells lowering the threshold for further phosphorylation under additional stress stimuli. p44/42 may be a precursor for STAT3 activation as aforementioned, and this makes sense in conjunction with the P-STAT3 blots as the HT1080 cells show a more prolonged expression of phosphorylated p44/42 and they also show a more prolonged P-STAT3 activation. The issue with the PathScan blots lies in the untreated samples which are inconsistent between different blots. It is possible that this was down to human error or biological variability. However, the samples treated with tunicamycin show reproducible results and therefore conclusions can still be made.

It can be concluded that the HeLa cells exhibit a more conventional cellular response to stress stimuli, undergoing a gradual increase in ER stress as the timepoints progress, with the bell shaped activation of p44/42 MAPK possibly acting as an upstream signalling component in the stress response.

With the HT1080 cells, the stress response is different, with earlier indicators of stress existing; possibly indicating a pre-existing low level ER stress response in the cells, or simply reflecting the result of the endogenous N-Ras mutation. Tunicamycin still affects the HT1080 cells and appears to do so more rapidly than the HeLa cells, but from these data it is difficult to conclude if there would be any clinical consequences with using tunicamycin as a treatment for different cell types. Therefore, the live cell imaging data provides phenotypic context to these results; enabling analysis on how the cell behaviour (motility) changes under treatment, and whether there are any morphological changes or apoptosis present.

4.3 The effect of stress on cell movement

The action of both tunicamycin and genestein on cells was investigated by live cell imaging (**Figures 3.2.1 to 3.2.4**). Whilst there is limited research on the links between ER stress and motility, there is certainly an existing link between increased stress and decreased cell migration. Activation of ERAD by the UPR results in the formation of

ERAD complexes which recognise subsets of misfolded proteins (Kim et al., 2015). One such complex consists of the ER-membrane resident ubiquitin ligase Hrd1 complexing with SEL1L which nucleates this ERAD complex (Mueller et al., 2008). Over-expression of SEL1L inhibits cellular migration of human pancreatic cancer cells (Cattaneo et al., 2005). This is through induction of the PTEN protein that causes G_1 stage cell cycle arrest and is known to inhibit cell proliferation, growth and motility (Kim et al., 2015). If cells are pushed towards an apoptotic phenotype, it makes sense that the motility would also decrease in this instance if the cells are dying. Previous studies have demonstrated that tunicamycin has an inhibitory effect on migration, both *in vivo* with epithelial sheet movement using organotypic cell cultures (Gipson et al., 1984) and *in vitro* with human airway epithelial cell wound repair (Dorscheid et al., 2001). The activation of the IRE1 and ATF6 pathways by tunicamycin also appeared to inhibit PDGF-BB induced migration in vascular smooth muscle cells (Yi et al., 2012). There is evidently a knock on effect with ER stress and migration but this may ultimately depend on the tissue environment in which the stressed cells lie (Sáez et al., 2014); as in cancer, ER stress promotes angiogenesis and invasion which contrasts somewhat to the discussed effects of tunicamycin.

4.3.1 Does tunicamycin affect cell motility differentially between HeLa and HT1080 cells?

The results seen here were certainly varied between cell types, with the HeLa cells showing a consistent change in phenotype when treated with tunicamycin. The graphs indicate that for both the repeat and the initial experiment, the tunicamycin does indeed inhibit the motility of the cells significantly (as confirmed by the 1 way ANOVA T-test). This significant decline in cellular migration fits with the known action of tunicamycin, and suggests that the stress response is affecting the behaviour of the cells in a way that is expected *in vitro*. The HT1080 cells however show a different pattern with a significant increase in motility seen in the tunicamycin treatment. This result is more variable than the HeLa cells however, and could indicate random variability in the cell motility when compared with the large replicable decline in migration in the HeLa cells. If the combined data is used to summarise and average out the data pools then it shows that the decline in motility seen in the mock vs

tunicamycin on the HeLa cells has a P value of <0.001 whereas in the HT1080 cells, the increase in motility between these two conditions has a P value of <0.01 which is significant to a lesser extent. Tunicamycin clearly affects the HeLa cells potently, inhibiting their motility, but with the HT1080 cells, the effect is less potent, and the trend – if any – is an increase in motility.

When looking at the action of genistein in conjunction with tunicamycin, the HeLa cells do not show any significant difference to the tunicamycin treatment alone. The genistein with tunicamycin treatment does show a similar decrease in motility compared to the mock, but it is clear that here, genistein does not have a synergistic effect with tunicamycin. Interestingly; the genistein on its own vs the mock treatment does show a decrease in motility that is significant. This could potentially be due to the genistein causing an increased susceptibility of the cell to any natural stress that may occur. The HeLa results show a nicely uniform pattern of how both tunicamycin and genistein affect the cells. Again though, in the HT1080 cells, the pattern of genistein action on the cells is variable, with a difference between the initial experiment and the repeat. The first experiment certainly showed a decrease of motility in the genistein with tunicamycin treatment when compared to just the tunicamycin, but this may be simply due to the possibly anomalous large increase in motility seen in the tunicamycin condition. In the second experiment, there is no significant difference with the addition of genistein. When looking at the combined result for the HT1080 cells, genistein + tunicamycin significantly decreases the motility of the cells compared to just the tunicamycin alone. This suggests that genistein does rescue the effects of tunicamycin on the HT1080 cells by restoring the cell motility to levels comparable with the mock treatment. Also no decrease in motility is seen in response to genistein treatment alone when compared to the mock.

Interestingly, the cell specific reactions to genistein here reflects what was seen in the earlier blot for GRP94. In the HeLa cells, untreated cells with genistein elicited an increase in the expression of the stress marker which reflects the decrease in motility seen in the presence of genistein in the HeLa cells (like the decrease in motility seen with tunicamycin). However, in the HT1080 cells GRP94 expression was decreased in

the untreated cells with genistein; the lower levels of this stress marker in the presence of genistein backs up the fact that no change in motility was seen when genistein was added to the untreated cells.

The cell morphology did not change at a gross level during live cell imaging; apart from the cells that are undergoing apoptosis. It is important to note that the images seen do not visualise the cell membrane however and instead are visualising the endoplasmic reticulum, and therefore changes in morphology may still be occurring beyond what can be seen in these experiments.

From these data, the clearest conclusion is that tunicamycin differentially affects HeLa cells and HT1080 cells in terms of their motility, with the HeLa cells showing a significant decrease in motility with tunicamycin as opposed to HT1080 cells which show either an increase in motility, or no change. The genistein itself seems to have no clear-cut effect on the motility of the cells, which may be simply because the pathways genistein acts upon do not affect motility. However if genistein was restoring ER stress and driving the cells towards apoptosis, a further decrease in motility would be expected when genistein is combined with tunicamycin.

4.4 Overall conclusions

In conclusion, the results here have demonstrated a differential protein expression profile between different cell types when subjected to pharmacologically induced stress. The P-STAT3 results have clearly shown a higher baseline level of activation in the HT1080 cells which is likely due to the N-Ras mutation inherent to this cell line. The P-STAT3 expression in the HeLa cells is likely indicative of PERK pathway activation in the UPR, but in the HT1080 cells, it may not be as clear cut due to the constitutive STAT3 activation. In terms of ER stress seen in the cells, it would appear overall that the HT1080 cells exhibit a low level, chronic stress response which may be transiently increased by tunicamycin, but ultimately this cell line seems to be showing a pro-survival phenotype when looking at the blots in conjunction with the live cell imaging. The HeLa cells on the other hand do not seem to exhibit the same initial low level stress response. The HeLa cells do seem to show an immediate reaction to tunicamycin with the expression of phospho-p44/42 like the HT1080 cells,

but ultimately seem to have a less constant and later activated response to the stress compared to the HT1080 cells.

It may ultimately be that the HT1080 cells and HeLa cells both react initially to the tunicamycin in the same way, but it is the later response that differs, with other stress indicators in the HeLa cells taking longer to appear, compared to the more continuous stress in the HT1080 cells. When viewed in conjunction with the live cell imaging it becomes clear that the HeLa cells are more sensitive to tunicamycin induced ER stress than the HT1080 cells, due to a significant inhibition of HeLa motility which may possibly precede apoptosis. This may be because the HT1080 cells have inherent mutations (N-Ras) that mean particular stress related pathways are already active. Therefore, it is possible that the threshold for ER stress to overwhelm the HT1080 cells and push them towards apoptosis instead of survival may be higher than the HeLa cells, due to a native stressed cellular environment in the HT1080 cells. This may suggest that the higher baseline stress response in the HT1080 cells results in irremediable stress that cannot be conventionally dealt with. The HeLa cells show increased sensitivity to stress, the effects of which are only evident towards the 6 hour timepoint in the blots, but are clearly evident in the live cell imaging via the gradual arrest of cell motility. The effects of genistein are mostly not evident, although a particularly interesting point is the decrease in phosphorylated AKT seen when genistein is added to the 10 minute tunicamycin treatment. This justifies the need for further investigation into how genistein may affect other stress related pathways, even if it does not noticeably influence aspects such as cell motility or observable apoptosis. **Figure 4.1** indicates the temporal differences in the expression of the main proteins that indicated reactions to the induced ER stress.

While the modulation of ER stress via genistein is still unclear; the differential reaction of the cells to tunicamycin suggests that therapy for ER stress related diseases such as ankylosing spondylitis and specific cancers may require specific drugs for different cell types. Inducing ER stress can clearly inhibit migration in HeLa cells but the lack of response seen in HT1080 cells may suggest that certain mutations can block the traditional response to increasing ER stress by creating an environment in the cell and ER that allows unresolvable stress to exist without interfering with

important cellular functions involved in disease pathology such as migration which is key for tumorigenesis.

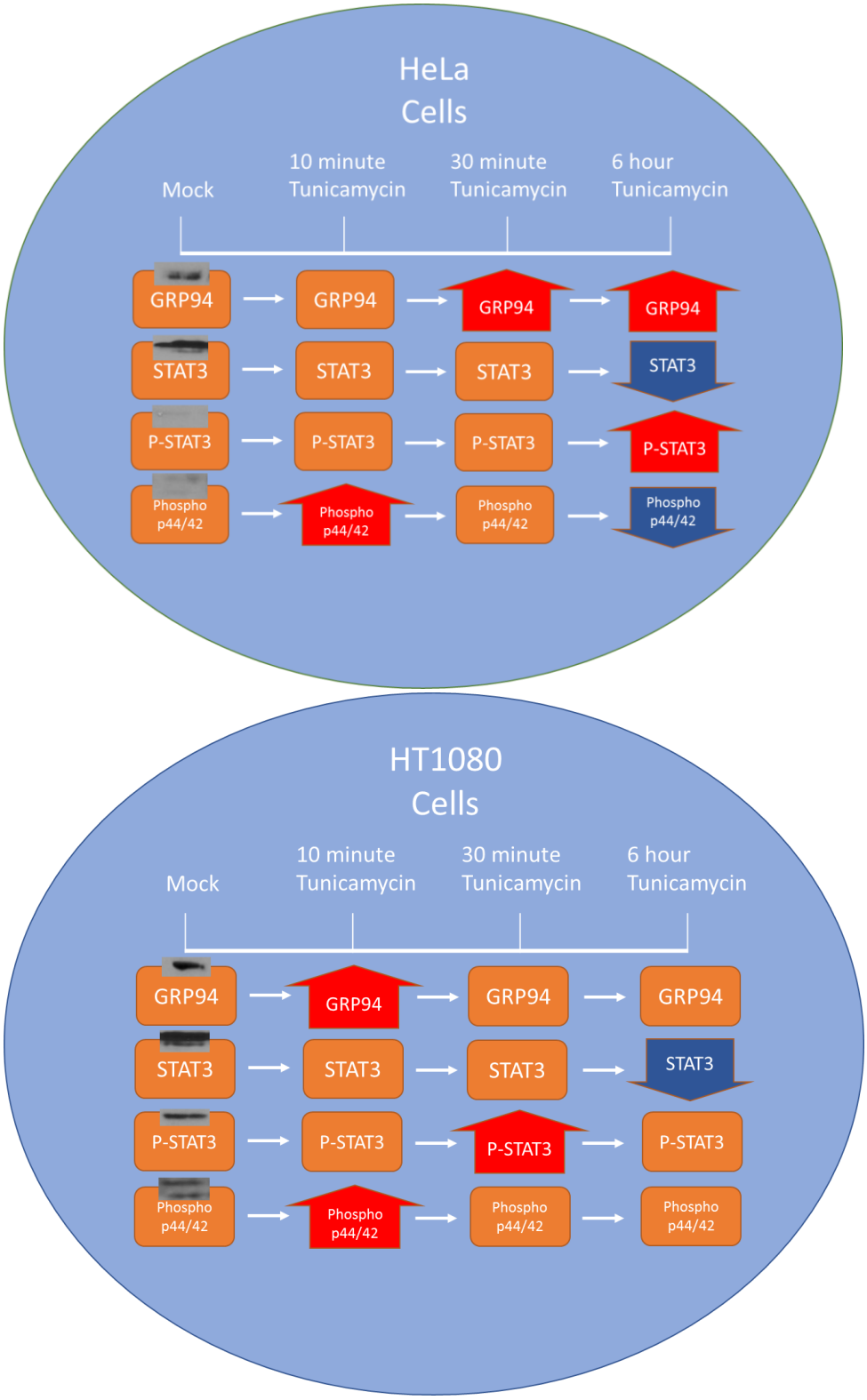

Figure 4.1: Temporal differences in ER stress induced protein expression between HeLa and HT1080 cells.

Flow chart showing how the expression of 4 proteins of interest (GRP94, STAT3, P-STAT3 and phospho-p44/42 MAPK) changes after various timed tunicamycin treatments. Initial untreated blots shown for comparison. Each change is relative to the previous time point, with a box representing no change, an upwards arrow indicating an increase in expression and a downwards arrow indicating a decrease in expression.

The difference between how the two cell lines react to induced ER stress may seem abstract, but it is likely due to the highly complex interlinking of various pathways involved in ER stress, and the possibility that mutations in various pathways and differing proteomes may also affect the cell behaviour. **Figure 4.2** shows the main observed consequences of tunicamycin induced ER stress in both HeLa cells and HT1080 cells, helping indicate the differences between the cell lines. It is also important to consider that these two cells are different cell types; with HT1080 cells being isolated from a fibrosarcoma (fibroblasts) and HeLa cells being isolated from a cervical adenocarcinoma (epithelial cells) Inherently; fibroblasts have a large and highly elaborate endoplasmic reticulum to fit their purpose as major components in ECM secretion (Baum and Duffy, 2011). Epithelial cells may also have a large endoplasmic reticulum for fat absorption and enzyme secretion (Friedman and Cardell, 1977); but perhaps a difference in purpose of the ER in these cell types may cause differential re-organisation of the ER when subjected to stress. These two cell types are also two very different types of cancer with distinct and different activating mutations that may well affect how they respond to stress.

4.5 Future directions

There is plenty of scope for further investigation after these results. Primarily, the reason behind the differential cellular response to stress needs to be investigated. Is this because of the mutations in HT1080 cells, or due to the different functions of these cell types? The action of genistein on modulating ER stress needs further investigation, and obtaining clean blots for the P-tyrosine expression profile would be a starting point. Then looking at more direct stress indicators such as a working BiP blot and other phosphorylated proteins involved in the UPR signalling pathways such as JNK would flesh out the data, and would demonstrate exactly what pathways were being activated in the UPR.

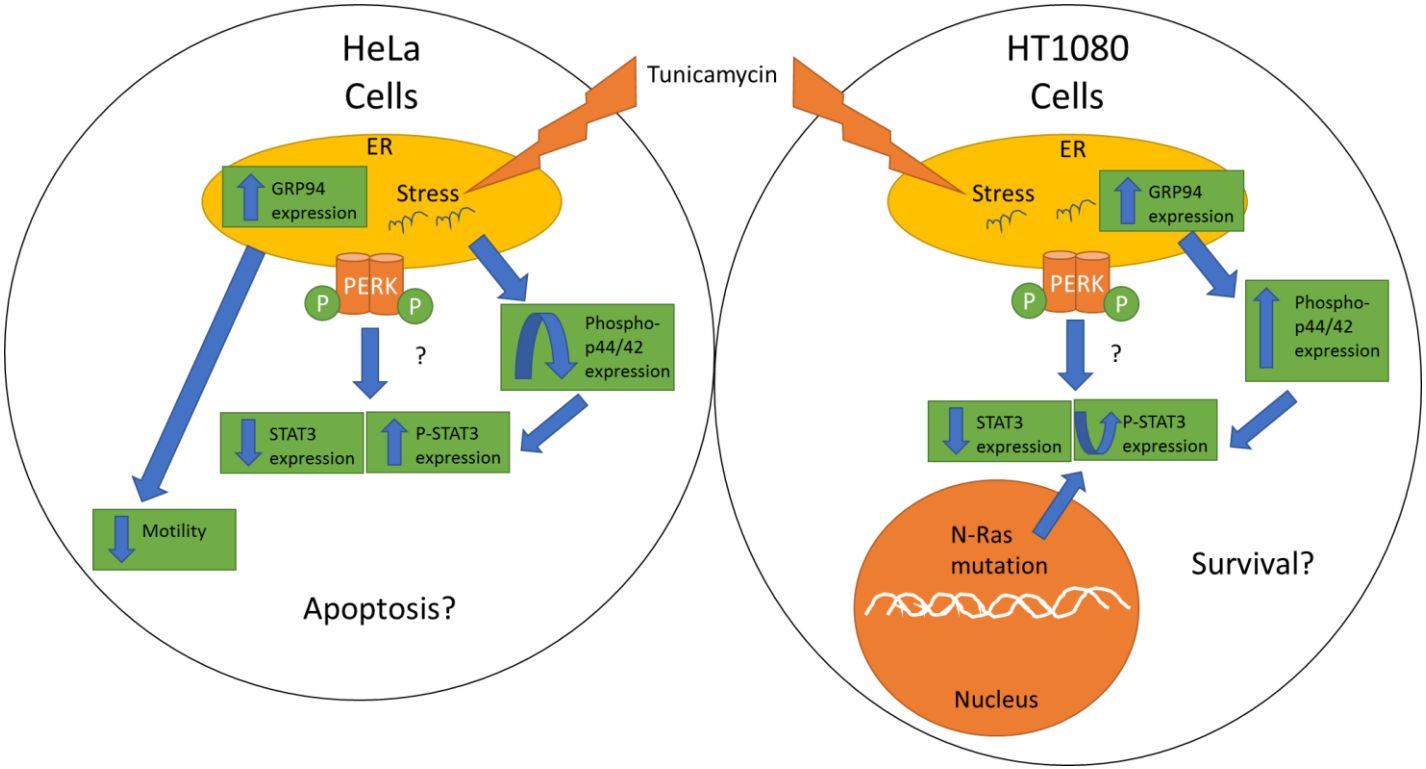

Figure 4.2: Tunicamycin induced stress elicits a differential response in HeLa and HT1080 cells.
Treatment of both HeLa and HT1080 cell lines resulted in an increase of GRP94 expression across both cell lines. In the HeLa cells, P-STAT3 expression was increased – a possible consequence of PERK activation. In the HT1080 cells, P-STAT3 expression decreased from a higher baseline level after 10 minutes of tunicamycin treatment and then increased again – the initial P-STAT3 expression possibly due to the endogenous N-Ras mutation in the HT1080 cells. In the HeLa cells, phospho-p44/42 MAPK increased at first and then decreased after 6 hours, whereas in the HT1080 cells, the expression was raised more consistently after tunicamycin treatment. P44/42 activity may have contributed to STAT3 phosphorylation. Motility was decreased in the HeLa cells after tunicamcycin treatment, but not in the HT1080 cells. While not directly observed, the live cell imaging results pointed to the HeLa cells moving towards apoptosis, and the HT1080 cells surviving under the ER stress.

=

Chapter 5: References

Ali, M.M.U., Bagratuni, T., Davenport, E.L., Nowak, P.R., Silva-Santisteban, M.C., Hardcastle, A., McAndrews, C., Rowlands, M.G., Morgan, G.J., Aherne, W., Collins, I., Davies, F.E., Pearl, L.H., 2011. Structure of the Ire1 autophosphorylation complex and implications for the unfolded protein response. EMBO J. 30, 894–905. https://doi.org/10.1038/emboj.2011.18

Allen, R.L., O'Callaghan, C.A., McMichael, A.J., Bowness, P., 1999. Cutting edge: HLA-B27 can form a novel beta 2-microglobulin-free heavy chain homodimer structure. J. Immunol. Baltim. Md 1950 162, 5045–5048.

Anfinsen, C.B., 1972. The formation and stabilization of protein structure. Biochem. J. 128, 737–749.

Arrington, D.D., Schnellmann, R.G., 2008. Targeting of the molecular chaperone oxygen-regulated protein 150 (ORP150) to mitochondria and its induction by cellular stress. Am. J. Physiol. - Cell Physiol. 294, C641–C650. https://doi.org/10.1152/ajpcell.00400.2007

Auf, G., Jabouille, A., Guérit, S., Pineau, R., Delugin, M., Bouchecareilh, M., Magnin, N., Favereaux, A., Maitre, M., Gaiser, T., von Deimling, A., Czabanka, M., Vajkoczy, P., Chevet, E., Bikfalvi, A., Moenner, M., 2010. Inositol-requiring enzyme 1alpha is a key regulator of angiogenesis and invasion in malignant glioma. Proc. Natl. Acad. Sci. U. S. A. 107, 15553–15558. https://doi.org/10.1073/pnas.0914072107

Back, S.H., Kaufman, R.J., 2012. Endoplasmic Reticulum Stress and Type 2 Diabetes. Annu. Rev. Biochem. 81, 767–793. https://doi.org/10.1146/annurev-biochem-072909-095555

BANERJEE, S., LI, Y., WANG, Z., SARKAR, F.H., 2008. MULTI-TARGETED THERAPY OF CANCER BY GENISTEIN. Cancer Lett. 269, 226–242. https://doi.org/10.1016/j.canlet.2008.03.052

Barnstable, C.J., Bodmer, W.F., Brown, G., Galfre, G., Milstein, C., Williams, A.F., Ziegler, A., 1978. Production of monoclonal antibodies to group A erythrocytes, HLA and other human cell surface antigens-new tools for genetic analysis. Cell 14, 9–20.

Baum, J., Duffy, H.S., 2011. Fibroblasts and Myofibroblasts: What are we talking about? J. Cardiovasc. Pharmacol. 57, 376–379. https://doi.org/10.1097/FJC.0b013e3182116e39

BAX BCL2 associated X, apoptosis regulator [Homo sapiens (human)] - Gene - NCBI [WWW Document], n.d. URL http://www.ncbi.nlm.nih.gov/gene/581 (accessed 9.6.16).

Benham, A.M., Cabibbo, A., Fassio, A., Bulleid, N., Sitia, R., Braakman, I., 2000. The CXXCXXC motif determines the folding, structure and stability of human Ero1-Lα. EMBO J. 19, 4493–4502. https://doi.org/10.1093/emboj/19.17.4493

Blais, J.D., Addison, C.L., Edge, R., Falls, T., Zhao, H., Wary, K., Koumenis, C., Harding, H.P., Ron, D., Holcik, M., Bell, J.C., 2006. Perk-dependent translational regulation promotes tumor cell adaptation and angiogenesis in response to hypoxic stress. Mol. Cell. Biol. 26, 9517–9532. https://doi.org/10.1128/MCB.01145-06

Bobrovnikova-Marjon, E., Grigoriadou, C., Pytel, D., Zhang, F., Ye, J., Koumenis, C., Cavener, D., Diehl, J.A., 2010. PERK promotes cancer cell proliferation and tumor growth by limiting oxidative DNA damage. Oncogene 29, 3881–3895. https://doi.org/10.1038/onc.2010.153

Braun, J., Bollow, M., Remlinger, G., Eggens, U., Rudwaleit, M., Distler, A., Sieper, J., 1998. Prevalence of spondylarthropathies in HLA-B27 positive and negative blood donors. Arthritis Rheum. 41, 58–67. https://doi.org/10.1002/1529-0131(199801)41:1<58::AID-ART8>3.0.CO;2-G

Cao, S.S., Kaufman, R.J., 2014. Endoplasmic Reticulum Stress and Oxidative Stress in Cell Fate Decision and Human Disease. Antioxid. Redox Signal. 21, 396–413. https://doi.org/10.1089/ars.2014.5851

Carrasco, D.R., Sukhdeo, K., Protopopova, M., Sinha, R., Enos, M., Carrasco, D.E., Zheng, M., Mani, M., Henderson, J., Pinkus, G.S., Munshi, N., Horner, J., Ivanova, E.V., Protopopov, A., Anderson, K.C., Tonon, G., DePinho, R.A., 2007. The Differentiation and Stress Response Factor XBP-1 Drives Multiple Myeloma Pathogenesis. Cancer Cell 11, 349–360. https://doi.org/10.1016/j.ccr.2007.02.015

Cattaneo, M., Fontanella, E., Canton, C., Delia, D., Biunno, I., 2005. SEL1L Affects Human Pancreatic Cancer Cell Cycle and Invasiveness through Modulation of PTEN and Genes Related to Cell–Matrix Interactions. Neoplasia N. Y. N 7, 1030–1038.

Chan, A.T., Kollnberger, S.D., Wedderburn, L.R., Bowness, P., 2005. Expansion and enhanced survival of natural killer cells expressing the killer immunoglobulin-like receptor KIR3DL2 in spondylarthritis. Arthritis Rheum. 52, 3586–3595. https://doi.org/10.1002/art.21395

Chang, S.-C., Momburg, F., Bhutani, N., Goldberg, A.L., 2005. The ER aminopeptidase, ERAP1, trims precursors to lengths of MHC class I peptides by a “molecular ruler” mechanism. Proc. Natl. Acad. Sci. U. S. A. 102, 17107–17112. https://doi.org/10.1073/pnas.0500721102

Chen, Y., Brandizzi, F., 2013. IRE1: ER stress sensor and cell fate executor. Trends Cell Biol. 23. https://doi.org/10.1016/j.tcb.2013.06.005

Cheriyath, V., Desgranges, Z.P., Roy, A.L., 2002. c-Src-dependent Transcriptional Activation of TFII-I. J. Biol. Chem. 277, 22798–22805.

Chial, H.J., Thompson, H.B., Splittgerber, A.G., 1993. A spectral study of the charge forms of Coomassie blue G. Anal. Biochem. 209, 258–266. https://doi.org/10.1006/abio.1993.1117

Clarke, H.J., Chambers, J.E., Liniker, E., Marciniak, S.J., 2014. Endoplasmic Reticulum Stress in Malignancy. Cancer Cell 25, 563–573. https://doi.org/10.1016/j.ccr.2014.03.015

Colbert, R.A., Tran, T.M., Layh-Schmitt, G., 2014. HLA-B27 Misfolding and Ankylosing Spondylitis. Mol. Immunol. 57. https://doi.org/10.1016/j.molimm.2013.07.013

Cortes, A., Pulit, S.L., Leo, P.J., Pointon, J.J., Robinson, P.C., Weisman, M.H., Ward, M., Gensler, L.S., Zhou, X., Garchon, H.-J., Chiocchia, G., Nossent, J., Lie, B.A., Førre, Ø., Tuomilehto, J., Laiho, K., Bradbury, L.A., Elewaut, D., Burgos-Vargas, R., Stebbings, S., Appleton, L., Farrah, C., Lau, J., Haroon, N., Mulero, J., Blanco, F.J., Gonzalez-Gay, M.A., Lopez-Larrea, C., Bowness, P., Gaffney, K., Gaston, H., Gladman, D.D., Rahman, P., Maksymowych, W.P., Crusius, J.B.A., van der Horst-Bruinsma, I.E., Valle-Oñate, R., Romero-Sánchez, C., Hansen, I.M., Pimentel-Santos, F.M., Inman, R.D., Martin, J., Breban, M., Wordsworth, B.P., Reveille, J.D., Evans, D.M., de Bakker, P.I.W., Brown, M.A., 2015. Major histocompatibility complex associations of ankylosing spondylitis are complex and involve further epistasis with ERAP1. Nat. Commun. 6. https://doi.org/10.1038/ncomms8146

Cullinan, S.B., Diehl, J.A., 2004. PERK-dependent activation of Nrf2 contributes to redox homeostasis and cell survival following endoplasmic reticulum stress. J. Biol. Chem. 279, 20108–20117. https://doi.org/10.1074/jbc.M314219200

Cullinan, S.B., Zhang, D., Hannink, M., Arvisais, E., Kaufman, R.J., Diehl, J.A., 2003. Nrf2 Is a Direct PERK Substrate and Effector of PERK-Dependent Cell Survival. Mol. Cell. Biol. 23, 7198–7209. https://doi.org/10.1128/MCB.23.20.7198-7209.2003

Dai, R.Y., Chen, S.K., Yan, D.M., Chen, R., Lui, Y.P., Duan, C.Y., Li, J., He, T., Li, H., 2010. PI3K/Akt promotes GRP78 accumulation and inhibits endoplasmic reticulum stress-induced apoptosis in HEK293 cells. Folia Biol. (Praha) 56, 37–46.

Dean, L.E., Jones, G.T., MacDonald, A.G., Downham, C., Sturrock, R.D., Macfarlane, G.J., 2014. Global prevalence of ankylosing spondylitis. Rheumatology 53, 650–657. https://doi.org/10.1093/rheumatology/ket387

Del Porto, P., D'Amato, M., Fiorillo, M.T., Tuosto, L., Piccolella, E., Sorrentino, R., 1994. Identification of a novel HLA-B27 subtype by restriction analysis of a cytotoxic gamma delta T cell clone. J. Immunol. Baltim. Md 1950 153, 3093–3100.

Dorscheid, D.R., Wojcik, K.R., Yule, K., White, S.R., 2001. Role of cell surface glycosylation in mediating repair of human airway epithelial cell monolayers. Am. J. Physiol. Lung Cell. Mol. Physiol. 281, L982-992.

Eletto, D., Dersh, D., Argon, Y., 2010. GRP94 in ER Quality Control and Stress Responses. Semin. Cell Dev. Biol. 21, 479–485. https://doi.org/10.1016/j.semcdb.2010.03.004

Esko, J.D., Bertozzi, C.R., 2009. Chemical Tools for Inhibiting Glycosylation, in: Varki, A., Cummings, R.D., Esko, J.D., Freeze, H.H., Stanley, P., Bertozzi, C.R., Hart, G.W., Etzler, M.E. (Eds.), Essentials of Glycobiology. Cold Spring Harbor Laboratory Press, Cold Spring Harbor (NY).

Fedorov, A.N., Baldwin, T.O., 1997. Cotranslational Protein Folding. J. Biol. Chem. 272, 32715–32718. https://doi.org/10.1074/jbc.272.52.32715

Friedman, H.I., Cardell, R.R., 1977. Alterations in the endoplasmic reticulum and golgi complex of intestinal epithelial cells during fat absorption and after termination of this process: A morphological and morphometric study. Anat. Rec. 188, 77–101. https://doi.org/10.1002/ar.1091880109

Galindo, I., Hernáez, B., Muñoz-Moreno, R., Cuesta-Geijo, M.A., Dalmau-Mena, I., Alonso, C., 2012. The ATF6 branch of unfolded protein response and apoptosis are activated to promote African swine fever virus infection. Cell Death Dis. 3, e341. https://doi.org/10.1038/cddis.2012.81

Gipson, I.K., Kiorpes, T.C., Brennan, S.J., 1984. Epithelial sheet movement: effects of tunicamycin on migration and glycoprotein synthesis. Dev. Biol. 101, 212–220.

Gogada, R., Yadav, N., Liu, J., Tang, S., Zhang, D., Schneider, A., Seshadri, A., Sun, L., Aldaz, C.M., Tang, D., Chandra, D., 2012. BIM, a proapoptotic protein, upregulated via transcription factor E2F1-dependent mechanism, functions as a prosurvival molecule in cancer. J. Biol. Chem. jbc.M112.386102. https://doi.org/10.1074/jbc.M112.386102

Gorman, J.D., Sack, K.E., Davis, J.C., 2002. Treatment of Ankylosing Spondylitis by Inhibition of Tumor Necrosis Factor α. N. Engl. J. Med. 346, 1349–1356. https://doi.org/10.1056/NEJMoa012664

Granados, D.P., Tanguay, P.-L., Hardy, M.-P., Caron, É., de Verteuil, D., Meloche, S., Perreault, C., 2009. ER stress affects processing of MHC class I-associated peptides. BMC Immunol. 10, 10. https://doi.org/10.1186/1471-2172-10-10

Gupta, S., Plattner, R., Der, C.J., Stanbridge, E.J., 2000. Dissection of Ras-dependent signaling pathways controlling aggressive tumor growth of human fibrosarcoma cells: evidence for a potential novel pathway. Mol. Cell. Biol. 20, 9294–9306.

Han, D., Lerner, A.G., Walle, L.V., Upton, J.-P., Xu, W., Hagen, A., Backes, B.J., Oakes, S.A., Papa, F.R., 2009. IRE1α Kinase Activation Modes Control Alternate Endoribonuclease Outputs to Determine Divergent Cell Fates. Cell 138, 562–575. https://doi.org/10.1016/j.cell.2009.07.017

Han, J., Back, S.H., Hur, J., Lin, Y.-H., Gildersleeve, R., Shan, J., Yuan, C.L., Krokowski, D., Wang, S., Hatzoglou, M., Kilberg, M.S., Sartor, M.A., Kaufman, R.J., 2013. ER-stress-induced transcriptional regulation increases protein synthesis leading to cell death. Nat. Cell Biol. 15, 481–490. https://doi.org/10.1038/ncb2738

Harding, H.P., Novoa, I., Zhang, Y., Zeng, H., Wek, R., Schapira, M., Ron, D., 2000. Regulated Translation Initiation Controls Stress-Induced Gene Expression in Mammalian Cells. Mol. Cell 6, 1099–1108. https://doi.org/10.1016/S1097-2765(00)00108-8

HAYAKAWA, R., HAYAKAWA, T., TAKEDA, K., ICHIJO, H., 2012. Therapeutic targets in the ASK1-dependent stress signaling pathways. Proc. Jpn. Acad. Ser. B Phys. Biol. Sci. 88, 434–453. https://doi.org/10.2183/pjab.88.434

He, C.H., Gong, P., Hu, B., Stewart, D., Choi, M.E., Choi, A.M.K., Alam, J., 2001. Identification of Activating Transcription Factor 4 (ATF4) as an Nrf2-interacting Protein IMPLICATION FOR HEME OXYGENASE-1 GENE REGULATION. J. Biol. Chem. 276, 20858–20865. https://doi.org/10.1074/jbc.M101198200

Hetz, C., 2012. The unfolded protein response: controlling cell fate decisions under ER stress and beyond. Nat. Rev. Mol. Cell Biol. 13, 89–102. https://doi.org/10.1038/nrm3270

Hetz, C., Martinon, F., Rodriguez, D., Glimcher, L.H., 2011. The Unfolded Protein Response: Integrating Stress Signals Through the Stress Sensor IRE1α. Physiol. Rev. 91, 1219–1243. https://doi.org/10.1152/physrev.00001.2011

Hewitt, E.W., 2003. The MHC class I antigen presentation pathway: strategies for viral immune evasion. Immunology 110, 163–169. https://doi.org/10.1046/j.1365-2567.2003.01738.x

Hoffmann, J.H., Linke, K., Graf, P.C., Lilie, H., Jakob, U., 2004. Identification of a redox-regulated chaperone network. EMBO J. 23, 160–168. https://doi.org/10.1038/sj.emboj.7600016

Hong, M., Lin, M., Huang, J., Baumeister, P., Hakre, S., Roy, A.L., Lee, A.S., 2005a. Transcriptional Regulation of the Grp78 Promoter by Endoplasmic Reticulum Stress ROLE OF TFII-I AND ITS TYROSINE PHOSPHORYLATION. J. Biol. Chem. 280, 16821–16828. https://doi.org/10.1074/jbc.M413753200

Hong, M., Lin, M., Huang, J., Baumeister, P., Hakre, S., Roy, A.L., Lee, A.S., 2005b. Transcriptional Regulation of the Grp78 Promoter by Endoplasmic Reticulum Stress ROLE OF TFII-I AND ITS TYROSINE PHOSPHORYLATION. J. Biol. Chem. 280, 16821–16828. https://doi.org/10.1074/jbc.M413753200

Hotamisligil, G.S., 2010. Endoplasmic Reticulum Stress and the Inflammatory Basis of Metabolic Disease. Cell 140, 900–917. https://doi.org/10.1016/j.cell.2010.02.034

Huang, Y., Qiu, J., Dong, S., Redell, M.S., Poli, V., Mancini, M.A., Tweardy, D.J., 2007. Stat3 isoforms, alpha and beta, demonstrate distinct intracellular dynamics with prolonged nuclear retention of Stat3beta mapping to its unique C-terminal end. J. Biol. Chem. 282, 34958–34967. https://doi.org/10.1074/jbc.M704548200

Huber, A.-L., Lebeau, J., Guillaumot, P., Pétrilli, V., Malek, M., Chilloux, J., Fauvet, F., Payen, L., Kfoury, A., Renno, T., Chevet, E., Manié, S.N., 2013. p58(IPK)-mediated attenuation of the proapoptotic PERK-CHOP pathway allows malignant progression upon low glucose. Mol. Cell 49, 1049–1059. https://doi.org/10.1016/j.molcel.2013.01.009

Hyoda, K., Hosoi, T., Horie, N., Okuma, Y., Ozawa, K., Nomura, Y., 2006. PI3K-Akt inactivation induced CHOP expression in endoplasmic reticulum-stressed cells. Biochem. Biophys. Res. Commun. 340, 286–290. https://doi.org/10.1016/j.bbrc.2005.12.007

Iurlaro, R., Muñoz-Pinedo, C., 2016. Cell death induced by endoplasmic reticulum stress. FEBS J. 283, 2640–2652. https://doi.org/10.1111/febs.13598

Kim, H., Bhattacharya, A., Qi, L., 2015. Endoplasmic reticulum quality control in cancer: Friend or foe. Semin. Cancer Biol., Theme Series - UPR in Cancer 33, 25–33. https://doi.org/10.1016/j.semcancer.2015.02.003

Kimura, K., Yamada, T., Matsumoto, M., Kido, Y., Hosooka, T., Asahara, S., Matsuda, T., Ota, T., Watanabe, H., Sai, Y., Miyamoto, K., Kaneko, S., Kasuga, M., Inoue, H., 2012. Endoplasmic Reticulum Stress Inhibits STAT3-Dependent Suppression of Hepatic

Gluconeogenesis via Dephosphorylation and Deacetylation. Diabetes 61, 61–73. https://doi.org/10.2337/db10-1684
Kozaci, L.D., Sari, I., Alacacioglu, A., Akar, S., Akkoc, N., 2009. Evaluation of inflammation and oxidative stress in ankylosing spondylitis: a role for macrophage migration inhibitory factor. Mod. Rheumatol. 20, 34–39. https://doi.org/10.1007/s10165-009-0230-9
Krämer, D.K., Bouzakri, K., Holmqvist, O., Al-Khalili, L., Krook, A., 2005. Effect of serum replacement with plysate on cell growth and metabolismin primary cultures of human skeletal muscle. Cytotechnology 48, 89–95. https://doi.org/10.1007/s10616-005-4074-7
Lamech, L.T., Haynes, C.M., 2015. The unpredictability of prolonged activation of stress response pathways. J. Cell Biol. 209, 781–787. https://doi.org/10.1083/jcb.201503107
Leblanc, V., Delumeau, I., Tocqué, B., 1999. Ras-GTPase activating protein inhibition specifically induces apoptosis of tumour cells. Oncogene 18, 4884–4889. https://doi.org/10.1038/sj.onc.1202855
Lee, A.-H., Iwakoshi, N.N., Glimcher, L.H., 2003. XBP-1 Regulates a Subset of Endoplasmic Reticulum Resident Chaperone Genes in the Unfolded Protein Response. Mol. Cell. Biol. 23, 7448–7459. https://doi.org/10.1128/MCB.23.21.7448-7459.2003
Lee, A.S., 2005. The ER chaperone and signaling regulator GRP78/BiP as a monitor of endoplasmic reticulum stress. Methods San Diego Calif 35, 373–381. https://doi.org/10.1016/j.ymeth.2004.10.010
Lemin, A.J., 2007. Characterisation of the oxidoreductase Erol-Lß and the misfolding of the secretory pathway substrate HLA-B27 (Unspecified). Durham University.
Lemin, A.J., Saleki, K., van Lith, M., Benham, A.M., 2007. Activation of the unfolded protein response and alternative splicing of ATF6α in HLA-B27 positive lymphocytes. FEBS Lett. 581, 1819–1824. https://doi.org/10.1016/j.febslet.2007.03.069
Leung-Hagesteijn, C., Erdmann, N., Cheung, G., Keats, J.J., Stewart, A.K., Reece, D.E., Chung, K.C., Tiedemann, R.E., 2013. Xbp1s-negative tumor B cells and pre-plasmablasts mediate therapeutic proteasome inhibitor resistance in multiple myeloma. Cancer Cell 24, 289–304. https://doi.org/10.1016/j.ccr.2013.08.009
Li, B., Yi, P., Zhang, B., Xu, C., Liu, Q., Pi, Z., Xu, X., Chevet, E., Liu, J., 2011. Differences in endoplasmic reticulum stress signalling kinetics determine cell survival outcome through activation of MKP-1. Cell. Signal. 23, 35–45. https://doi.org/10.1016/j.cellsig.2010.07.019
Li, X., Zhang, K., Li, Z., 2011. Unfolded protein response in cancer: the Physician's perspective. J. Hematol. Oncol.J Hematol Oncol 4, 8. https://doi.org/10.1186/1756-8722-4-8
Lindholm, D., Wootz, H., Korhonen, L., 2006. ER stress and neurodegenerative diseases. Cell Death Differ. 13, 385–392. https://doi.org/10.1038/sj.cdd.4401778
Liu, C.Y., Schröder, M., Kaufman, R.J., 2000. Ligand-independent dimerization activates the stress response kinases IRE1 and PERK in the lumen of the endoplasmic reticulum. J. Biol. Chem. 275, 24881–24885. https://doi.org/10.1074/jbc.M004454200
Liu, T., Qian, W.-J., Gritsenko, M.A., Camp, D.G., Monroe, M.E., Moore, R.J., Smith, R.D., 2005. Human Plasma N-Glycoproteome Analysis by Immunoaffinity Subtraction, Hydrazide Chemistry, and Mass Spectrometry. J. Proteome Res. 4, 2070–2080. https://doi.org/10.1021/pr0502065
Marais, R., Light, Y., Paterson, H.F., Marshall, C.J., 1995. Ras recruits Raf-1 to the plasma membrane for activation by tyrosine phosphorylation. EMBO J. 14, 3136–3145.

Marzec, M., Eletto, D., Argon, Y., 2012. GRP94: an HSP90-like protein specialized for protein folding and quality control in the Endoplasmic Reticulum. Biochim. Biophys. Acta 1823, 774–787. https://doi.org/10.1016/j.bbamcr.2011.10.013

Mayer, M.P., Bukau, B., 2005. Hsp70 chaperones: Cellular functions and molecular mechanism. Cell. Mol. Life Sci. 62, 670–684. https://doi.org/10.1007/s00018-004-4464-6

McCullough, K.D., Martindale, J.L., Klotz, L.O., Aw, T.Y., Holbrook, N.J., 2001. Gadd153 sensitizes cells to endoplasmic reticulum stress by down-regulating Bcl2 and perturbing the cellular redox state. Mol. Cell. Biol. 21, 1249–1259. https://doi.org/10.1128/MCB.21.4.1249-1259.2001

McGonagle, D., 2009. Entheses, enthesitis and enthesopathy. Arthritis Res. UK, Topical Reviews.

Meares, G., Benveniste, E., 2013. ER stress and neuroinflammation: connecting the unfolded protein response to JAK/STAT signaling (P5196). J. Immunol. 190, 198.5-198.5.

Meares, G.P., Liu, Y., Rajbhandari, R., Qin, H., Nozell, S.E., Mobley, J.A., Corbett, J.A., Benveniste, E.N., 2014. PERK-Dependent Activation of JAK1 and STAT3 Contributes to Endoplasmic Reticulum Stress-Induced Inflammation. Mol. Cell. Biol. 34, 3911–3925. https://doi.org/10.1128/MCB.00980-14

Mueller, B., Klemm, E.J., Spooner, E., Claessen, J.H., Ploegh, H.L., 2008. SEL1L nucleates a protein complex required for dislocation of misfolded glycoproteins. Proc. Natl. Acad. Sci. 105, 12325–12330. https://doi.org/10.1073/pnas.0805371105

Nicknam, M.H., Mahmoudi, M., Amirzargar, A.A., Jamshidi, A.R., Rezaei, N., Nikbin, B., 2009. HLA-B27 subtypes and tumor necrosis factor alpha promoter region polymorphism in Iranian patients with ankylosing spondylitis. Eur. Cytokine Netw. 20, 17–20. https://doi.org/10.1684/ecn.2009.0143

Oslowski, C.M., Urano, F., 2011. Measuring ER stress and the unfolded protein response using mammalian tissue culture system. Methods Enzymol. 490, 71–92. https://doi.org/10.1016/B978-0-12-385114-7.00004-0

Parham, P., Ohta, T., 1996. Population Biology of Antigen Presentation by MHC Class I Molecules. Science 272, 67–74. https://doi.org/10.1126/science.272.5258.67

Parker, R., Phan, T., Baumeister, P., Roy, B., Cheriyath, V., Roy, A.L., Lee, A.S., 2001. Identification of TFII-I as the Endoplasmic Reticulum Stress Response Element Binding Factor ERSF: Its Autoregulation by Stress and Interaction with ATF6. Mol. Cell. Biol. 21, 3220–3233. https://doi.org/10.1128/MCB.21.9.3220-3233.2001

Paul, M.K., Mukhopadhyay, A.K., 2004. Tyrosine kinase – Role and significance in Cancer. Int. J. Med. Sci. 1, 101–115.

Pierce BCA Protein Assay Kit - Thermo Fisher Scientific [WWW Document], n.d. URL https://www.thermofisher.com/order/catalog/product/23225 (accessed 8.2.16).

Pirkmajer, S., Chibalin, A.V., 2011. Serum starvation: caveat emptor. Am. J. Physiol. - Cell Physiol. 301, C272–C279. https://doi.org/10.1152/ajpcell.00091.2011

Plattner, R., Gupta, S., Khosravi-Far, R., Sato, K.Y., Perucho, M., Der, C.J., Stanbridge, E.J., 1999. Differential contribution of the ERK and JNK mitogen-activated protein kinase cascades to Ras transformation of HT1080 fibrosarcoma and DLD-1 colon carcinoma cells. Oncogene 18, 1807–1817. https://doi.org/10.1038/sj.onc.1202482

Puthalakath, H., O'Reilly, L.A., Gunn, P., Lee, L., Kelly, P.N., Huntington, N.D., Hughes, P.D., Michalak, E.M., McKimm-Breschkin, J., Motoyama, N., Gotoh, T., Akira, S., Bouillet, P., Strasser, A., 2007. ER stress triggers apoptosis by activating BH3-only protein Bim. Cell 129, 1337–1349. https://doi.org/10.1016/j.cell.2007.04.027

Rawson, R.B., 2002. Regulated intramembrane proteolysis: from the endoplasmic reticulum to the nucleus. Essays Biochem. 38, 155–168.

Reimold, A.M., Iwakoshi, N.N., Manis, J., Vallabhajosyula, P., Szomolanyi-Tsuda, E., Gravallese, E.M., Friend, D., Grusby, M.J., Alt, F., Glimcher, L.H., 2001. Plasma cell differentiation requires the transcription factor XBP-1. Nature 412, 300–307. https://doi.org/10.1038/35085509

Romero-Ramirez, L., Cao, H., Nelson, D., Hammond, E., Lee, A.-H., Yoshida, H., Mori, K., Glimcher, L.H., Denko, N.C., Giaccia, A.J., Le, Q.-T., Koong, A.C., 2004. XBP1 is essential for survival under hypoxic conditions and is required for tumor growth. Cancer Res. 64, 5943–5947. https://doi.org/10.1158/0008-5472.CAN-04-1606

Ron, D., Walter, P., 2007. Signal integration in the endoplasmic reticulum unfolded protein response. Nat. Rev. Mol. Cell Biol. 8, 519–529. https://doi.org/10.1038/nrm2199

Rutkowski, D.T., Arnold, S.M., Miller, C.N., Wu, J., Li, J., Gunnison, K.M., Mori, K., Sadighi Akha, A.A., Raden, D., Kaufman, R.J., 2006. Adaptation to ER stress is mediated by differential stabilities of pro-survival and pro-apoptotic mRNAs and proteins. PLoS Biol. 4, e374. https://doi.org/10.1371/journal.pbio.0040374

Sáez, P.J., Villalobos-Labra, R., Westermeier, F., Sobrevia, L., Farías-Jofré, M., 2014. Modulation of endothelial cell migration by ER stress and insulin resistance: a role during maternal obesity? Front. Pharmacol. 5. https://doi.org/10.3389/fphar.2014.00189

Sano, R., Reed, J.C., 2013. ER stress-induced cell death mechanisms. Biochim. Biophys. Acta BBA - Mol. Cell Res. 1833, 3460–3470. https://doi.org/10.1016/j.bbamcr.2013.06.028

Schittenhelm, R.B., Sian, T.C.C.L.K., Wilmann, P.G., Dudek, N.L., Purcell, A.W., 2015. Revisiting the arthritogenic peptide theory: quantitative not qualitative changes in the peptide repertoire of HLA-B27 allotypes. Arthritis Rheumatol. Hoboken NJ 67, 702–713. https://doi.org/10.1002/art.38963

Seger, R., Krebs, E.G., 1995. The MAPK signaling cascade. FASEB J. Off. Publ. Fed. Am. Soc. Exp. Biol. 9, 726–735.

Shamji, M.F., Bafaquh, M., Tsai, E., 2008. The pathogenesis of ankylosing spondylitis. Neurosurg. Focus 24, E3. https://doi.org/10.3171/FOC/2008/24/1/E3

Shiau, M., Lo, M., Chang, C., Yang, T., Ho, K., Chang, Y., 2007. Association of tumour necrosis factor α promoter polymorphisms with ankylosing spondylitis in Taiwan. Ann. Rheum. Dis. 66, 562–563. https://doi.org/10.1136/ard.2006.065888

Sieper, J., Braun, J., Rudwaleit, M., Boonen, A., Zink, A., 2002. Ankylosing spondylitis: an overview. Ann. Rheum. Dis. 61, iii8-iii18. https://doi.org/10.1136/ard.61.suppl_3.iii8

Spagnuolo, C., Russo, G.L., Orhan, I.E., Habtemariam, S., Daglia, M., Sureda, A., Nabavi, S.F., Devi, K.P., Loizzo, M.R., Tundis, R., Nabavi, S.M., 2015. Genistein and Cancer: Current Status, Challenges, and Future Directions. Adv. Nutr. Int. Rev. J. 6, 408–419. https://doi.org/10.3945/an.114.008052

Stam, N.J., Spits, H., Ploegh, H.L., 1986. Monoclonal antibodies raised against denatured HLA-B locus heavy chains permit biochemical characterization of certain HLA-C locus products. J. Immunol. 137, 2299–2306.

Stosic-Grujicic, S., Stojanovic, I., Maksimovic-Ivanic, D., Momcilovic, M., Popadic, D., Harhaji, L., Miljkovic, D., Metz, C., Mangano, K., Papaccio, G., Al-Abed, Y., Nicoletti, F., 2008. Macrophage migration inhibitory factor (MIF) is necessary for progression of autoimmune diabetes mellitus. J. Cell. Physiol. 215, 665–675. https://doi.org/10.1002/jcp.21346

Szegezdi, E., Logue, S.E., Gorman, A.M., Samali, A., 2006. Mediators of endoplasmic reticulum stress-induced apoptosis. EMBO Rep. 7, 880–885. https://doi.org/10.1038/sj.embor.7400779

(tasc), T.A.-A.-A.S.C., (wtccc2), the W.T.C.C.C. 2, Evans, D.M., Spencer, C.C.A., Pointon, J.J., Su, Z., Harvey, D., Kochan, G., Oppermann, U., Dilthey, A., Pirinen, M., Stone, M.A., Appleton, L., Moutsianas, L., Leslie, S., Wordsworth, T., Kenna, T.J., Karaderi, T., Thomas, G.P., Ward, M.M., Weisman, M.H., Farrar, C., Bradbury, L.A., Danoy, P., Inman, R.D., Maksymowych, W., Gladman, D., Rahman, P., (sparcc), S.R.C. of C., Morgan, A., Marzo-Ortega, H., Bowness, P., Gaffney, K., Gaston, J.S.H., Smith, M., Bruges-Armas, J., Couto, A.-R., Sorrentino, R., Paladini, F., Ferreira, M.A., Xu, H., Liu, Y., Jiang, L., Lopez-Larrea, C., Díaz-Peña, R., López-Vázquez, A., Zayats, T., Band, G., Bellenguez, C., Blackburn, H., Blackwell, J.M., Bramon, E., Bumpstead, S.J., Casas, J.P., Corvin, A., Craddock, N., Deloukas, P., Dronov, S., Duncanson, A., Edkins, S., Freeman, C., Gillman, M., Gray, E., Gwilliam, R., Hammond, N., Hunt, S.E., Jankowski, J., Jayakumar, A., Langford, C., Liddle, J., Markus, H.S., Mathew, C.G., McCann, O.T., McCarthy, M.I., Palmer, C.N.A., Peltonen, L., Plomin, R., Potter, S.C., Rautanen, A., Ravindrarajah, R., Ricketts, M., Samani, N., Sawcer, S.J., Strange, A., Trembath, R.C., Viswanathan, A.C., Waller, M., Weston, P., Whittaker, P., Widaa, S., Wood, N.W., McVean, G., Reveille, J.D., Wordsworth, B.P., Brown, M.A., Donnelly, P., 2011. Interaction between ERAP1 and HLA-B27 in ankylosing spondylitis implicates peptide handling in the mechanism for HLA-B27 in disease susceptibility. Nat. Genet. 43, 761–767. https://doi.org/10.1038/ng.873

Tkach, M., Rosemblit, C., Rivas, M.A., Proietti, C.J., Flaqué, M.C.D., Mercogliano, M.F., Beguelin, W., Maronna, E., Guzmán, P., Gercovich, F.G., Deza, E.G., Elizalde, P.V., Schillaci, R., 2013. p42/p44 MAPK-mediated Stat3Ser727 phosphorylation is required for progestin-induced full activation of Stat3 and breast cancer growth. Endocr. Relat. Cancer 20, 197–212. https://doi.org/10.1530/ERC-12-0194

Tournier, C., Hess, P., Yang, D.D., Xu, J., Turner, T.K., Nimnual, A., Bar-Sagi, D., Jones, S.N., Flavell, R.A., Davis, R.J., 2000. Requirement of JNK for stress-induced activation of the cytochrome c-mediated death pathway. Science 288, 870–874.

Turkson, J., Bowman, T., Adnane, J., Zhang, Y., Djeu, J.Y., Sekharam, M., Frank, D.A., Holzman, L.B., Wu, J., Sebti, S., Jove, R., 1999. Requirement for Ras/Rac1-Mediated p38 and c-Jun N-Terminal Kinase Signaling in Stat3 Transcriptional Activity Induced by the Src Oncoprotein. Mol. Cell. Biol. 19, 7519–7528.

Turner, M.J., Delay, M.L., Bai, S., Klenk, E., Colbert, R.A., 2007. HLA-B27 up-regulation causes accumulation of misfolded heavy chains and correlates with the magnitude of the unfolded protein response in transgenic rats: Implications for the pathogenesis of spondylarthritis-like disease. Arthritis Rheum. 56, 215–223. https://doi.org/10.1002/art.22295

Uchio, N., Oma, Y., Toriumi, K., Sasagawa, N., Tanida, I., Fujita, E., Kouroku, Y., Kuroda, R., Momoi, T., Ishiura, S., 2007. Endoplasmic reticulum stress caused by aggregate-prone proteins containing homopolymeric amino acids. FEBS J. 274, 5619–5627. https://doi.org/10.1111/j.1742-4658.2007.06085.x

Ulianich, L., Terrazzano, G., Annunziatella, M., Ruggiero, G., Beguinot, F., Di Jeso, B., 2011. ER stress impairs MHC Class I surface expression and increases susceptibility of thyroid cells to NK-mediated cytotoxicity. Biochim. Biophys. Acta BBA - Mol. Basis Dis. 1812, 431–438. https://doi.org/10.1016/j.bbadis.2010.12.013

Upton, J.-P., Wang, L., Han, D., Wang, E.S., Huskey, N.E., Lim, L., Truitt, M., McManus, M.T., Ruggero, D., Goga, A., Papa, F.R., Oakes, S.A., 2012. IRE1α Cleaves Select microRNAs During ER Stress to Derepress Translation of Proapoptotic Caspase-2. Science 338, 818–822. https://doi.org/10.1126/science.1226191

Urano, F., Wang, X., Bertolotti, A., Zhang, Y., Chung, P., Harding, H.P., Ron, D., 2000. Coupling of stress in the ER to activation of JNK protein kinases by transmembrane protein kinase IRE1. Science 287, 664–666.

Urra, H., Dufey, E., Avril, T., Chevet, E., Hetz, C., 2016. Endoplasmic Reticulum Stress and the Hallmarks of Cancer. Trends Cancer 2, 252–262. https://doi.org/10.1016/j.trecan.2016.03.007

Usuki, F., Fujimura, M., Yamashita, A., 2013. Endoplasmic reticulum stress preconditioning attenuates methylmercury-induced cellular damage by inducing favorable stress responses. Sci. Rep. 3, 2346. https://doi.org/10.1038/srep02346

Vakifahmetoglu-Norberg, H., Zhivotovsky, B., 2010. The unpredictable caspase-2: what can it do? Trends Cell Biol. 20, 150–159. https://doi.org/10.1016/j.tcb.2009.12.006

van der Linden, S.M., Valkenburg, H.A., de Jongh, B.M., Cats, A., 1984. The risk of developing ankylosing spondylitis in HLA-B27 positive individuals. A comparison of relatives of spondylitis patients with the general population. Arthritis Rheum. 27, 241–249.

Vidal, R.L., Hetz, C., 2013. Unspliced XBP1 controls autophagy through FoxO1. Cell Res. 23, 463–464. https://doi.org/10.1038/cr.2013.9

Wang, M., Kaufman, R.J., 2014. The impact of the endoplasmic reticulum protein-folding environment on cancer development. Nat. Rev. Cancer 14, 581–597. https://doi.org/10.1038/nrc3800

Wang, Y., Alam, G.N., Ning, Y., Visioli, F., Dong, Z., Nör, J.E., Polverini, P.J., 2012. The unfolded protein response induces the angiogenic switch in human tumor cells through the PERK/ATF4 pathway. Cancer Res. 72, 5396–5406. https://doi.org/10.1158/0008-5472.CAN-12-0474

Wei, S.-G., Yu, Y., Weiss, R.M., Felder, R.B., 2016a. Endoplasmic Reticulum (ER) Stress Induces p44/42 Mitogen-Activated Protein Kinase (MAPK) Signaling, Inflammation and Renin-Angiotensin System (RAS) Activity in Forebrain and Contributes to Sympathetic Nerve Activity in Heart Failure Rats. FASEB J. 30, 1005.2-1005.2.

Wei, S.-G., Yu, Y., Weiss, R.M., Felder, R.B., 2016b. Inhibition of brain mitogen-activated protein kinase signaling reduces central endoplasmic reticulum stress and inflammation and sympathetic nerve activity in heart failure rats. Hypertension 67, 229–236. https://doi.org/10.1161/HYPERTENSIONAHA.115.06329

Wu, A.H., Yu, M.C., Tseng, C.-C., Pike, M.C., 2008. Epidemiology of soy exposures and breast cancer risk. Br. J. Cancer 98, 9–14. https://doi.org/10.1038/sj.bjc.6604145

Yan, L., Spitznagel, E.L., 2009. Soy consumption and prostate cancer risk in men: a revisit of a meta-analysis. Am. J. Clin. Nutr. 89, 1155–1163. https://doi.org/10.3945/ajcn.2008.27029

Yi, N., Chen, S.-Y., Ma, A., Chen, P.-S., Yao, B., Liang, T.-M., Liu, C., 2012. Tunicamycin inhibits PDGF-BB-induced proliferation and migration of vascular smooth muscle cells through induction of HO-1. Anat. Rec. Hoboken NJ 2007 295, 1462–1472. https://doi.org/10.1002/ar.22539

Yoshida, H., Matsui, T., Yamamoto, A., Okada, T., Mori, K., 2001. XBP1 mRNA Is Induced by ATF6 and Spliced by IRE1 in Response to ER Stress to Produce a Highly Active Transcription Factor. Cell 107, 881–891. https://doi.org/10.1016/S0092-8674(01)00611-0

Zambrano-Zaragoza, J., Francisco, Agraz-Cibrian, J.M., Gonz&#xe1, lez-Reyes, C., Dur&#xe1, n-Avelar, M. de J., s, Vibanco-P&#xe9, Rez, N., Zambrano-Zaragoza, J., Francisco, Agraz-Cibrian, J.M., Gonz&#xe1, lez-Reyes, C., Dur&#xe1, n-Avelar, M. de J., s, Vibanco-P&#xe9, Rez, N., 2013. Ankylosing Spondylitis: From Cells to Genes, Ankylosing Spondylitis: From Cells to Genes. Int. J. Inflamm. Int. J. Inflamm. 2013, 2013, e501653. https://doi.org/10.1155/2013/501653, 10.1155/2013/501653

Zarubin, T., Han, J., 2005. Activation and signaling of the p38 MAP kinase pathway. Cell Res. 15, 11–18. https://doi.org/10.1038/sj.cr.7290257

Zhang, K., Kaufman, R.J., 2004. Signaling the Unfolded Protein Response from the Endoplasmic Reticulum. J. Biol. Chem. 279, 25935–25938. https://doi.org/10.1074/jbc.R400008200

Zhang, X., Yuan, Y., Jiang, L., Zhang, J., Gao, J., Shen, Z., Zheng, Y., Deng, T., Yan, H., Li, W., Hou, W.-W., Lu, J., Shen, Y., Dai, H., Hu, W.-W., Zhang, Z., Chen, Z., 2014. Endoplasmic reticulum stress induced by tunicamycin and thapsigargin protects against transient ischemic brain injury. Autophagy 10, 1801–1813. https://doi.org/10.4161/auto.32136

Zhou, H.-B., Chen, J.-J., Wang, W.-X., Cai, J.-T., Du, Q., 2004. Apoptosis of human primary gastric carcinoma cells induced by genistein. World J. Gastroenterol. WJG 10, 1822–1825. https://doi.org/10.3748/wjg.v10.i12.1822

Zhou, Y., Lee, A.S., 1998a. Mechanism for the Suppression of the Mammalian Stress Response by Genistein, an Anticancer Phytoestrogen From Soy. J. Natl. Cancer Inst. 90, 381–388. https://doi.org/10.1093/jnci/90.5.381

Zhou, Y., Lee, A.S., 1998b. Mechanism for the Suppression of the Mammalian Stress Response by Genistein, an Anticancer Phytoestrogen From Soy. JNCI J. Natl. Cancer Inst. 90, 381–388. https://doi.org/10.1093/jnci/90.5.381

Zwanzig, R., Szabo, A., Bagchi, B., 1992. Levinthal's paradox. Proc. Natl. Acad. Sci. U. S. A. 89, 20–22.